THE
PHYSICAL REVIEW
A Journal of Experimental and Theoretical Physics Established by E. L. Nichols in 1893
VOL. 54, NO. 1 JULY 1, 1938 SECOND SERIES

Measurements of Gamma-Ray Ionization Currents in Air at High Pressures and High Gradients

JAMES W. BROXON AND GEORGE T. MERIDETH
University of Colorado, Boulder, Colorado
(Received April 27, 1938)

With weak sources of gamma-rays, ionization currents in air were measured at pressures between 20 and 200 atmospheres with collecting fields varied from less than 1 volt/cm to 4500 volts/cm. At all pressures, ionization currents were found to continue increasing with increase of collecting field intensity throughout the range employed. The ionization current measured with a particular collecting field intensity does not continue to increase with pressure but has a maximum value in the neighborhood of 140 atmospheres. Rates of collection of negative ions were found under all conditions to be greater than rates of collection of positive ions under the same conditions.

RECENT and current detection of cosmic radiation by the high pressure ionization method must be interpreted in terms of meager knowledge of high pressure ionization phenomena. A study of these has been begun at this laboratory. This paper presents measurements of ionization currents in air extending to 200 atmospheres and 4500 volts per cm, at room temperature. Measurements at higher and lower temperatures have been made and are being prepared for publication.

A preliminary report[1] of such observations has already been given. However, several alterations in the equipment have been introduced during the last few years, and in this paper are included only data obtained within the last year with what we consider our most satisfactory arrangement, herein described.

The currents were measured by the usual null method with quadrant electrometer, used by Broxon[2] in cosmic-ray measurements. The high pressure, steel, ionization chamber is represented in longitudinal section in Fig. 1, drawn to scale with fair accuracy. The long neck and the forms of the electrodes were necessitated by the considerable temperature variations imposed. It should be noted that the guard, G, restricted the region of collection of ions by the collection electrode, E, to a quite well-defined volume (of 520 cc) in the main body of the bomb.

The source of gamma-radiation, S_1, was a $RaBr_2$ concentrate sealed for three years in a heavy walled straight glass tube, sealed in its turn in cylinder, C_1. S_1 will be referred to as the "central source."

The source, S_2, consisted of the same type of $RaBr_2$ concentrate sealed in two nearly completely semicircular glass tubes placed together to form a nearly circular source of gamma-radiation located, as shown, beneath the ionization chamber and separated from it by a central

[1] J. W. Broxon and G. T. Merideth, Phys. Rev. **49**, 415 (1936).

[2] J. W. Broxon, Phys. Rev. **37**, 1320 (1931).

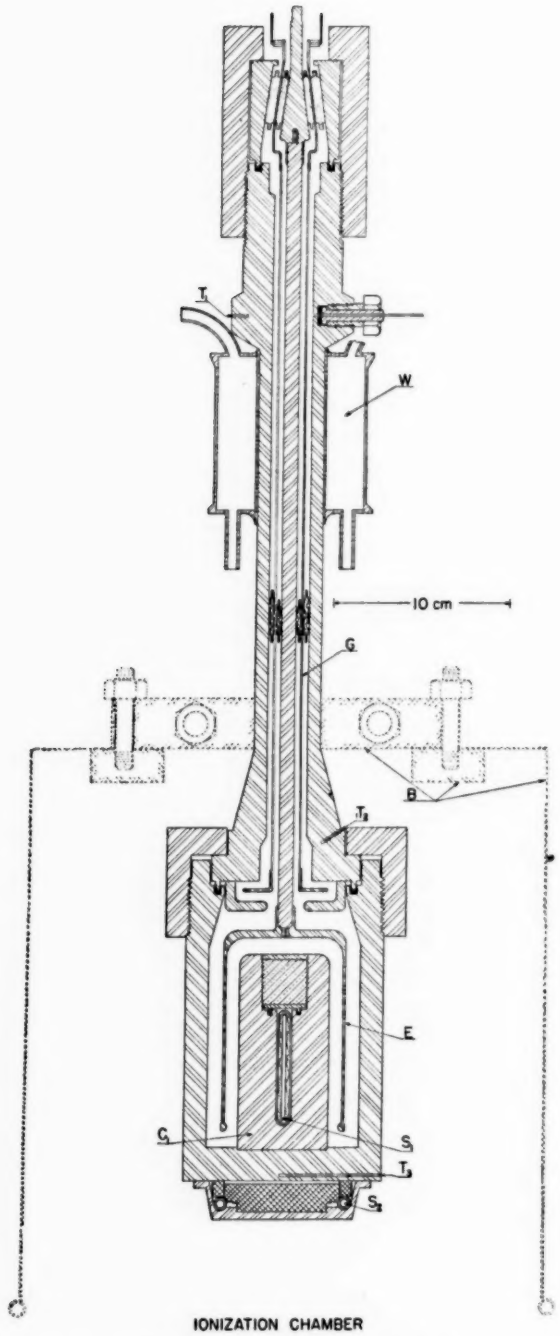

FIG. 1. High pressure ionization chamber.

plate and ring of lead. S_2 will be referred to as the "ring source." When S_1 was in its position as shown, S_2 and its container were removed from the vicinity of the chamber. When S_2 was in its position as shown, S_1 was removed, but C_1 was left in position.

The outer radius of C_1, the inner and outer radii of the cylindrical portion of the collecting electrode, E, and the inner radius of the chamber were, respectively, 2.54 cm, 3.32 cm, 3.46 cm, and 4.32 cm.

The water cooler, W, was employed to prevent extreme temperature variations of the conical and ring-shaped amber insulators during determination of the temperature effect,[3] and was detached when not needed.

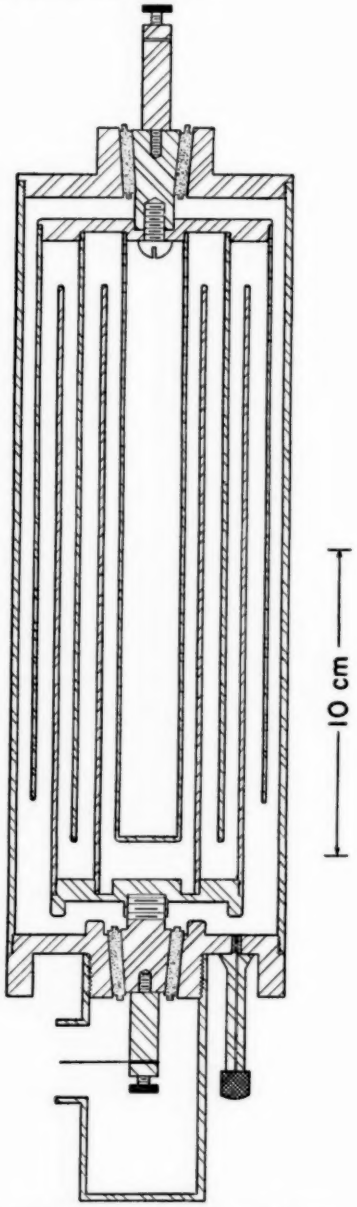

FIG. 2. Compensation condenser.

[3] J. W. Broxon and G. T. Merideth, Phys. Rev. **52**, 252 (1937).

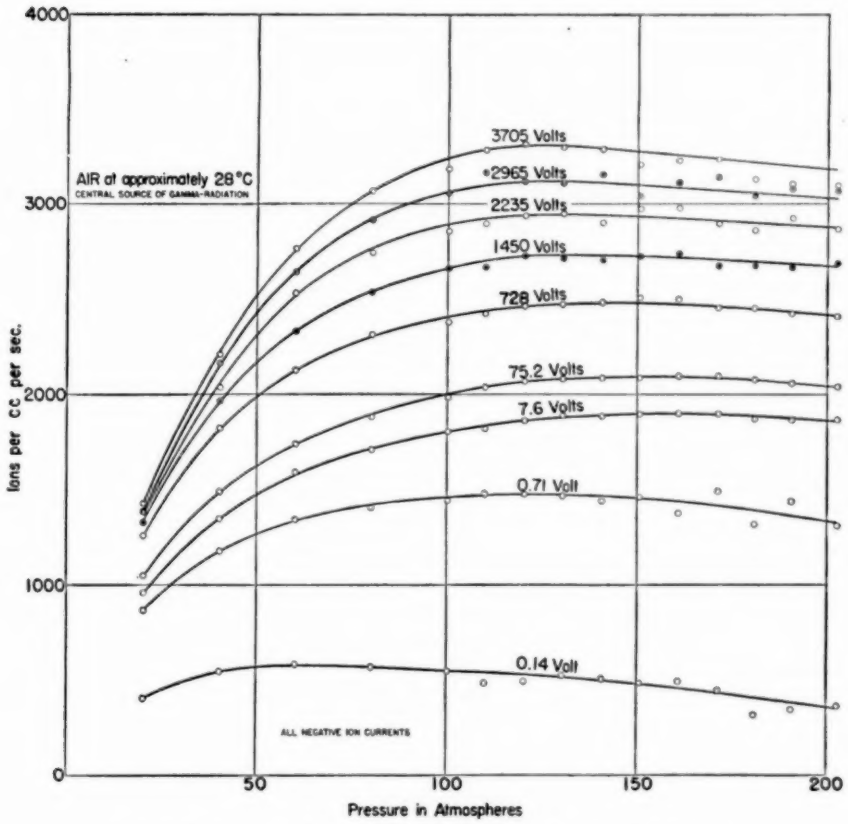

FIG. 3. Pressure ionization current curves, with central source.

B, drawn in broken lines, represents a detachable container for an oil bath employed only for high temperature measurements, the entire chamber being inverted from the position shown when B was in use.

T_1, T_2, and T_3 represent small drill holes at whose bottoms thermocouple junctions were located to determine the temperatures at these places in the cases of measurements not made at room temperature.

Figure 2 represents the well-guarded compensation condenser employed for the final measurements. Amber insulation was employed here as elsewhere for the central system. The condenser contained air at local atmospheric pressure, but was sealed and was separated from the ionization chamber and its radiation source by a distance of a few feet and an intervening brick and cement wall. The compensation condenser thus contributed only a small and nearly constant contrary ionization current. It provided a constant factor for the conversion of the rate of application of P.D. across it, into ionization currents. The condenser was calibrated by comparison with a Günther and Tegetmeyer variable air condenser which was carefully calibrated for us by the National Bureau of Standards after the calibration chart supplied by the makers was found to lead to inconsistent values with different condenser settings. The National Bureau of Standards calibration was made by the method of Rosa and Dorsey,[4] and ours by the usual electrometer method,[5] the variable condenser being substituted for the ionization chamber. The electrostatic induction coefficient between the high potential electrode of the compensation condenser and the central or collecting system was 154.2 cm. That between the high potential electrode of the ionization chamber and the central system was 50 cm when the chamber was evacuated.

[4] E. B. Rosa and N. E. Dorsey, Bull. Nat. Bur. Stand. **3**, No. 4, 541 (1907).
[5] J. W. Broxon, Phys. Rev. **37**, 1338 (1931).

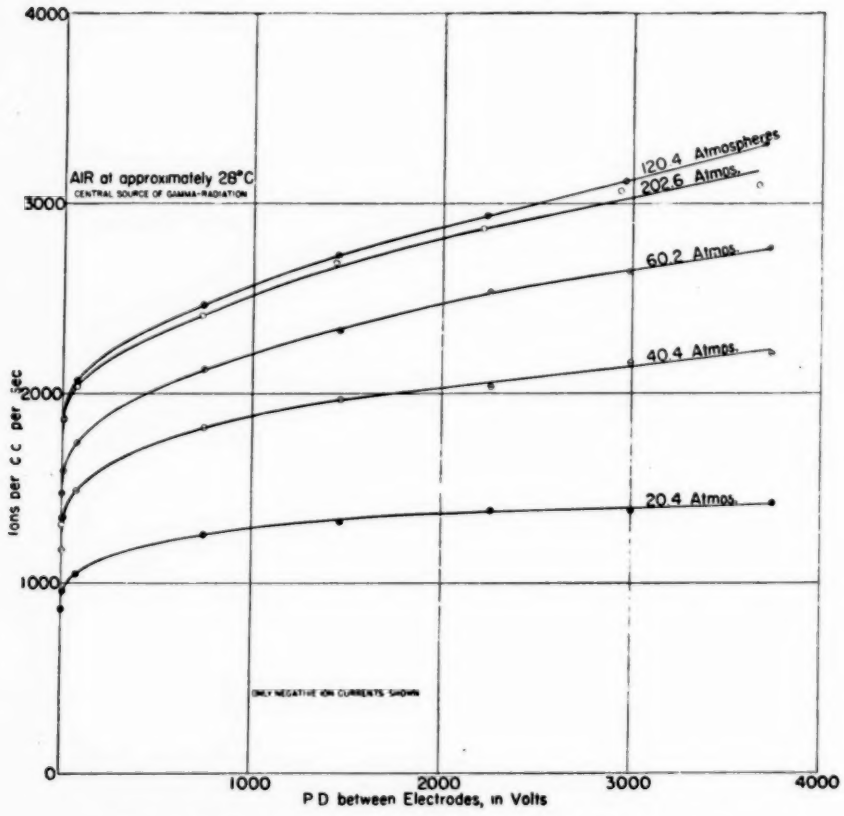

FIG. 4. Voltage ionization current curves, with central source.

Voltmeters of various appropriate ranges were employed for measurement of the potentials applied across the resistance capacitance compensation bridge arrangement, and the actual fractions of these applied across the ionization chamber were calculated from the ratios of the resistances which were measured at each pressure by an Eppley precision bridge. The ionization current compensation voltages were determined by a Weston model 1 microammeter with series resistance. All these meters were calibrated by means of a Leeds and Northrup type K potentiometer and standard cell, and standard or carefully determined resistances. Batteries supplied the low P.D.'s. For a time we used three high potential generators to supply 3500 volts, and a rectifier for an additional 1000. The high potential observations herein described, however, were all made with the aid of a 5000-volt, 0.25 amp., full wave rectifier, constructed by the General Electric Company and obtained with their cooperation. It was supplied with a filter found by them to pass a ripple of only 0.078 percent at maximum potential and full load. A Variac in the input circuit of the transformer provided for fine variation of the output direct voltage from zero to the maximum.

As usual, the air was allowed to stand a month or more after compression before being used. It was passed into the ionization chamber slowly over a trough containing P_2O_5, and then through alternate, tightly packed wads of glass wool and cotton, and finally, through a fine brass screen. After experiencing considerable difficulty with apparently erratic high conductivity of the air at the high pressures and highest gradients, we adopted the practice of carefully removing lint from the interior of the chamber with the aid of special illumination and a magnifying glass while assembling it, and then maintaining a P.D. of about 2000 volts between the long neck and the guard tube, providing a strong field through which the air must pass on its way to the ionization chamber, proper. This appeared to

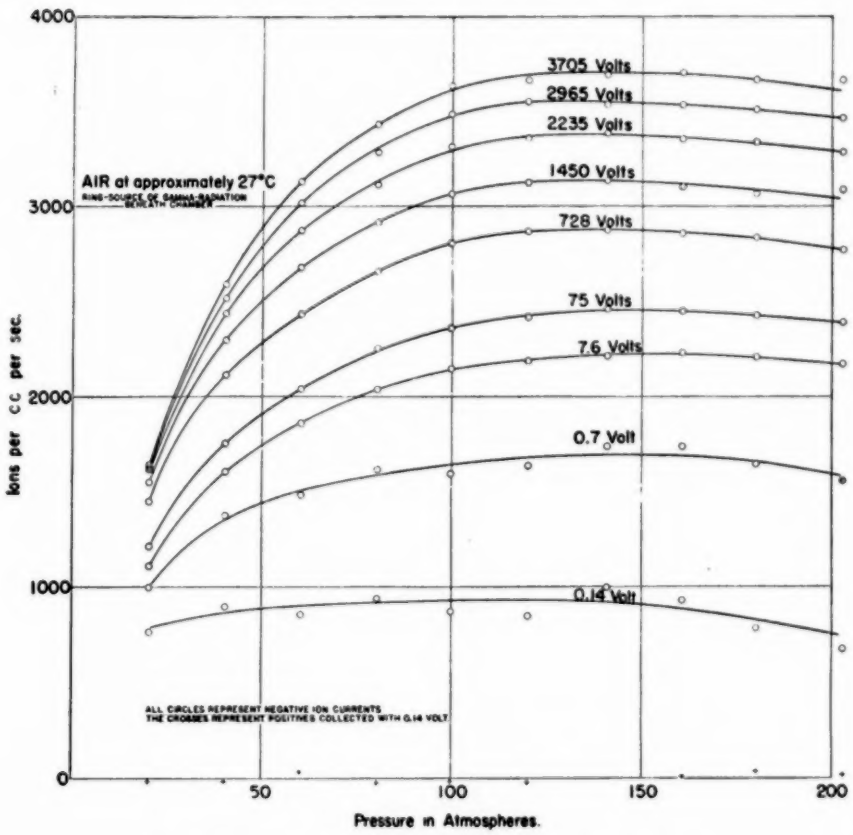

FIG. 5. Pressure ionization current curves, with ring source.

improve conditions materially, but did not always insure satisfactory functioning.

Pressures were measured by a new Ashcroft-American Bourdon type gauge calibrated by the National Bureau of Standards. Errors in pressure determination may have been 1 percent.

Except at the very low gradients, it was customary to collect the ions for periods of three, four or five minutes, after "balancing" or adjusting the equipment so that no large or permanent deflection was caused by suddenly impressing or withdrawing 5000 volts from the system, and after establishing steady current flow. The average of four such independent observations was normally determined and the points plotted in the diagrams represent these averages. An occasional reading was discarded when its large deviation from the average clearly indicated an error in observing or recording. Very high gradient current observations accepted as satisfactory were reproducible minima. At the lowest gradients, two observations were usually made, with ten- or fifteen-minute collection periods.

In Fig. 3, the ionization currents in ions per cc per sec. obtained with the central source, are plotted as ordinates with total pressures in atmospheres as abscissae. At the several pressures, observations were made with the same definite over-all potentials impressed across the compensation bridge system. Because of the increase in the dielectric coefficient of the air with increase in pressure, a slightly smaller fraction of the total impressed P.D. was actually across the ionization chamber at the higher than at the lower pressures. This is shown in Fig. 4, where the current is plotted against the actual voltage across the ionization chamber, for a few selected pressures. The variation of current with voltage in the voltage interval involved was found so small, however, that in the pressure current diagrams the currents measured with a constant

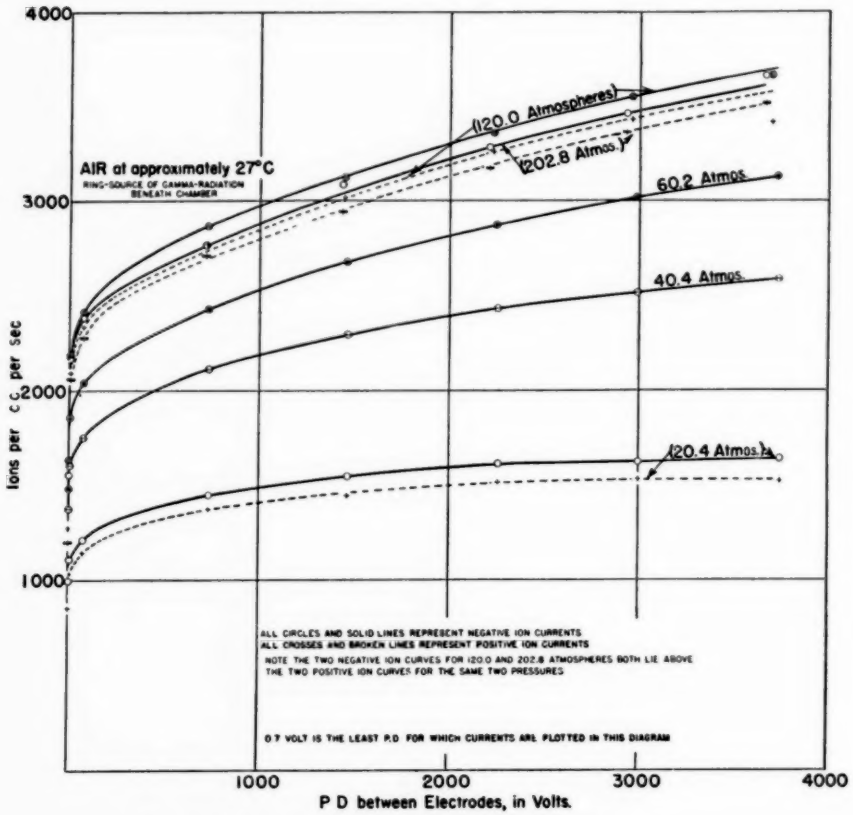
4000
3000
2000
1000
Ions per c.c. per sec
AIR at approximately 27°C
RING-SOURCE OF GAMMA-RADIATION BENEATH CHAMBER
(120.0 Atmospheres)
(202.8 Atmos.)
60.2 Atmos.
40.4 Atmos.
(20.4 Atmos.)
ALL CIRCLES AND SOLID LINES REPRESENT NEGATIVE ION CURRENTS
ALL CROSSES AND BROKEN LINES REPRESENT POSITIVE ION CURRENTS
NOTE THE TWO NEGATIVE ION CURVES FOR 120.0 AND 202.8 ATMOSPHERES BOTH LIE ABOVE THE TWO POSITIVE ION CURVES FOR THE SAME TWO PRESSURES
0.7 VOLT IS THE LEAST P.D. FOR WHICH CURRENTS ARE PLOTTED IN THIS DIAGRAM
1000
2000
3000
4000
P D between Electrodes, in Volts.

FIG. 6. Voltage ionization current curves, with ring source.

over-all potential were plotted without correction for the capacitance variation, the voltage designated for each curve being the mean of the voltages across the ionization chamber at the extremes of pressure. All values plotted in the case of the central source represent negative ion currents, or the rate of collection of negative ions (per cc) upon the central system.

In Fig. 5 are plotted the pressure current relations observed with the ring source of radiation, each curve corresponding to a definite, over-all, impressed P.D., the average P.D. across the ionization chamber being designated as in Fig. 3. Figure 6 gives the voltage current relations observed with the ring source, at approximately the same pressures for which corresponding curves are shown in Fig. 4 for the central source. The lowest voltage values plotted, both in Fig. 4 and in Fig. 6, correspond to 0.71 volt across the chamber, the values at 0.14 volt being omitted from these curves. In Fig. 6 both negative and positive ion currents are given for 20.4, 120 and 202.8 atmospheres. In Fig. 5, positive ion currents depending on single observations with an impressed chamber P.D. of 0.14 volt are designated by plus signs near the pressure axis. Values designated below this axis represent the

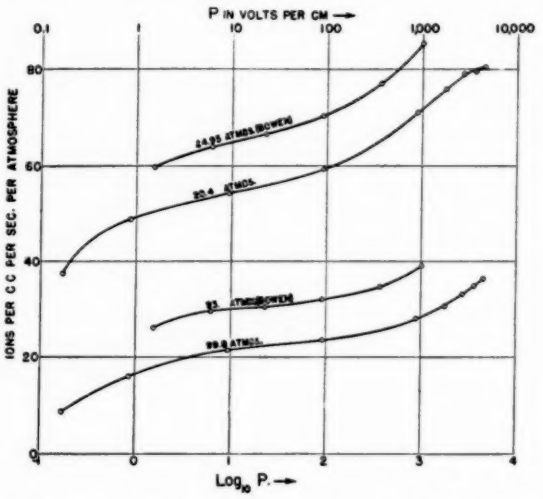

FIG. 7. Log gradient ionization current *per atmosphere.*

actual collection of negative ions although the small P.D. was impressed in such a manner as to force positive ions toward the central system. In all cases not designated, only negative ion currents are represented in Figs. 3–6.

As has been mentioned, the design of the ionization chamber was influenced by the requirement of rather large temperature variation. To this end, complete uniformity of collection field was sacrificed. Accurate computations of the effects of the nonuniformity of field which existed would probably be impossible. Even when good approximations to the field strength at particular points in the region of considerable nonuniformity had been made, it would be difficult to form a reliable conclusion regarding the relation of any function of this to the resultant current measured. Relative to this situation it is fortunate that we have observations made by Bowen[6] with particular care as to uniformity of field, with nearly the same ion densities produced in air by the same type of radiation, and with gradients extending over a considerable fraction of the range we employed. For comparison with his values, the P.D. (in volts) across the ionization chamber was divided by 0.82, the mean radial distance in cm across the ionized region between electrodes, to obtain an effective gradient for our observations. In Fig. 7 are given Bowen's curves for 24.95 and 93 atmospheres, and our own (negative ion currents) for 20.4 and 98.8 atmospheres, with the ring source, actual numerical values being designated in all cases. As was done by Bowen, the currents in ions per cc per sec. *per atmosphere* are plotted as ordinates, and the *logarithms* of the gradients as abscissae. This exaggerates the low gradient end of the curve considerably, but serves to bring out clearly the dependence of the currents upon collecting field in the region of low fields, and provides an excellent comparison of values in the region of Bowen's measurements. The curves indicate that the departure from uniformity of the field in our ionization chamber was not sufficient to affect materially the measured currents. The similarity of the relations is brought out even more clearly in Table I.

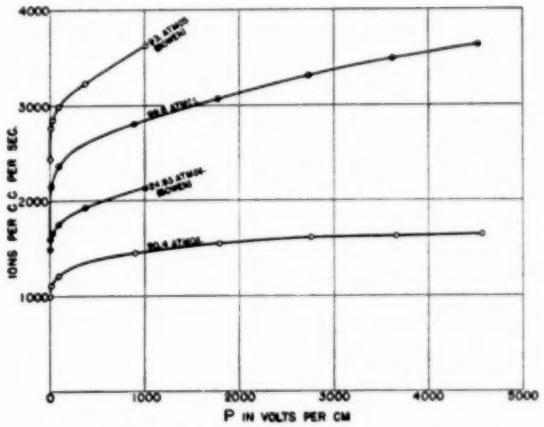

FIG. 8. Gradient ionization current.

In columns 2 and 5 are listed the values given tabularly by Bowen[6] opposite the gradients he employed, in column 1. In columns 3 and 6 are given our own values for these gradients as read from our curves in Fig. 7. Column 4 gives the ratios of Bowen's values for 24.95 atmospheres to our own for the comparable pressure of 20.4 atmospheres. The ratio is seen to be constant throughout Bowen's range of gradients, within the accuracy of the observations. In column 7 are listed the ratios of Bowen's 93-atmosphere values to our corresponding values at the comparable pressure of 99.8 atmospheres. In this case the ratio varies somewhat in the very low gradient region, but again remains constant within the

[6] I. S. Bowen, Phys. Rev. **41**, 24 (1932).

TABLE I. *Ionization currents at various gradients.*

GRADIENT (V/CM)	I AT 24.95 ATMOS. (IONS-CC^{-1}-SEC.$^{-1}$-ATMOS.$^{-1}$) (BOWEN)	I AT 20.4 ATMOS. (IONS-CC^{-1}-SEC.$^{-1}$-ATMOS.$^{-1}$) (B. AND M.)	$\frac{I \text{ AT } 24.95}{I \text{ AT } 20.4}$	I AT 93 ATMOS. (IONS-CC^{-1}-SEC.$^{-1}$-ATMOS.$^{-1}$) (BOWEN)	I AT 99.8 ATMOS. (IONS-CC^{-1}-SEC.$^{-1}$-ATMOS.$^{-1}$) (B. AND M.)	$\frac{I \text{ AT } 93}{I \text{ AT } 99.8}$
1.55	59.8	50.5	1.18	26.2	17.9	1.46
6.2	63.9	53.5	1.19	29.7	21.0	1.41
23.0	66.5	56.0	1.19	30.6	22.4	1.37
91.5	70.2	59.4	1.18	32.1	23.6	1.36
367.	77.1	65.2	1.18	34.8	25.6	1.36
1009.	85.5	71.8	1.19	39.1	28.5	1.37

accuracy of observation for all gradients above 23 volts/cm.

In Fig. 8 are designated the same data represented in Fig. 7, ordinates in this instance representing currents directly in ions per cc per second, and abscissae the actual gradients, in accordance with our usual mode of representation. This brings out more clearly the relations among the high gradient values.

Certain of the curves in Figs. 3–6 may appear to the reader to have been drawn without adequately weighting certain individual plotted points. In drawing individual curves, it was borne in mind that each was but a member of a family; and in drawing the voltage current curves, the smoothed out pressure current curves were observed, and *vice versa*. On these bases we believe that the curves represent very well the designated relations, although there is necessarily some arbitrariness.

Perhaps the most striking feature of the pressure current curves is the broad but apparently definite maximum displayed by each. Erikson[7] has observed such maxima with very much higher ion current densities (estimated at 2×10^5 to 10^7 ions per cc per sec. *per atmosphere* by Bowen and Cox).[8] In his curves for the three highest gradients he employed, 2500 volts, 1050 volts and 102 volts, across 0.8 cm between small cylindrical electrodes, the maxima occur in the region between 140 and 160 atmospheres. For smaller gradients, however, the maxima occur at regularly lower pressures, that for his 8.3-volt curve being at about 30 atmospheres. In our measurements with the ring source, Fig. 5, all the maxima occur in the region between 130 and 150 atmospheres for all gradients, the maxima for the 75.2-volt and the 7.6-volt curves occurring at perhaps slightly higher pressures than those for the higher gradients. With the exception of the 0.14-volt curve, all the curves of the central source pressure current family appear to have maxima in the region between 120 and 150 atmospheres, the highest pressures again corresponding to maxima of the 75.2-volt and 7.6-volt curves.

Sievert[9] has observed similar maxima with ions produced by x-rays, at 50 to 60 atmospheres.

The two families of pressure current curves obtained with the two sources resemble each other closely, but are not identical in form. Values were read from the two sets of curves at 10-atmosphere intervals and compared. Excluding the 0.14-volt values, it was found that the ratio of the ring source current to the central source current for the same pressure and gradient, remained between 1.1 and 1.2 for all pressures and gradients. However, there appeared no striking regularity of variation of the ratio between those limits.

Both sets of voltage current curves, Figs. 4 and 6, show the current continues to increase with voltage for all voltages and pressures employed, some of the curves appearing to be nearly linear at the high potential ends. The curves indicate that even at 20 atmospheres a gradient of 4500 volts per cm is not sufficient to produce saturation, but that the current is still dependent upon the gradient. This is in agreement with observations of Clay and van Tijn.[10]

Clay and van Tijn have also observed the negative ion current values larger than positive ion current values under otherwise identical conditions, illustrated in the curves of Fig. 6. On the other hand, Cox[11] was unable to observe this effect with the equipment used by Bowen and himself. We have made many observations over a long period, under varied conditions as to details of guard, insulation, position and intensity of radiation source, compensation condenser, source of applied P.D., pressure, gradient, and temperature, but in all these cases in which we have collected both kinds of gamma-ray ions under apparently identical conditions, we have observed larger rates of collection of the negatives.

It is possibly significant that in all cases the gamma-radiation initially penetrated the high potential electrode and then the collecting electrode, although when the central source was employed the radiation served both as "emergent" and "incident" at corresponding

[7] H. A. Erikson, Phys. Rev. **27**, 473 (1908).
[8] I. S. Bowen and E. F. Cox, Phys. Rev. **51**, 232 (1937).
[9] R. M. Sievert, Nature **129**, 792 (1932).
[10] J. Clay and M. A. van Tijn, Physica **2**, 825 (1935). Note "positive" and "negative" should be exchanged in section 3, p. 827 and in the captions for Figs. 1 and 2, p. 828 of their paper. See p. 650 of J. Clay and M. A. van Tijn, Physica **4**, 648 (1937).
[11] E. F. Cox, Phys. Rev. **51**, 55 (1937).

surfaces of both electrodes. Rutherford[12] found in 1901 that unequal currents resulted from intense, unsymmetrical ionization of dry air. It is rather interesting that with the arrangement he employed, Rutherford actually collected greater negative than positive ion currents. With the ionization confined to the immediate neighborhood of the high potential electrode, he found for certain impressed voltages that the ratio of the negative to the positive ion currents received at the collecting electrode equalled the ratio of the mobilities of the corresponding ions in air. At both higher and lower voltages the ratio approached unity. The difference between currents of the two signs was also considerably decreased by the introduction of various vapors, particularly alcohol. In our observations the numerical difference between the weak currents of the two signs does not appear to depend much upon the pressure or intensity of the collecting field. The "positive" ion current values of Fig. 5 collected with a very low impressed P.D. show the effect of contact potentials, of course.

[12] E. Rutherford, Phil. Mag. **2**, 210 (1901).

JULY 1, 1938 PHYSICAL REVIEW VOLUME 54

The Analysis of High Gradient, High Pressure, Gamma-Ray, Air Ion Current Measurements, by Zanstra's Adaptation of Jaffé's Columnar Theory

JAMES W. BROXON AND GEORGE T. MERIDETH
University of Colorado, Boulder, Colorado

(Received April 27, 1938)

A brief survey of theories advanced to explain the chief characteristics of high pressure ionization current measurements is given. The equation developed by Zanstra from Jaffé's theory of recombination of the ions formed by a single particle, yielding a linear relation between the reciprocal of the measured current and a function of the collecting field intensity and pressure, was applied to our high pressure, gamma-ray, ionization current measurements. The curves yielded were not linear, but departure from linearity was rather small in the region of high gradients. By extrapolation, "saturation" current values were obtained. These "saturation" currents were found to vary linearly with the air density over certain pressure ranges, as found by Clay and van Tijn, but changes in slope at very high pressures would indicate a modification of Clay's "wall" radiation theory if the analysis is regarded as reliable.

THAT measured gamma-ray ionization currents in air at high pressures depend upon the pressure in much the same manner as do cosmic-ray ionization currents has been demonstrated by Compton, Bennett and Stearns[1] and by Broxon.[2] Tarrant[3] made a similar observation consequent to his gamma-ray measurements. Gross[4] pointed out that Florance's[5] beta-ray ionization pressure curves also closely resemble the gamma-ray curves of Bowen[6] and the cosmic-ray curves of Broxon,[7] over Florance's range of 70 atmospheres. This situation has necessitated theoretical treatment designed to clarify those ionization phenomena which result in measurements of such striking similarity associated with these radiations of different nature and vastly different penetrating power. It has also provided us with the means of investigating and interpreting high pressure cosmic-ray ionization measurements by conducting gamma-ray ionization current measurements under conveniently controllable conditions.

Attempted explanations of the characteristics of recent measurements of cosmic-ray and gamma-ray ionization currents at high pressures are interestingly similar to initial attempts at explaining alpha-ray and gamma-ray currents measured a quarter of a century earlier. Many of the same characteristics are outstanding in

[1] A. H. Compton, R. D. Bennett and J. C. Stearns, Phys. Rev. **39**, 873 (1932).
[2] J. W. Broxon, Phys. Rev. **42**, 321 (1932).
[3] G. T. P. Tarrant, Proc. Roy. Soc. **A135**, 223 (1932).
[4] B. Gross, Zeits. f. Physik **80**, 125 (1933).
[5] D. C. H. Florance, Phil. Mag. **25**, 172 (1913).
[6] I. S. Bowen, Phys. Rev. **41**, 24 (1932).
[7] J. W. Broxon, Phys. Rev. **37**, 1320 (1931).

both instances, and the fundamental points of view have been duplicated.

To explain relations between current and intensity of collecting field observed in connection with work on recombination of alpha-ray ions, Bragg and Kleeman,[8] in 1906, used a suggestion made by Rutherford[9] in 1904, assuming a "process of recombination of newly-formed ions with the atoms from which they have just been separated. The effects of it are proportional to the number of ions formed in a cubic cm in unit time, not to the product of the existing numbers of positives and negatives. They are independent of the shape of the ionization chamber, and in this they differ from those of general recombination. They depend directly on pressure, and vary greatly from gas to gas." They did some quantitative work, deciding that fields of the order of 1000 volts/cm would be necessary to affect this "initial" recombination considerably.

In 1908 Erikson[10] used this "initial" (sometimes called "preferential" or "selective") recombination hypothesis in explaining his extensive measurements of high pressure gamma-ray ionization currents.

However, Moulin,[11] in 1911, found this inadequate to explain his measurements, particularly with reference to the dependence of experimental currents upon collecting fields, and invoked a suggestion he attributed to Langevin (apparently 1902 or 1903) that the preponderance of recombination among the ions formed by a single ionizing particle is strikingly effective, writing: *Pour interpréter le phénomène de recombinaison initiale, M. Langevin a proposé une autre hypothèse qui fait intervenir une recombinaison générale entre tous les ions produits par une même particule α, sur laquelle un champ extérieur doit avoir une action marqueé puisqu'il peut diminuer le nombre total de rencontres qui ont lieu entre ces différents ions. Cette interprétation, qui a servi de point de départ aux recherches qui vont suivre, est basée sur l'hypothèse que les ions produits par chaque particule α s'éloignent relativement peu de la trajectoire et sont, initialement, distribués en colonnes, . . .*

Jaffé,[12] in 1913, proceeded further with the "columnar" (sometimes called "initial") recombination development of Moulin, deducing formulae relating rate of collection of ions to magnitude and direction of the collecting field and involving the coefficients of ionic recombination, mobility, and diffusion. Jaffé assumed an initial probable cylindrical distribution of the ions, and set up a differential equation for which he was able to obtain only an approximate solution.

Meanwhile, in 1909, Wilson[13] had explained the current-pressure relation he had observed in gamma-ray and natural ionization current measurements extending to 40 and 45 atmospheres, in terms of the supposed considerable contribution to the ionization by secondary radiations excited in the walls of the ionization chamber. He attributed his "wall" radiation hypothesis to McLennan[14] who worked on gamma-ray subsidiaries in 1907. Wilson offered some mathematical development.

After the World War when the study of the penetrating (cosmic) radiation was resumed, certain investigators, notably Professor Swann, appreciated the advantages offered by the high pressure ionization chamber. Measurements of this type again raised many of the old questions.

In 1920 Downey[15] employed the "wall" radiation hypothesis to explain the natural ionization current-pressure relation she observed at pressures extending to 58 atmospheres. In 1926 Broxon[16] extended the pressure range and provided some mathematical development of the hypothesis, later[2] concluding that it was inadequate to explain all the phenomena.

In 1932 Compton, Bennett and Stearns[1] pointed out inadequacies in the "wall" hypothesis, and applied the hypothesis of "initial" recombination of ions with atoms from which they were separated. They were able to explain the cosmic-ray current-pressure relations observed by Broxon,[7]

[8] W. H. Bragg and R. D. Kleeman, Phil. Mag. **11**, 466 (1906).
[9] E. Rutherford, *Radioactivity* (1904), p. 33.
[10] H. A. Erikson, Phys. Rev. **27**, 473 (1908).
[11] M. Moulin, Ann. de chim. et phys. **22**, 26 (1911).
[12] G. Jaffé, Ann. d. Physik 4, **42**, 303 (1913).
[13] W. Wilson, Phil. Mag. **17**, 216 (1909).
[14] J. C. McLennan, Phil. Mag. **14**, 760 (1907).
[15] K. M. Downey, Phys. Rev. **16**, 420 (1920); **20**, 186 (1922).
[16] J. W. Broxon, Phys. Rev. **28**, 1071 (1926). (Also see reference 7.)

as well as dependences upon temperature and upon the nature of the gas. They concluded that in air at 20°C fields of the order of 40,000 volts/cm would be necessary to affect this "initial" recombination.

At about the same time Millikan and Bowen[17] also drew attention to the "initial" recombination hypothesis, but offered no mathematical treatment. Bowen,[6] Gross,[18] Lea,[19] and Harig[20] have all objected to the "initial" recombination treatment by Compton, Bennett and Stearns[1] because of their conclusion relative to the lack of dependence of current upon field intensity at high values less than the critical value they specify.

Gross,[18, 4] by means of certain assumptions relative to dependence of the ion constants upon pressure and temperature, adapted Jaffé's[12] "columnar" theory formulae to high pressure measurements, including consideration of "general" or "volume" recombination not restricted to columns. He succeeded in approximating the high density gamma-ray current-pressure curves of Erikson[10] at the several collecting field intensities he used, Broxon's[7, 21] cosmic-ray curves in air and nitrogen, Bowen's[6] low density gamma-ray curves, and Florance's[5] beta-ray curves, as well as temperature effects observed at high pressures.

Harig[20] also used the "columnar" hypothesis and Jaffé's calculations to explain Bowen's observations. Lea[19] criticized Gross' treatment of the problem, and introduced the assumption that the ion distribution is better represented by "clusters" symmetrical relative to points than by "columns" symmetrical relative to lines, these clusters perhaps being arranged in columns. He concluded that "cluster" recombination may roughly be regarded as accounting for the dependence of currents upon pressure, and "columnar" recombination, for the dependence upon the collecting field.

Zanstra[22] has written formula (32′) of the paper by Jaffé[12] in the form

$$\frac{1}{i}=\frac{1}{I}+\frac{q}{I}f(x). \qquad \text{(A)}$$

Here i is the measured ionization current and I the supposed "saturation" current which could be obtained by an infinite collecting field, so that i/I is the same as Jaffé's N_∞'/N_0, both "initial" and "general" recombination being neglected and only "columnar" recombination considered.

In this equation, $q=\alpha N_0/8\pi D$, where α is the "coefficient of recombination" among ions of a column, N_0 is the initial line density of ions in a column, and D is the ionic "diffusion coefficient." Also,

$$f(x)=e^x(j\pi/2)H_0^{(1)}(jx),$$

where $j=\sqrt{(-1)}$ and $H_0^{(1)}$ is designated by Gross[18] *eine Hankelsche Funktion nullter Ordnung*, values of $jH_0^{(1)}(jx)$ being given in *Table of Functions* by Janke and Emde. In this,

$$x=(buE\sin\phi/2D)^2,$$

where b is a "column parameter" proportional to the initial mean radial displacement of the ions in a column, u is the ionic "mobility" assumed the same for ions of both signs, E is the intensity of the collecting field, and ϕ is the angle between column axis and collecting field (or $\sin^2\phi$ may be replaced by an "average" value unless ϕ is predominantly small).

Assuming u/D independent of the pressure, and the average $(b\sin\phi)$ inversely proportional to the pressure, Zanstra decided that for high pressure gamma-ray ionization currents in air collected with strong fields, $x=1.24(10)^{-4}(E/p)^2$ to a sufficient degree of approximation, p being the pressure in atmospheres and E being measured in volts/cm. Zanstra pointed out that as E approaches ∞, $f(x)$ approaches 0. Hence the $(1/i)$ intercept of the line represented by Eq. (A), linear in $f(x)$, must represent the reciprocal of the "saturation" current collected at infinite field intensity if the relation is correct. Graphs representing $f(x)$ for values of x from 10^{-8} to 12 are given by Zanstra.

Zanstra emphasized that the relation should be obeyed only at high field intensities where "general" recombination is eliminated. He ap-

[17] R. A. Millikan and I. S. Bowen, Nature **128**, 582 (1931).
[18] B. Gross, Zeits. f. Physik **78**, 271 (1932).
[19] D. E. Lea, Proc. Camb. Phil. Soc. **30**, 80 (1933–34).
[20] G. Harig, Physik. Zeits. Sowjetunion **5**, 637 (1934).
[21] J. W. Broxon, Phys. Rev. **38**, 1704 (1931).
[22] H. Zanstra, Physica **2**, 817 (1935).

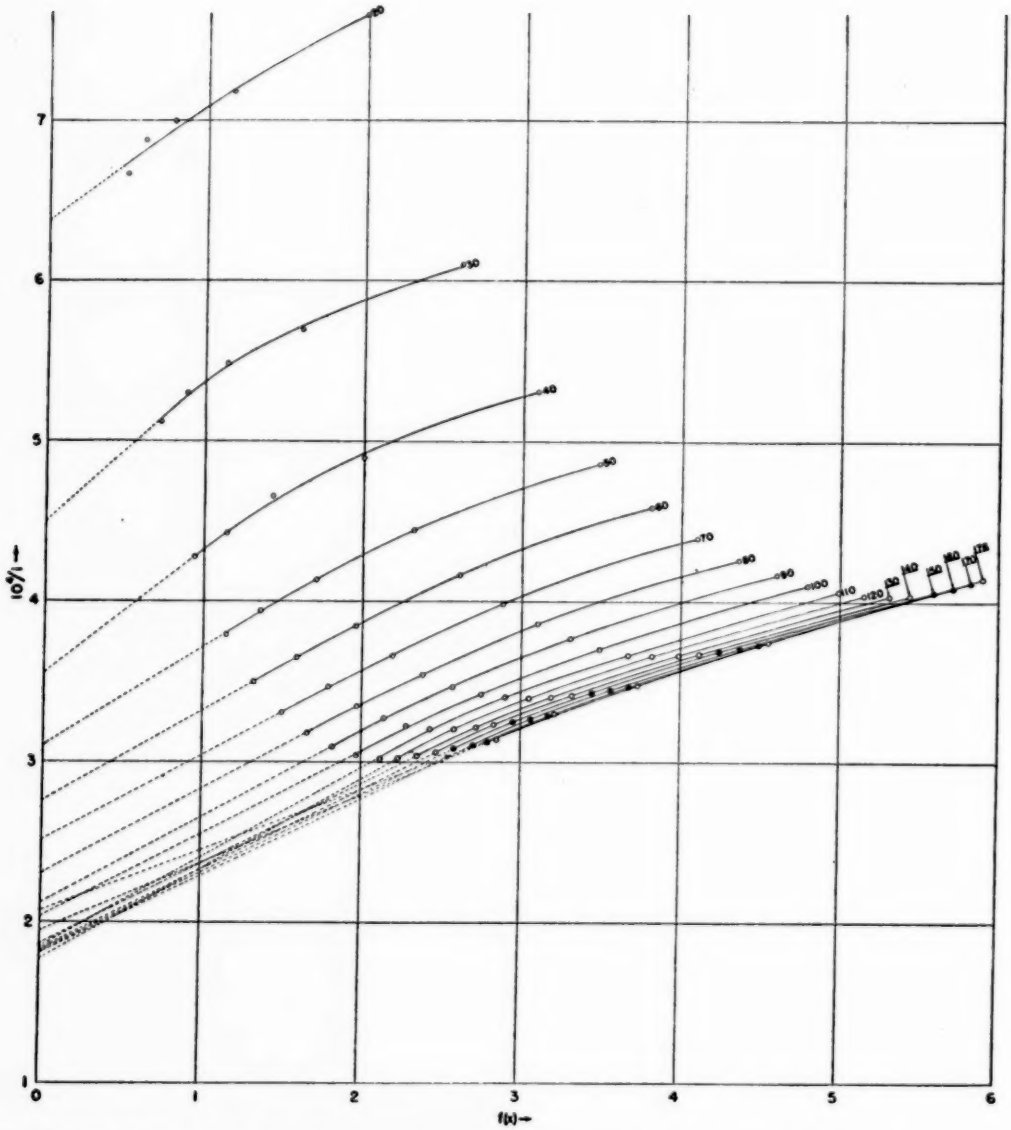

FIG. 1. Jaffé-Zanstra function curves corresponding to our measurements with central source. Air at 28°C. Central source of gamma-radiation. Numbers at upper ends of curves represent specific gravity relative to air at N.T.P.

plied the theory to Erikson's[10] measurements, finding the linear relation obeyed by those data, and extrapolated to find the "saturation" currents. He also pointed out that for specified field intensities the accuracy of determination of I decreases with increase of P and the consequent greater extrapolation necessitated.

Clay[23] and Clay and van Tijn[24] applied Zanstra's deductions to their measurements of gamma-ray and cosmic-ray ionization currents in various gases at high pressures, and found the linear relation between $1/i$ and $f(x)$ obeyed for large collecting field intensities. Clay[23] found the "saturation" current to increase linearly with pressure at different rates in different pressure ranges, and explained the situation in terms of secondary radiations produced in the gas and in the walls of the vessel.

Bowen and Cox[25] have criticized the work of

[23] J. Clay, Physica 2, 811 (1935).
[24] J. Clay and M. A. van Tijn, Physica 2, 825 (1935).
[25] I. S. Bowen and E. F. Cox, Phys. Rev. 51, 232 (1937).

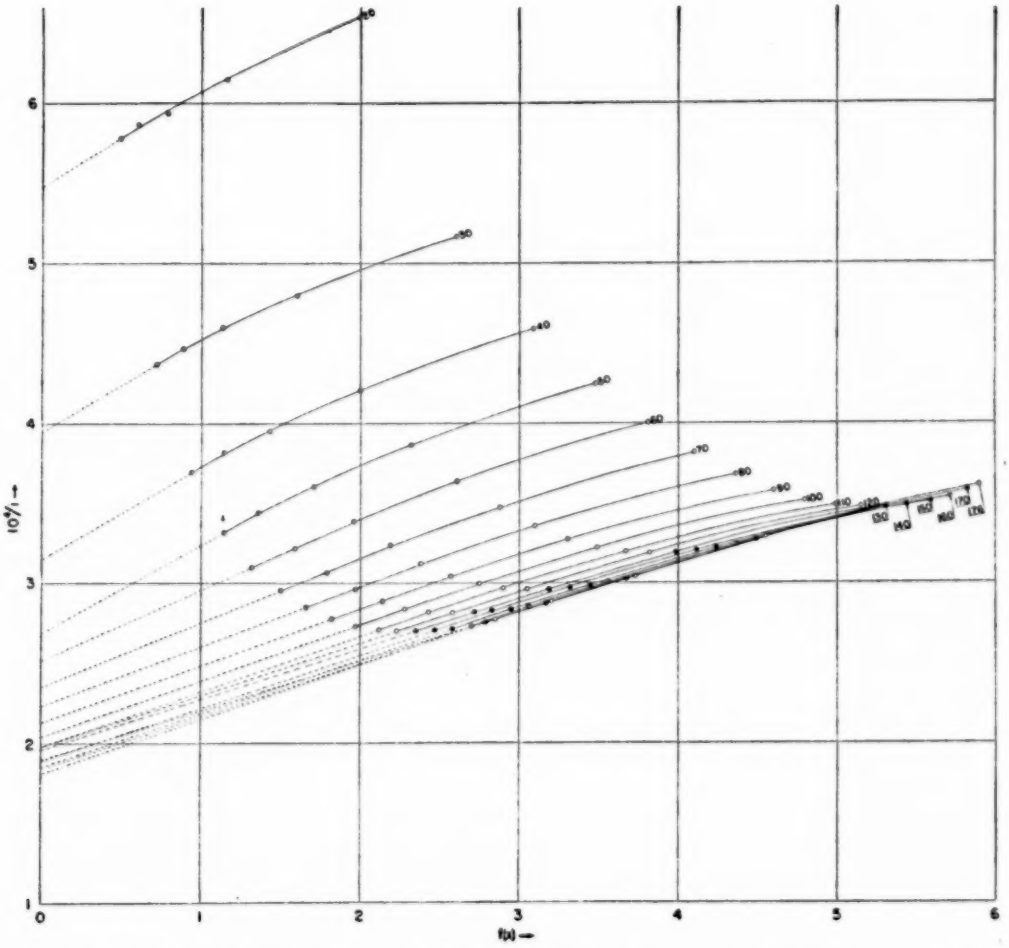

FIG. 2. Jaffé-Zanstra function curves corresponding to our measurements with ring-source. Air at 27°C. Ring-source of gamma-radiation beneath chamber. Numbers at upper ends of curves represent specific gravity relative to air at N.T.P.

Zanstra and Clay and van Tijn. Applying Zanstra's equation to their own measurements, they obtained a curve concave toward the $f(x)$ axis rather than a straight line. They emphasized the necessity of very low ion densities such as employed in their own measurements, in order to assure freedom from "general" or "volume" recombination.

Clay[26] then showed that "volume" recombination could not have affected his measurements, and pointed out that the collecting fields employed by Bowen and Cox were too weak to provide a proper test of the Zanstra equation. Clay and van Tijn[27] have provided striking evidence in favor of this method of analysis by deducing Eve's constant from measurements of gamma-ray ionization currents in air at pressures extending to 147 atmospheres.

Our recent measurements[28] of gamma-ray ionization currents in air provide a desirable test of this theory which presumes to evaluate actual "saturation" currents (or rates of *production* of ions?) in gases at high pressures. We employed the same low ion densities advocated by Bowen and Cox, and the range of collecting field intensities and pressures found satisfactory by Clay and van Tijn.

In Fig. 1 are the curves obtained by substituting in Zanstra's equation our experimental values observed with the central source of

[26] J. Clay, Phys. Rev. **52**, 143 (1937).
[27] J. Clay and M. A. van Tijn, Physica **4**, 648 (1937).
[28] J. W. Broxon and G. T. Merideth, Phys. Rev. **54**, 1 (1938).

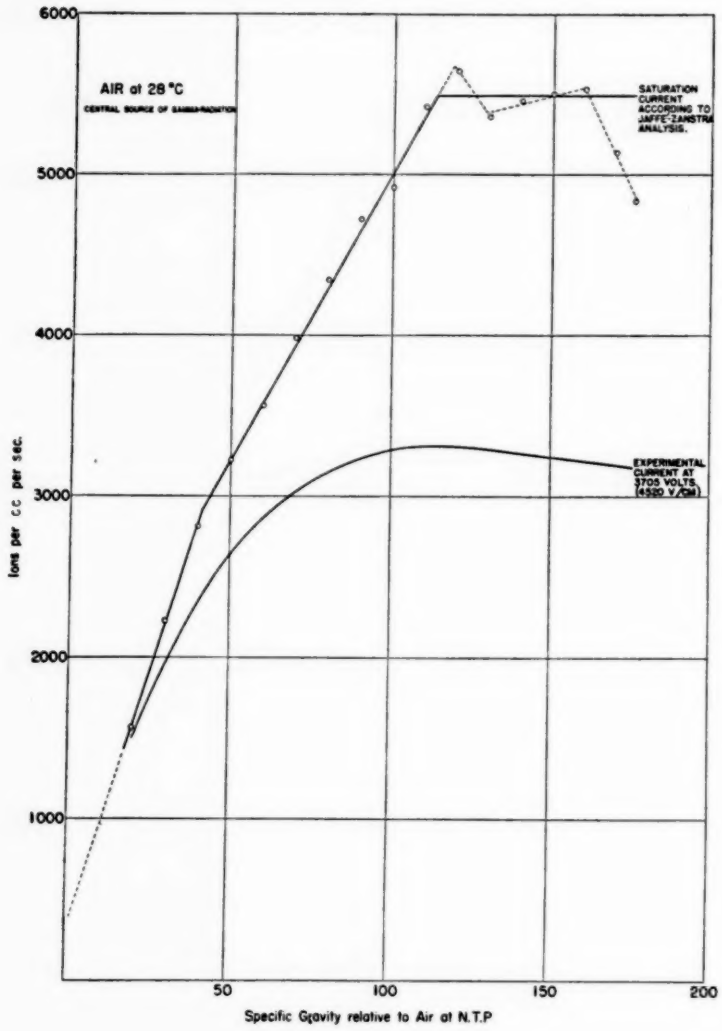

FIG. 3. "Saturation" current curve corresponding to our observations with central source, together with experimental curve obtained with strongest collecting field.

radiation. σ, the specific gravity of the air relative to air at 0°C and standard atmospheric pressure, was substituted for p in the expression for x. E was obtained by dividing the voltage across the chamber by 0.82 cm, as was done in obtaining the gradients of Figs. 7 and 8 of the preceding paper. Values of i for a particular density of air were read from the family of curves of Fig. 3 of the preceding paper, the smoothed-out curves being regarded as more reliable than individual observations. Such series of values were determined at pressures corresponding to intervals of 10 in the specific gravity, and a Zanstra curve constructed for each set. Only values corresponding to the five highest gradients we employed, within the range suggested by Clay, are included in the diagram.

The curves of Fig. 2 correspond precisely to those of Fig. 1, but are obtained from the ring-source curves of Fig. 5 of the preceding paper.

It will be observed that all the curves of Figs. 1 and 2 are somewhat concave toward the $f(x)$ axis, in the sense noted by Bowen and Cox[25] but in many cases the curvature is very slight. The curvature was found much more pronounced in the same sense in the region of low field intensities, not shown. Since the curves were not straight, extrapolations were attempted by producing tangents to the curves at their high gradient termini where the ideal should have been most nearly approached.

Reciprocals of the intercepts on the $1/i$ axis of the extrapolations of the curves in Figs. 1 and 2 are plotted as "saturation" currents in

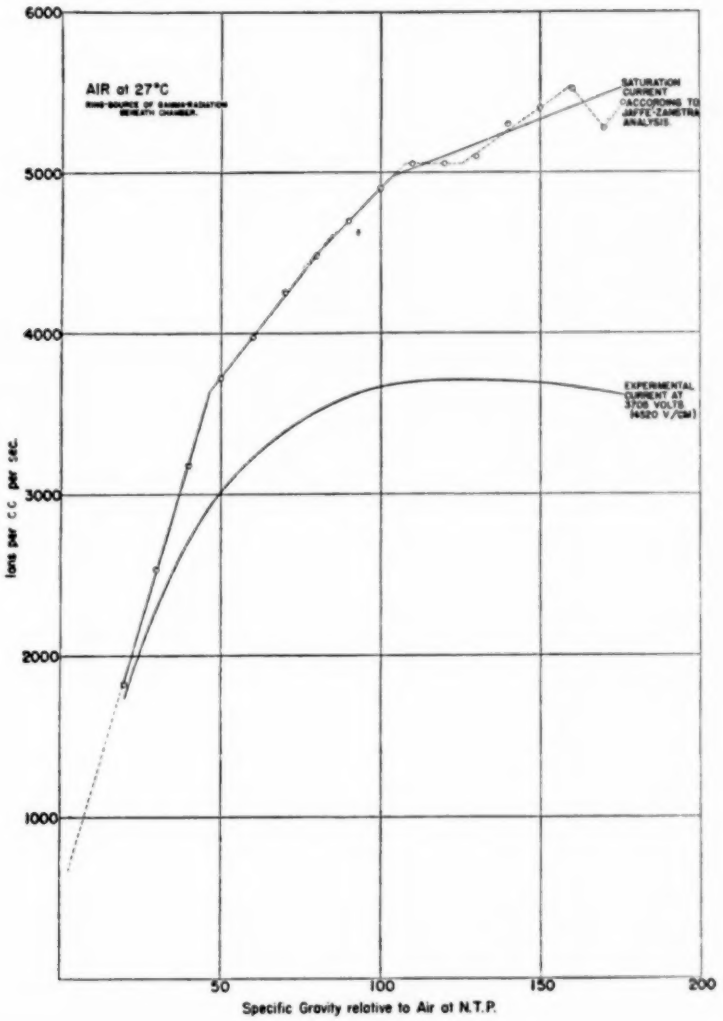

FIG. 4. "Saturation" current curve corresponding to our observations with ring-source, together with experimental curve obtained with strongest collecting field.

Figs. 3 and 4, respectively, against the specific gravity of the air. As the theory predicts, the "saturation" curves in each case lie above the experimental curves obtained with the highest field intensity employed, throughout the pressure range. As Clay and his associates found, the "saturation" current curves are made up of straight line segments, at least at the lower pressures. As in their curves, extrapolations of the low pressure segments to zero density cut the current axes above the origins. The first breaks in the curves occur at about $\sigma = 41$ and $\sigma = 46$, or pressures of about 45 and 50 atmospheres at 28°C. They correspond to breaks in the curves of Clay and van Tijn at about 40 atmospheres, the slope being less steep above the break than below in each case. In this connection it may be noted that their electrode spacing was slightly less than ours.

The "saturation" currents show a new feature, however, in that a second break occurs at about $\sigma = 114$ or 126 atmospheres in Fig. 3, and at a somewhat lower pressure in Fig. 4. A very slight break is indicated at $\sigma = 80$ or 87 atmospheres, also, in the second case. Whereas in Fig. 4, corresponding to the ring source, the "saturation" current continues to increase with pressure at a further decreased rate above the high pressure break, the central-source curve of Fig. 3 indicates the attainment of a maximum "saturation" current or even a possible decrease, although it should be remembered that the extent of extrapolation (with accompanying decrease of accuracy) increases rapidly with

pressure. In this connection Zanstra's[22] calculations from Erikson's data, represented in Fig. 5, are interesting in that they also show a high-pressure break in the "saturation" current curve, which may be significant in spite of the wide limits of error indicated. However, Clay and van Tijn[27] attained pressures of 147 atmospheres without the appearance of the additional break.

If Clay's explanation of the breaks in terms of the absorption of "wall" radiations is to be applied, it would seem to be necessary to invoke a dual type of "wall" radiation to explain our new breaks in the neighborhood of 130 atmospheres. The possibly horizontal portion of the "saturation" curve of Fig. 3 may call to mind attempts by Broxon to explain the pressure effect entirely in terms of "wall" radiation.

Relative to the similarities of the experimental and theoretical curves corresponding to the two sources of radiation, the diversity of directions of excited beta-rays relative to exciting gamma-rays should be borne in mind, together with the fact brought out by Jaffé that except in case of very accurate collimation in the direction of the collecting field, there is little dependence of experimental current upon angle between columns and field, even in the case of alpha-rays.

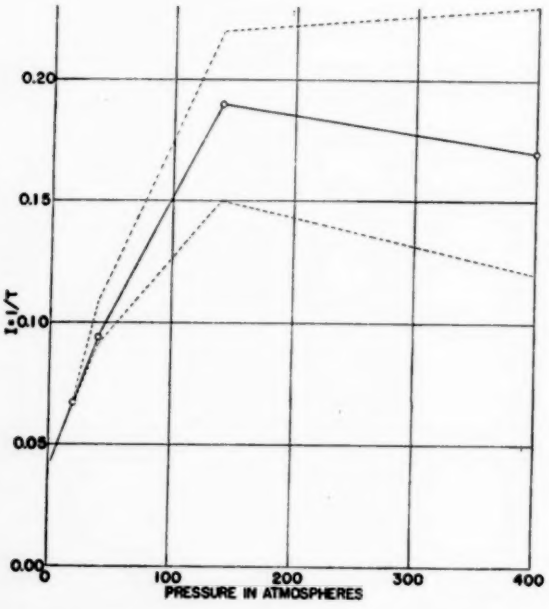

FIG. 5. "Saturation" current curve corresponding to Erikson's measurements, as calculated by Zanstra. Dotted lines represent limits of error estimated by Zanstra.

In Fig. 6 are given the Zanstra curves for the currents obtained upon collection of negative and positive ions, respectively, at the three pressures at which both currents are shown in Fig. 6 of the preceding paper. Intercept values for ions of the two signs at a particular pressure do not appear to be identical as in the case of Clay and van Tijn.[24]

We have also measured ionization currents produced in air at 100 atmospheres by a larger supply of radium located about 65 cm beneath the ionization chamber. The negative-ion currents measured at the five highest gradients were almost exactly 9.7 times as great as the corresponding currents obtained with the central source, throughout this range of gradients. Again negative-ion currents were larger than the positives. The Zanstra curves for both negatives and positives (not shown) had the small curvature toward the $f(x)$ axis, but in this instance the intercept values for the extrapolated curves might well be considered identical.

By way of criticism of the theory applied herein and of other theories, it should be emphasized that assumptions relative to the ionic "coefficients" at high pressures have been necessary in a region where little and in some instances no experimental work has been done. Moreover, because of the complexity of the problem, over-simplification is likely. It is interesting that in order to obtain an approximate solution to his differential equation, Jaffé[12] made the simplifying assumption that the radial distribution of ions in a column is determined entirely by diffusion and not at all by recombination, the latter supposedly affecting only the gross ion content of the widening column. As Jaffé points out, this amounts to assuming that the rate of recombination is not proportional to the square of the ion density at a point in the column, or to assuming that the "coefficient of recombination" is variable, being least at the axis where the ion density is greatest, and increasing exponentially with the square of the radial distance. Thus at a distance a little less than the mean distance of the ions from the axis the "coefficient of recombination" is presumed to be twice as great as at the axis, and at a distance twice as great as the mean radial distance

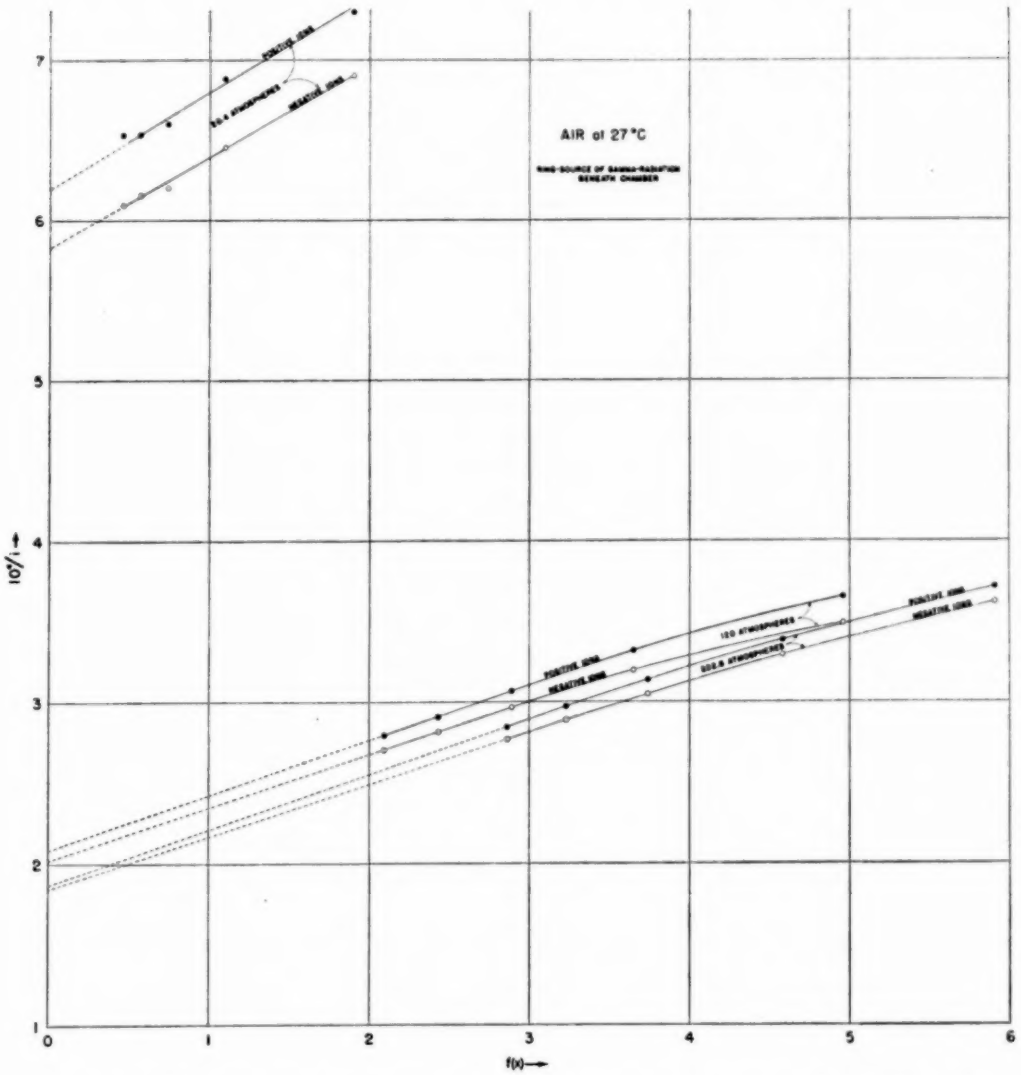

FIG. 6. Jaffé-Zanstra function curves corresponding to our measurements of "negative" and "positive" ion currents at three pressures.

of the ions, the "coefficient of recombination" is about 23 times as great as at the axis. This is inherent in all theories which begin with Jaffé's final equation.

It appears practically universally to be assumed that for a given intensity of a penetrating radiation passing through a specified volume of gas, the rate of production of ions and hence the theoretical "saturation" current which may or may not be capable of measurement, must be directly proportional to the amount of the gas present in that volume. It may possibly be worth mentioning again[2] that if it is conceivable that radiation energy may eventually, through the agency of subsidiary radiations or otherwise, be dissipated in any manner other than by the production of ions, then this universal assumption may not be justified.

Range and Specific Ionization of Alpha-Particles

M. G. Holloway and M. Stanley Livingston
Cornell University, Ithaca, New York

(Received April 6, 1938)

A study of the specific ionization of polonium alpha-particles near the end of their range with a shallow ionization chamber and linear pulse amplifier has resulted in an accurate determination of the single particle specific ionization curve and the range energy relation in this region. The method used is to compare the average single particle ionization in chambers of different depths and from the differences to obtain the ionization of particles of residual range less than the depth of the chambers. The single particle specific ionization curve differs from earlier determinations and shows the necessity of a correction to the accepted values of absolute mean range of all alpha-particle groups. The value suggested for the mean range of Th C′ (at 15°C and 760 mm) is 8.570±0.007 cm; for Po it is 3.842±0.006 cm. It is shown that extrapolated ranges obtained from ionization measurements differ from those obtained from number distance curves; an empirical relation is suggested to convert such values to mean range. A corrected range energy relation for alpha-particles extending down to zero range is obtained by combining the results of the present investigations with earlier determinations.

Introduction

ONE of the most essential relations for the analysis of nuclear disintegration data is that between alpha-particle range and energy. In the region in which alpha-particle groups from natural radioactive sources are available (between 5.3 and 10.5 Mev) precision measurements of the energies have been made with a magnetic deflection technique.[1, 2] The extrapolated ranges from ionization measurements near the end of the range have been accurately observed for a few natural alpha-groups,[3, 4] while the relative values of mean range have been obtained for most of them.[5] Lewis and Wynn-Williams[5] correlated these measurements and established an absolute mean range scale (Th C′ alphas = 8.533 cm at 15°C and 760 mm). In the region below 5.3 Mev (Po = 3.8 cm) several attempts have been made to measure reduced ranges and energies by slowing down the particles in absorbers.[6, 7] These have resulted in extending the relation down to about 3 Mev with reasonable accuracy. A few points on the curve at still lower energies can be computed from atomic mass values and disintegration data, with somewhat less accuracy. The ranges and energies of extremely low energy alphas have been obtained from studies of alpha-particle recoils in He gas.[8] An analysis of the existing experimental evidence, supplemented by a theoretical calculation (valid for the higher energies) for which the constants were determined in the well-known region of natural alphas, has been made by Bethe,[9] and has resulted in a range energy relation which seems to be in reasonable agreement with most disintegration results. The accuracy claimed for this relation below 0.5 Mev is 10 percent, between 0.5 and 2.0 Mev 50 kv (~5 percent), and between 2 and 5 Mev 30 kv (~1 percent).

In the analysis of those nuclear disintegrations from which very short range alpha-particles are observed,[10] the poor accuracy of the range energy relation has been a serious handicap. It has affected the accuracy of the values obtained for neutron energies when measured through the ranges of recoil He atoms. Studies of the energy distribution of neutrons emitted from excited heavy nuclei, which are expected to be of the order of 1 or 2 Mev, also will require a more exact knowledge of the low range region.

This paper reports a method for the accurate determination of the specific ionization of a single alpha-particle and the range energy relation for alpha-particles in the low energy region, extending down to essentially zero range. The results require a new analysis of the Cavendish

[1] Rutherford, Wynn-Williams, Lewis and Bowden, Proc. Roy. Soc. **139**, 617 (1933).
[2] Briggs, Proc. Roy. Soc. **157**, 183 (1936).
[3] Henderson, Phil. Mag. **42**, 538 (1921).
[4] I. Curie, Ann. de physique **3**, 299 (1925).
[5] Lewis and Wynn-Williams, Proc. Roy. Soc. **136**, 349 (1932).
[6] Mano, Ann. de physique **1**, 407 (1934).
[7] Briggs, Proc. Roy. Soc. **114**, 341 (1927).
[8] Blackett and Lees, Proc. Roy. Soc. **134**, 658 (1932).
[9] Livingston and Bethe, Rev. Mod. Phys. **9**, 261 (1937).
[10] Livingston and Hoffman, Phys. Rev. **53**, 227 (1938).

results and give a more exact determination of the absolute range. The work was started with the intention of establishing the position of the mean range of an alpha-particle group with relation to the physical face of a shallow ionization chamber. It was found that this position was a decided function of the electrical characteristics of the amplifier and counter circuits. In order to specify the range as measured by the shallow ionization chamber technique to a better accuracy than the depth of the chamber (usually about 2 mm), it is necessary to know the effective "electrical face" or "electrical center" of the chamber, the relative size of the noise level of the amplifier to alpha-particle pulse heights, the amplitude response characteristic of the amplifier, the grid bias on the recording thyratron, the penetration of the particle into the chamber to produce a count at this bias, etc. In the discussion to follow these various factors are analyzed and methods suggested for determining their effects on the observed values of range.

Discussion

In order to discuss the features pertaining to range measurements it is necessary to define the terms to be used. A very helpful analysis has been given by King and Rayton.[11] Since the loss of energy of alpha-particles through the processes of ionization and excitation occurs in discrete amounts, the energy loss will show statistical fluctuations and the particle ranges will be distributed about a *mean* or most probable value. This distribution may be closely approximated by a Gaussian function:

$$f(x)dx=(1/(\pi^{\frac{1}{2}}\alpha))e^{-(R_0-x)^2/\alpha^2}dx;$$

where $f(x)dx$ is the fraction (of the total number of particles) having a range ending between x and $x+dx$, R_0 is the mean range, α/R_0 is the dimensionless range straggling coefficient, usually indicated by the symbol ρ, and α, the *range straggling parameter*, is the half-width of the distribution curve at $1/e$ of the maximum. Such a distribution is illustrated in Fig. 1 (A), where α has the value 0.062 cm (for Po). Integration of $f(x)dx$ results in a *number distance* curve, similar to those obtained experimentally, in which the mean range is the distance at half-maximum (the point of inflection of the curve). It follows from this that the mean range of a collimated group of alpha-particles is that for which half the particles have a greater, and half a smaller range. The intercept of the essentially straight line portion of the number distance curve is an *extrapolated number distance range* of the particle group, and is the most readily determined feature of experimental number distance curves. It can readily be shown that the difference between these mean and extrapolated ranges, s, is a linear function of the straggling parameter: $s=\frac{1}{2}\pi^{\frac{1}{2}}\alpha$. Such a curve is also indicated in Fig. 1 (B), extrapolating to a value $s=\frac{1}{2}\pi^{\frac{1}{2}}(0.062)=0.055$ cm.

As an alpha-particle moves through a gas it loses energy by ionization and excitation of the gas atoms. The ionization produced per cm length of path (by a single alpha or by a group of alphas) is called the specific ionization (of the single alpha or group of alphas). We will call the specific ionization as measured in a chamber of finite depth (1 to 2 mm) the *specific ionization*, and the value which this approaches as the chamber is made infinitely thin the *differential specific ionization*. The specific ionization is a function of the distance from the end of the

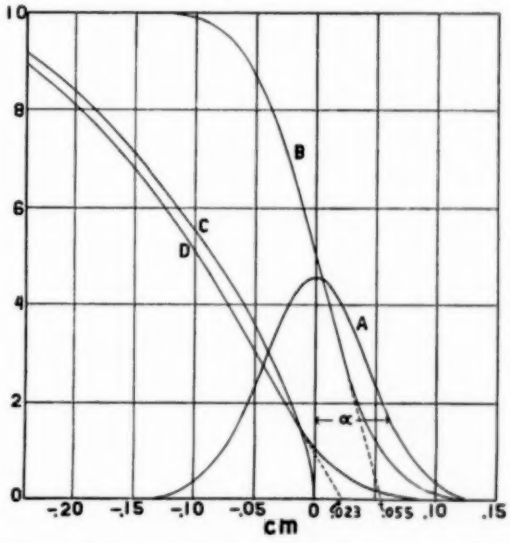

Fig. 1. Characteristics of range curves for polonium alphas. *A*, Range straggling distribution about the mean range; *B*, number distance curve showing extrapolated range; *C*, differential specific ionization of a single alpha-particle of mean range; *D*, average ionization (Bragg) curve for a group of alpha-particles with the range distribution of curve *A*, showing the ionization extrapolated range.

[11] King and Rayton, Phys. Rev. **51**, 826 (1937).

range. The curve of specific ionization against distance from the end of the range for a collimated group of alphas is called a *Bragg curve*. This curve rises asymptotically from zero at the end of the range to a maximum at about 5 or 6 mm from the end, and then decreases slowly to 0.5 of the maximum for particles of about 2.5 cm residual range. The specific ionization curve for a *single* alpha was first obtained experimentally by a study of the photographic density of alpha-particle tracks in a cloud chamber.[12] The chief result of the present investigation is to obtain this curve with accuracy up to the extreme end of the range. As the Bragg curve is the specific ionization of a group of alphas, it is then the resultant of the ionization curve of the single alpha and the straggling distribution of particles in the group. It shows a pronounced tail due to straggling. An extrapolation of the essentially linear front of this curve to zero ionization (first suggested by Marsden and Perkins[13]) results in an *extrapolated ionization range* which is not the same as the extrapolated number distance range obtained from the number distance curve. The ranges measured and reported by Henderson,[3] Curie[4] and others are extrapolated ionization ranges obtained from Bragg curves.

In order to illustrate these features we have plotted in Fig. 1 (C) the single particle differential specific ionization curve obtained from these experiments. The method of taking the data, which will be described in detail later, eliminates the effects of straggling, and so the end of this curve is exactly the mean range. We have also computed the expected shape of the Bragg curve from this single particle curve and the range straggling indicated in the distribution curve ($\alpha=0.062$ cm). This is plotted in Fig. 1 (D), and has an extrapolated intercept 0.023 cm greater than the mean range, but 0.032 cm less than the range extrapolated from the number distance curve. In a latter section of this paper we amplify this analysis to show how the absolute mean range may be determined from the observed Bragg curves of certain standard alpha-particle groups.

The present practice in nuclear physics is to observe the number distance curve and obtain the extrapolated number distance range therefrom. This method has two advantages; that it leads directly to the mean range through subtraction of the quantity $s=\frac{1}{2}\pi^{\frac{1}{2}}\alpha$, and for which α can be determined from the observed straggling of the front of the number distance curve; and that it represents a range value independent of the shape of the Bragg curve. The mean range may be determined from the extrapolated ionization range only through an empirical relation such as that deduced by Lewis and Wynn-Williams:[5] $x=0.8\alpha-0.06$ mm, in which x is the difference between mean range and extrapolated ionization range. It is our impression that the distinction between these two extrapolated ranges is not generally recognized. With the new evidence which we present we find the difference between mean and extrapolated range in the two cases to differ by more than a factor 2.

In the measurement of alpha-particle ranges three essentially different techniques have been used; photographic observation of particle track lengths in a cloud chamber, measurements with sensitive charge measuring devices of the ionization produced in a short length of path, and counting techniques usually involving shallow ionization chambers and pulse amplifiers.

Histographic plots of the lengths of tracks observed in a cloud chamber show a most probable value which is interpreted as the mean range of the group. The absolute range measurements are handicapped by the difficulties of determining gas density at the instant of formation of the track, and the uncertainty of determining the exact end of the range in the region where the specific ionization is rapidly decreasing. The range distribution, however, leads directly to a good estimate of straggling, if errors of measurement are considered.[4, 14]

Ionization measurements, such as those of Henderson,[3] Curie,[4] and Naidu,[15] have resulted in the most consistent data, and from the curves obtained the extrapolated intercepts can be determined with precision. The conversion of such values to mean range requires a knowledge of the specific ionization curve of the single alpha, and of the straggling, including the effects

[12] Feather and Nimmo, Proc. Camb. Phil. Soc. **24**, 139 (1938).
[13] Marsden and Perkins, Phil. Mag. **27**, 690 (1914).
[14] Rayton and Wilkins, Phys. Rev. **51**, 818 (1937).
[15] Naidu, Ann. de physique **1**, 72 (1934).

of the depth of chamber. If properly analyzed, however, it offers possibilities of giving the most exact determinations of range since measurements come from large numbers of alpha-particles, and may be carried out under reduced pressures so that the errors in distance measurements are negligible and the effective chamber depth small.

The shallow ionization chamber technique may be used either to count the number of particles arriving at a certain point (the number distance curve), or, by measuring the size of the pulses, to determine the energy loss by ionization in the chamber. In the first method, the total number of pulses is counted, regardless of size. The most readable quantity from such experimental data is the extrapolated number distance range. Determination of the exact mean range of the particles is handicapped, however, by the finite resolution of the chamber due to its depth. Each experimental apparatus has its own noise level, or background, and only those pulses are counted which are larger than a certain minimum determined by the noise level. This result is usually obtained experimentally by applying the output pulses to a thyratron (grid-controlled gaseous discharge tube) on which the grid bias is adjusted so that the tube flashes and records counts only for pulses greater than a set value. This means that very small pulses, such as those due to particles just entering the chamber, are not counted, and so a minimum depth of penetration corresponding to this value must be added to the distance to the face of the chamber. In order to determine this penetration it is necessary to know the variation of ionization with distance from the end of the range.

This variation can be determined if measurements are taken of the size of pulses obtained from a chamber of given depth, in which case the pulse heights are proportional to the ionization produced in the chamber. This can be obtained by determining the thyratron bias just sufficient to count such pulses or by measuring the height of oscillographic records of the pulses. A spread in pulse heights will be observed due to the range straggling; the average pulse height will be proportional to the ionization of the average alpha-particle in the range straggling distribution. Such measurements give at the same time an alternative direct determination of the end of the range of the average alpha.

In both of these applications of the shallow chamber and counter the resolution can be improved by decreasing the depth of the chamber either physically or by reducing the pressure. With number distance data this results in a smaller correction for penetration and a more accurate result; in number bias curves it makes the error due to the curvature of the specific ionization relation smaller. A most valuable modification of the counter method came from the development of the differential ionization chamber[16] in which the ionization from two adjacent shallow chambers with opposite applied potentials is collected upon a common grid. For particles crossing both chambers the ionization essentially cancels, giving no pulse; only those particles are recorded which stop within the chamber. The resolution of the instrument was further improved by recording only those pulses within set limits of magnitude, effectually measuring particles stopping in a shallow region near the common grid. A peaked curve is obtained broadened by range straggling; the position of this peak represents the point of maximum rate of change of ionization along the path of the alpha-particle. This represents a characteristic range differing from the mean range only by a constant difference, and this difference depends upon the measuring apparatus and not upon the straggling of the alpha-group. The differential chamber technique was used by Lewis and Wynn-Williams[5] and others in the Cavendish Laboratory in their measurements of the relative mean ranges of the natural alpha-groups. All the methods described except that yielding mean pulse heights have the inherent disadvantage of including the range straggling in all observations.

Bohr[17] first suggested that the tail at the end of the Bragg curve was due to the statistical nature of the energy loss and calculated the expected straggling. For Po alphas the straggling parameter, α, computed from the Bohr expression is 0.042 cm; that obtained[14] from the wave mechanical treatment of Bethe[18] is 0.046

[16] Rutherford, Ward and Wynn-Williams, Proc. Roy. Soc. **129**, 211 (1930).
[17] Bohr, Phil. Mag. **30**, 581 (1915).
[18] Bethe, Ann. d. Physik **5**, 325 (1930).

cm. Since all experimental determinations have led to larger values, it has been suggested that such theoretical values are too low because the energy loss by excitation of the inner electrons is neglected.[19] The observed distribution in range nearly always includes other sources of straggling, due to such factors as thickness of the alpha-particle source, finite depth of the measuring chamber, noise or background fluctuations in the amplifiers or electrometers, statistical errors in measurement, etc. The value obtained for the range straggling parameter depends in most instances on the success in identifying and measuring the straggling due to these other factors. The α for Po has been variously reported as: 0.064,[4] 0.052,[14] 0.067[20] cm.

Briggs[21] has made direct measurements of the straggling in mica by magnetic analysis of the energy distribution of Ra C′ alphas after traversing different thicknesses of mica foils. His results, when reduced to air, showed a nearly linear relation between α^2 and distance in the first 4.5 cm where the results had a reasonable consistency. Rutherford, Ward and Lewis[22] extrapolated this relation to obtain an α for the longer range Th C′ alphas. Lewis and Wynn-Williams[5] used Briggs' results to obtain the straggling parameters for all natural alpha-particles. Their absolute values for α may be subject to question, and we will discuss the possible errors in a later section. There are good indications, however, that the variation of α with range is essentially correct and that the relative values are significant. We have chosen to use the Lewis and Wynn-Williams values where needed in this analysis, recognizing the possibility of errors in the absolute values. These values refer to the range straggling parameter only, and so do not necessarily apply to the straggling observed in a particular experiment. We will expect, therefore, that each experiment will have a straggling including types other than range straggling and so will usually be greater than the Cavendish value for the group.

[19] Reference 9, p. 283.
[20] Schulze, Zeits. f. Physik **94**, 104 (1935).
[21] Briggs, Proc. Roy. Soc. **114**, 313 (1927).
[22] Rutherford, Ward and Lewis, Proc. Roy. Soc. **131**, 684 (1931).

Experimental Arrangement and Calibrations

The alpha-particle source used in these investigations was a relatively weak source of polonium (0.5 mC) deposited on palladium from a 0.1N HCl solution saturated with hydrogen.[23] The source was about one year old but had not become appreciably thicker than its original condition. The number-range curves obtained show a straggling of only about 1.4 that of the best obtained in experimental measurements. The method of taking data was such as to record only mean ranges, and so eliminate the effects of straggling. In the supplementary experiments on measurements of the absolute mean range a fresh source was prepared and compared with the above to determine the necessary correction for the thickness of the source. This fresh source was prepared in the manner described by Rutherford by placing a drop of purified Po solution of 0.1N HNO_3 on nickel, and washing thoroughly before tarnish appeared. It was found to have a straggling only slightly greater than the accepted value for range straggling alone, but the intensity of the source was much weaker.

The ionization chamber was designed to allow the depth to be varied and determined to better than 0.05 mm, by mounting the back plate on a screw of 1 mm pitch. The front face was a closely woven nickel screen from a radio tube, rolled flat and mounted to form the high potential electrode. Microscope measurements showed the grid apertures to be rectangular, of 0.20 by 0.40 mm size; the flattened grid was 0.18 mm thick. The movable back plate was a brass disk $\frac{3}{4}$ inch in diameter and surrounded by a guard ring. It was insulated with amber rings and connected to the grid of the first amplifier tube with a 5-inch lead. The computed electrical capacity of the 1 mm chamber and shielded lead was 5.5 $\mu\mu f$. The source support was arranged to be moved between machined guides perpendicular to the chamber face by means of a 1 mm pitch steel screw equipped with a divided drum and index, and calibrated with a traveling microscope. The alpha-particles from the source

[23] Kanne, Phys. Rev. **52**, 380 (1937). The authors wish to thank Dr. Kanne for supplying the polonium source.

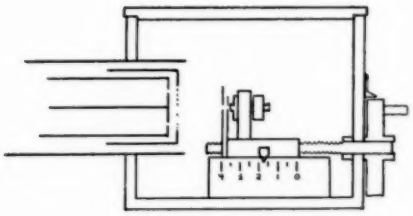

FIG. 2. Diagrammatic sketch of shallow ionization chamber and movable source holder with calibrated screw.

were collimated by two small holes having an average diameter of 0.0435 cm in thin brass sheets 0.365 cm apart immediately in front of the source. The physical distance between source and the inside surface of the grid forming the chamber face was obtained with a traveling microscope; it was found by trial that the distance could be determined to better than 0.005 mm. This was obtained at one setting of the scale and relative distances read off the drum and scale. A scale drawing of the physical arrangement is shown in Fig. 2.

All observations were made at room temperature and pressure and reduced to 15°C and 760 mm of Hg. The barometric pressure was read at intervals of ½ hour during a run and the pressure at the time of the individual readings interpolated from a time chart of the variations. The pressure readings were corrected for the temperature of the mercury column through standard conversion tables, to the 0°C at which the barometer was calibrated. A 1/10°C thermometer near the chamber was read at 5 min. intervals. The total temperature and pressure correction varied between 7.6 and 8.1 percent during one run, and between 5.8 and 6.2 percent during the others.

The pulse amplifier and the counting circuit require special attention, since upon their performance depends much of the accuracy of the results. The amplifier is the resistance capacity coupled type employed by Wynn-Williams,[24] Dunning[25] and others. The usual care was taken in design to eliminate interstage coupling by having for each stage two shielded compartments, one for the tube and the other for the decoupling resistors and condensers. The input stage used a 38 tube operating at low plate and screen potentials. The second, third and fourth stages were voltage amplifiers (6C6 tubes). In the last two stages a 56 tube was used to drive a 210 tube, which had 475 volts plate potential in order to maintain linearity for large plate swings. The output of the amplifier was controlled by means of a potentiometer before the fifth stage. The gain of the amplifier was such that with a 2 mm chamber placed at the peak of the Bragg curve output pulses of a mean height of 250 volts could be obtained. The six stages of amplification were used in order to reduce the gain required of each stage. This insured that each tube would operate on only the linear part of its characteristic. The entire amplifier and thyratron circuit was enclosed in a copper shielding case which allowed operation undisturbed by the cyclotron oscillator in the same room. Five separate power supplies furnished the d.c. potentials for the entire amplifier. The high potential for the ionization chamber came from one supply. The first amplifier stage, with plate and screen voltages of the order of 10 volts, had a separate supply with very good filtering. The second, third and fourth stages had a common supply, as did the fifth and sixth. The latter two, being power stages, required very good regulation of their plate potentials. Another supply was necessary for the thyratron circuit as the flashing of this tube would seriously affect any other tube using the same power supply. The 60-cycle 110-volt supply for the amplifier was a 12 kw synchronous motor generator set which after a half-hour's running gave a very constant voltage.

The thyratron used for measuring output pulse heights was an RCA 885, chosen from several for its reproducibility. Operating at 130 volts plate potential it had a "flash-point" of −14.5 volts grid potential, varying slightly with plate potential and the ambient temperature. The calibration runs to be described below show that the thyratron has a linear characteristic between pulse height and negative grid potential above the flash point. The grid bias supply and meter limited the range of operation to −100 volts, so the gain of the amplifier was adjusted to supply pulse heights of a maximum of 85

[24] Wynn-Williams and Ward, Proc. Roy. Soc. **131**, 391 (1931).
[25] Dunning, Rev. Sci. Inst. **5**, 387 (1934).

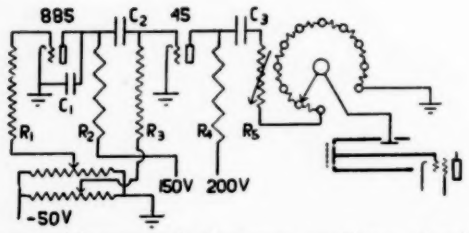

FIG. 3. Diagram of thyratron oscillator circuit for producing pulses of varying amplitudes and time constants; used to simulate alpha-particle pulses in calibrating the amplifier.

volts (when the chamber was set at the position of the peak of the Bragg curve).

In determining the amplitude response characteristic of the amplifier a circuit was used which gave uniform voltage pulses very similar in shape to those produced by an alpha-particle (Fig. 3). In this way the amplifier could be tested under conditions comparable to the counting of alpha-particles. It consisted of an 885 "thyratron oscillator" with condenser C_1 and grid potential adjusted to give a flash frequency of about 1000 per minute. The 45 tube was used to control the size of the pulses and to obtain a convenient inversion. The output was applied to a potential divider composed of ten 200 ohm metallized resistors and a variable resistor R_5. The taps of the voltage divider were connected to a small plate near the grid of the first stage amplifier tube, allowing potential pulses to be induced on the grid of known relative sizes and of a common shape. The time constant controls C_2, C_3 and R_4 were adjusted to make the pulse shapes indistinguishable from those due to alpha-particles, as determined by the use of a cathode-ray oscilloscope with a sweep frequency of 800/sec. The amplitude control R_5 was then set to give an output pulse from the amplifier of the order of 85 volts when the potential divider was set for the maximum. The uniform height pulses were superimposed upon the natural noise of the amplifier; a plot of counts against bias of the amplifier thyratron resulted in a curve similar to that obtained for alpha-particles except for the smaller straggling, which in this case is only that due to noise. The bias for half-maximum counting rate was determined for the various taps of the voltage divider by obtaining points just above and just below half-maximum. These mean bias values are plotted against the fraction of the maximum pulse height in Fig. 4. The plot is seen to be linear over the entire range and to extrapolate to the thyratron flash point of -14.5 volts for zero pulse height. The result makes it reasonably certain that the amplifier is linear in its amplitude response to voltage pulses over its working range. Since the size of a voltage pulse is proportional to the charge collected in the ionization chamber, it may be assumed that the mean pulse height will be proportional to the ionization produced in the chamber. Here and throughout this paper by *mean pulse height* we mean the difference between the mean thyratron bias and the flash point bias.

A noise background is always present in the amplifier, consisting of pulses, both positive and negative, with shapes determined by the time constant of the amplifier, and of such number that data cannot be taken at low bias voltages. Amplifier noise is due to the statistical fluctuations in electron current in the tubes and resistances of the first stage, and the ionization of residual gas in the tube. The use of low plate and screen voltages on the first tube (about 10 volts) reduces the gas noise. Microphonic response to acoustical noise or vibration may be minimized by mounting chamber and tubes on sponge rubber supports. It was found that the noise depended strongly upon the condition of charge or discharge of the filament battery; best results were obtained by discharging to about 0.9 of the capacity of the battery after full charge. The noise level sets a lower limit to the thyratron bias at which the counter is reliable. This was at -33 volts in the calibration run plotted in Fig. 4, or about 18 volts less than the -14.5 volt flash point. In the experiments to be described the noise amounted to about $\frac{1}{4}$ the maximum alpha-particle pulse height in the 1 mm chamber and $\frac{1}{6}$ that for the 2 mm chamber. In deeper chambers the noise is relatively smaller, although nearly the same in absolute magnitude. In general, there is nothing to be gained by distorting the response of the amplifier in order to suppress the noise, as the lower limit of observations exists whether the noise is visible in the oscilloscope or not, and produces a proportionate bias straggling.

Some confusion exists in the literature as to what is meant by the noise background of a pulse amplifier. The r.m.s. value, usually obtained from observations of the noise pattern on the oscilloscope screen, has no significance in counting experiments. The effective noise level is that below which reliable data cannot be taken because of the number of noise counts. This may be several times greater than the r.m.s. value. In describing the operation of a pulse amplifier the usual method is to give a signal to noise ratio, reported by several experimenters to be as large as 50/1. This is probably due either to the use of an r.m.s. value of noise, or to a nonlinearity in the amplifier response, discriminating against the small noise pulses. This last feature is valuable in simple counting experiments, and is readily obtained by adjusting the grid bias of any one of the amplifier tubes. The signal noise ratio has no meaning, however, unless the amplifier has been adjusted to be strictly linear and calibration runs made. An indication of the true signal noise ratio may be obtained from the straggling of number bias curves with alphas near the beginning of their range (for which the range straggling is small). The curves of Fig. 8 (to be described later) show a definite straggling, chiefly due to noise for chamber settings near the source; this straggling spread would have to be less than 1/50 of the average bias value to indicate a ratio of 50/1. No such sharp bias cut-off curves have been reported, and the indication is that such high signal-noise ratios are due to imperfect adjustment of the amplifier and nonlinear response characteristics. However, the signal to noise ratio of 6/1 obtained with the amplifier used in these experiments probably could be improved by a more careful selection of the tube for the first stage.

The instrumental straggling due to noise was determined from the slopes of the curves from which the half-maximum bias values plotted in Fig. 4 were obtained. An average slope was found to extrapolate from the half-maximum to zero in 4.6 volts of bias; this is the "s" for the straggling due to noise, in terms of volts of bias. With the uniform pulses there is no other source of straggling included, such as range or thick source effects. In the low bias region in which the data to be described later were taken it is found that the variation of bias voltage with distance is about 23 volts/mm, which corresponds to a noise straggling parameter α_2 of 0.023 cm. This figure will be used in the analysis of the observed straggling.

Observations and Analysis of the Method

When the collimated beam of alpha-particles was allowed to enter the chamber, and the counting rate observed as a function of distance from the source with a fixed thyratron bias, a number distance curve was obtained. This curve was similar to the analytic curve illustrated in Fig. 1, except for a slight unsymmetrical flattening near the top, due to the particles coming from the deeper layers of the source. It was found that number distance curves obtained with different bias settings led to curves which were displaced relative to each other. In Fig. 5 is shown a set of such curves obtained with a 1 mm chamber for bias settings varying from the minimum (just above the noise level of the amplifier) to a maximum (where a few counts are obtained for particles of maximum ionization). For the four lower bias values the curves have a common shape, showing parallel slopes and having the flat top characteristic of true number distance curves. Within this region the mean range and the extrapolated number distance

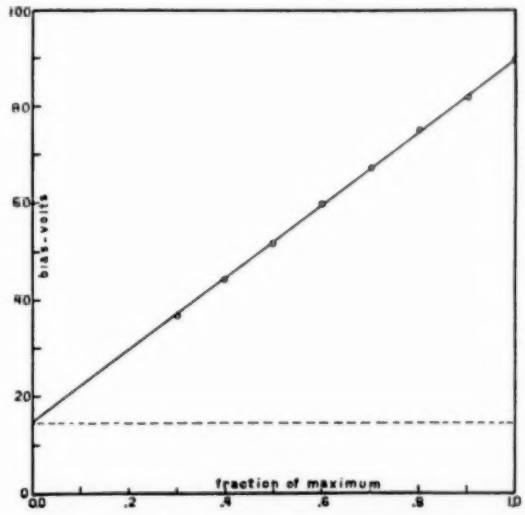

Fig. 4. Amplitude response characteristic of the pulse amplifier showing a linear response above the thyratron flash point.

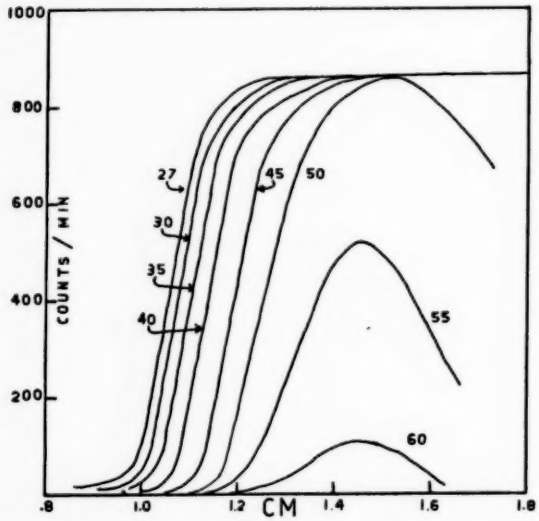

FIG. 5. Number distance curves obtained with the 1 mm depth chamber for a series of thyratron bias voltages, showing the manner in which observed ranges depend upon bias.

range could be obtained by determining the depth of penetration specified by the bias settings. The four higher bias curves all show maxima and changing slopes. The maximum is sharpest at about 55 volts and represents the position of the peak of the Bragg curve at the center of the chamber.[26] This is seen to be about 4 mm from the mean range (half-maximum) indicated by the lowest bias curve. In this region of changing slopes we are measuring the number of particles having a specific ionization greater than that specified by the bias setting.

The difficulty of analyzing such number distance curves is twofold. First, since the curves were taken only for bias values above the noise level, they do not give directly a measurement of the mean range or extrapolated number distance range, which are defined for zero pulse height (zero ionization). A plot of the extrapolated intercepts against pulse height does not result in a straight line and so cannot be extrapolated to zero pulse height with any precision; the same is true of the position of half-maximum representing the mean range. Furthermore, the ionization collected in the chamber does not start sharply at the grid face; there is an effective "electrical face" of the chamber at some distance in front of the grid face itself. Fields of 0.1 the value in the chamber may exist at distances of the order of the grid aperture on the outside of the grid.[27] So the electrical face of the chamber may be several tenths of a mm in front of the grid, and the chamber may have a correspondingly greater "electrical depth."[28]

A method has been devised to determine the position of the electrical face of the chamber, and at the same time to obtain the shape of the extrapolation to zero pulse height. This is accomplished by taking, for a series of biases, number distance curves for two depths of chamber, "1" mm and "2" mm, near the end of the range. The figures are in quotes to indicate that the true electrical depths as determined from the experiments will be different in each case. The physical conditions for the two cham-

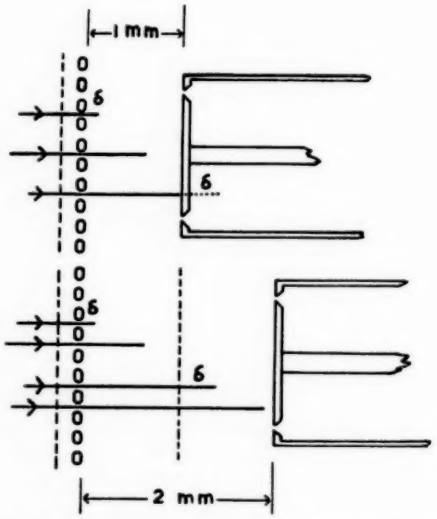

FIG. 6. Schematic diagram of chambers of 1 and 2 mm physical depth, with the external "electrical face" indicated by a dotted line. Particles with residual range δ at the electrical face produce equal ionizations in the two chambers; those with range δ at the back of the 1 mm chamber give different ionizations, the difference being the ionization of a particle of range δ.

[26] This high bias condition is valuable in separating groups of particles of different ranges; the distance between corresponding parts of the curves for different ranges at the same bias will be the difference in range. It can also be used to distinguish between particles of different specific ionizations, such as alpha-particles and protons. The counts for extremely high bias (60 volts) are probably due to a favorable superposition of noise fluctuations with the particle pulses.

[27] Brüche and Scherzer, *Geometrische Elektronenoptik* (Springer, 1934).

[28] The use of a grounded grid in front of the high potential grid might eliminate the extension of the electrical field. However, there is no advantage in this, since for any arrangement an experimental test must be made to determine the effective face.

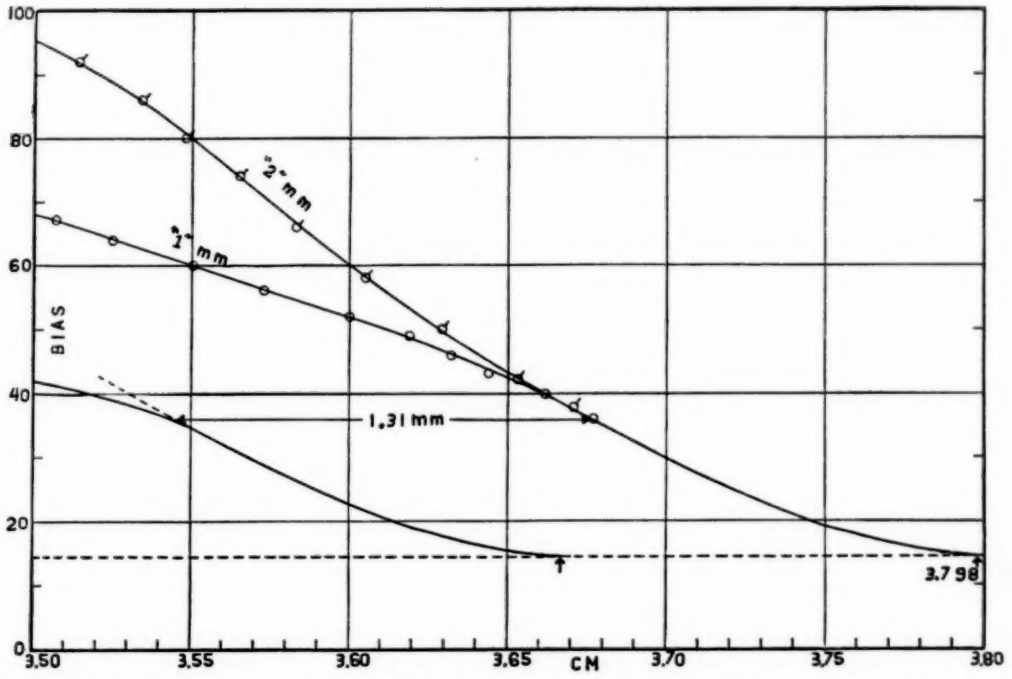

FIG. 7. Plot of observed distance for half-maximum counting rate as a function of bias voltage, for chambers with depths of 1 and 2 mm. The difference curve shown below, and also shifted to the right to join smoothly to the experimental curves, gives the ionization of particles of residual range less than 1 mm. The required shift of 1.31 mm represents the electrical depth of the 1 mm chamber.

bers are represented schematically in Fig. 6. Particles having residual ranges δ at the face of the chamber less than the depth of the "1" mm chamber will produce identical ionizations in the two chambers.[29] Particles having residual range δ at the *back* of the "1" mm chamber will produce different ionizations in the two chambers. This difference will be uniquely the ionization of particles of residual range δ, where δ is less than the 1 mm difference between the two chamber depths. It should be noted that for an alpha which does not completely cross the chamber (i.e., has residual range δ) it is not the specific ionization (averaged over the chamber depth) which is measured, but the

$$I_t(x) = \int_0^{\delta} I(x)dx,$$

where $I_t(x)$ is the total ionization from the end of range, and $I(x)$ is the differential specific ionization. The "2" mm chamber then gives us the total ionization of particles having a residual range up to about 2 mm.

For a number of different bias voltages and with the 1 mm chamber a series of observations were made of the positions for which the counting rate was half maximum. The maximum rate was measured with the chamber set at the peak of the Bragg curve (about 4500 counts/5 minutes). The distance to the source was increased until the counting rate was just above half-maximum (2250 to 3000 in 5 minutes) and then just below (1500 to 2250). The exact distance corresponding to half-maximum was then obtained by a linear interpolation. The bias voltages are plotted against the corresponding distances for half-maximum in Fig. 7. An entirely similar set of readings made with a physical depth of 2 mm and the same collecting field is also plotted in Fig. 7. These two curves are found to merge at their low bias ends, but to diverge for higher bias values. In order to analyze such data it is necessary that the

[29] Since it was possible that the change in electrical field due to doubling the depth of the chamber might result in a different collection time for the ions and so a different pulse height, observations were taken with full and half-voltage on each chamber. The results were identical, indicating that the collection time was very short compared to the time constant of the amplifier, and that there was no appreciable shift in the position of the electrical face.

two curves overlap, and the relative chamber depths to accomplish this result had been determined in previous preliminary observations.

Smooth curves are drawn through the experimental points and the differences between these curves plotted separately in Fig. 7. We have assumed a power relation between total ionization I_t and residual range R, *viz.* $I_t = R^n$, n being in general a function of R. Such a relation is found to hold with good accuracy over the last mm of the difference curve, with $n = 1.64$. Using this relation we find the end of the difference curve to be at 3.667 cm. If the effective depths of the two chambers had been exactly 1 and 2 mm, shifting of the difference curve by 1 mm should have made it coincide with the "2" mm curve. It is found, however, that the difference curve must be shifted 1.31 cm (at 15°, 760 mm) to make a smooth fit. This represents the electrical depth of the "1" mm chamber. All distance measurements were taken to the inside face of the grid, and corrected to 15°C, 760 mm. The 1 mm physical depth of the chamber has a reduced value of 0.92 mm, so the "electrical face" is at a position $1.31 - 0.92 = 0.39$ mm in *front* of the inner face of the grid to which measurements were made. The "2" mm chamber has then a depth of $0.92 + 1.31 = 2.33$ mm. The abscissae of Fig. 7 represent the distance to the electrical face of the chamber at 15°, 760 mm; the indicated end of range is at $3.667 + 0.131 = 3.798$ cm. From the magnitude of the experimental fluctuations of the data plotted in Fig. 7, and from the assumption made in extrapolating the difference curve, we estimate the probable error in the determination of the end of range to be ± 0.008 cm. *The end of the range is now defined by the extrapolation to zero total ionization of the total ionization distance curve of the single particle of mean range by use of the range exponent found to hold over the last mm of path.*

When counts are taken as a function of bias voltage with the chamber set at a fixed position, a number bias curve is obtained. Such a curve shows the distribution of pulse heights about a half-maximum or mean value. Half of the alpha-particles produce more ionization than this value, and half produce less. Therefore this mean bias value represents the specific ionization of the alpha-particle having a range equal to the mean range of the group. This follows from the fact that in a group of alphas half have their individual specific ionization curves shifted to one side of the specific ionization curve of the alpha of mean

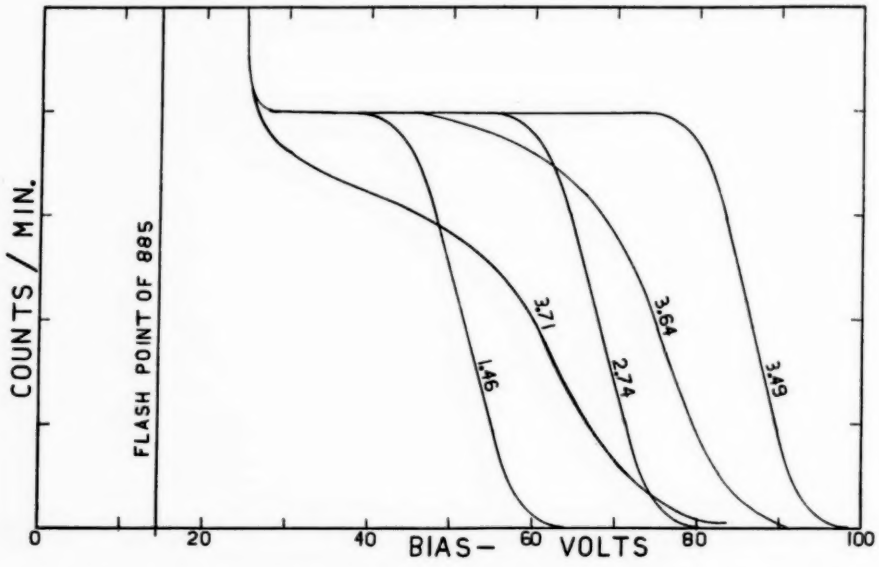

FIG. 8. Number bias curves obtained with the 1 mm depth chamber for settings at various distances from the source. The mean bias (for half-maximum counting rate) represents the specific ionization of the average alpha; the slopes of the curves are determined by the instrumental straggling, increased near the end of the range by range straggling.

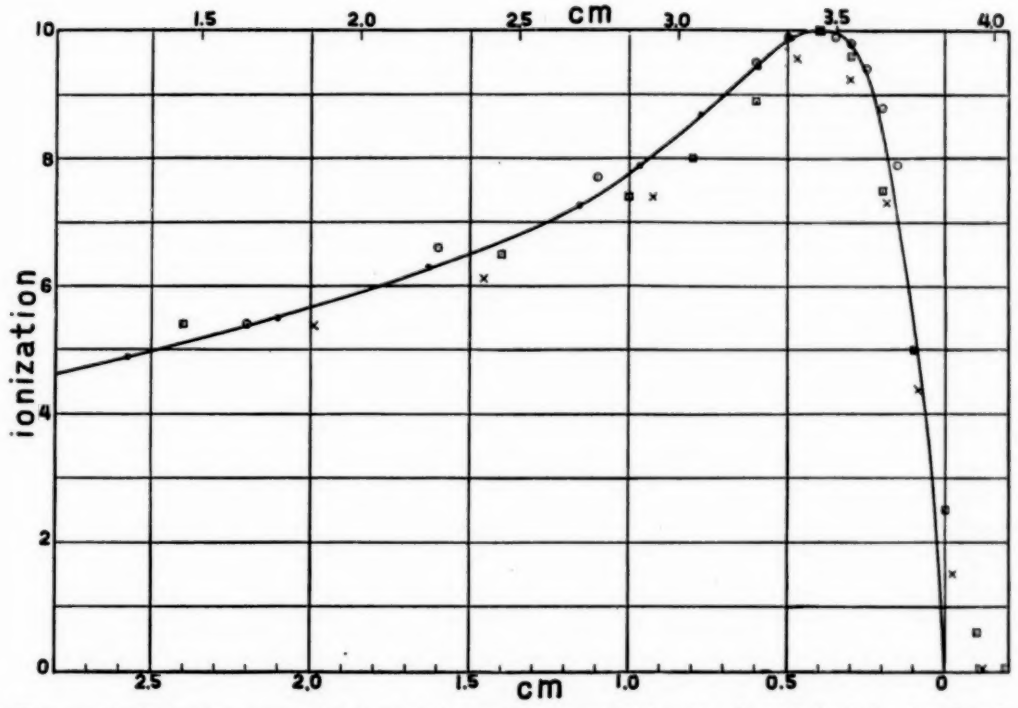

FIG. 9. The specific ionization curve of a single alpha-particle corrected for the effect of the finite chamber depth. The experimental points (small solid circles) are the values of mean bias plotted against the position of the electrical center of the chamber. The scattered points are taken from other reported single particle ionization curves: Feather and Nimmo (large circles), Stetter and Jentschke (squares), and Schulze (crosses).

range, and half to the other side. Due to the finite slope of the specific ionization curve those alphas with curves shifted to one side will produce greater (or less) ionization than those with curves shifted to the other side.

A family of number bias curves obtained for several settings of the chamber position is shown in Fig. 8. The figures on the curves represent the distance between source and chamber. In each curve a straggling of pulse heights about the mean value is observed, and a linear portion which can be extrapolated to the axis. Where the range straggling is small (close to source), the slopes are nearly uniform and can be used to determine the straggling in pulse heights due to the instrument alone. The slopes increase with increasing distance, due to the effects of the range straggling of the individual particles on their ionization in the region of rapidly decreasing specific ionization. The most significant feature of one of these curves is the half-maximum or mean bias. As the distance between source and chamber is increased this mean bias increases, reaching a maximum when the chamber is set at the peak of the Bragg curve. With further increase the mean bias drops rapidly. A plot of pulse heights obtained from such mean bias values, as a function of distance, is the specific ionization of the alpha-particle of mean range.

Using a "1" mm chamber the bias for half-maximum counting rate was determined at different points along the path. For each setting of position three bias values were used, one to determine the maximum counting rate (35 volts) and the others at biases giving counting rates just above and just below half-maximum. The mean bias value is obtained by linear interpolation between the latter two points. The corresponding mean pulse height is proportional to the ionization per 1.31 mm length of path when plotted against the distance to the "electrical center" of the chamber ($\frac{1}{2}(1.31)-0.39=0.27$ mm *behind* the physical face). It is desirable to have the differential specific ionization rather than that in any finite depth of chamber. This requires a correction for the variation of the specific ionization in the chamber depth, which can be determined from the curvature of the observed

curve.[30] The corrected curve is shown in Fig. 9; it shows $I(x)$, the differential specific ionization (relative to that at the peak), for a single alpha-particle as a function of distance from the end of the range. The small heavy circles are experimental points. For comparison with the results of other observers points are indicated taken from the reported single particle ionization curves of Feather and Nimmo,[12] Schulze,[20] and Stetter and Jentschke,[31] matched at the peak. The method described above is neither valid nor practicable within the last 1.31 mm of range, but points can be obtained in this region from the slope of the bias distance curve of Fig. 7. The curve in Fig. 7 represents $I_t(x)$, the total ionization up to 2.23 mm residual range. But since

$$I_t(x)=\int_0^x I(x)dx, \quad I(x)=dI_t(x)/dx.$$

In this manner $I(x)$ can be obtained for the last 2.23 mm of range.

A larger scale plot of the end of the curve beyond the peak is shown in Fig. 10. Here the dotted curve is drawn through the observed points (circles) with the 1.31 mm chamber. The solid curve is corrected to zero chamber depth (the differential specific ionization) and extended to zero residual range by means of the points obtained from the slope of the bias distance curve (crosses). The resulting curve fits the experimental points accurately and shows an essentially vertical intercept at the end of the range.[32]

A graphical integration of the areas under the curves of Figs. 9 and 10 was next performed to obtain a relation between range and total ionization. If we assume that the energy loss per ion pair remains constant throughout this region, the integration gives a relative range energy relation for alpha-particles having a range equal to the mean range of the group. This requires that the ratio between energy loss by ionization and by excitation remain constant. We consider this assumption to be the chief cause of uncertainty in the range energy relation. The curve obtained was adjusted to match the natural alpha relation in the region between 2.5 and 2.8 cm residual

[30] Let $f(x)$ be the ordinate representing the observed ionization in a chamber of depth l, whose center is at x. Then:

$$f(x)=E(x+\tfrac{1}{2}l)-E(x-\tfrac{1}{2}l), \quad (1)$$

where $E(x)$ is the energy of a particle of residual range x. By the expansion of the right-hand side of (1) in a Taylor's series about x:

$$f(x)=l\left(\frac{dE}{dx}+\frac{1}{6}\left(\frac{l}{2}\right)^2\frac{d^3E}{dx^3}+\cdots\right). \quad (2)$$

Similarly, if we expand $f(x+\frac{1}{2}l)+f(x-\frac{1}{2}l)$ about the point x:

$$f(x+\tfrac{1}{2}l)+f(x-\tfrac{1}{2}l)=2f(x)+l(\tfrac{1}{2}l)^2d^3E/dx^3+\cdots. \quad (3)$$

Since the ionization $I(x)=ldE/dx$, by combining (2) and (3) we obtain:

$$I(x)=(4/3)f(x)-(1/6)f(x+\tfrac{1}{2}l)-(1/6)f(x-\tfrac{1}{2}l),$$

where $I(x)$ is the differential specific ionization at x.

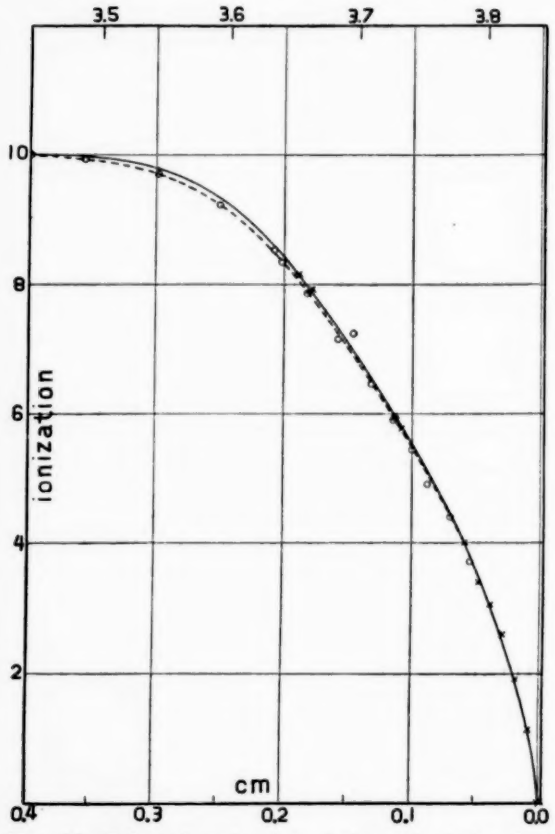

FIG. 10. Enlarged scale plot of the end of the single particle specific ionization curve, showing observed points from number bias data (circles) and from the slope of the range bias curve of Fig. 7 (crosses). The solid curve is the differential specific ionization, corrected for the effect of finite chamber depth.

[31] Stetter and Jentschke, Physik. Zeits. **36**, 441 (1935).

[32] The assumption of a constant range exponent used in obtaining the extreme end of range makes the shape of this extrapolation uncertain within the last 0.1 mm. The known phenomena of capture and loss of charge in this region would suggest that the true ionization curve has a slight extension at the foot. However, in order to provide a satisfactory standard on which to base range determinations we have used the assumption of constant range exponent resulting in the vertical intercept.

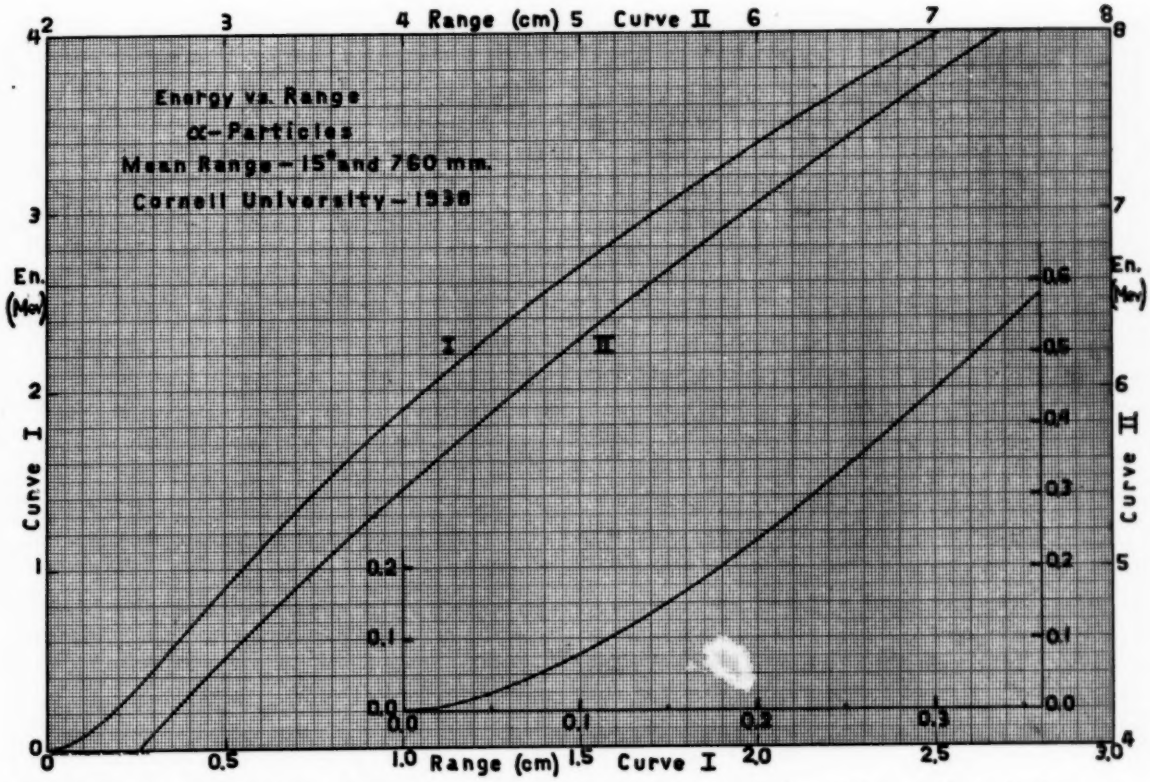

FIG. 11. Energy *vs.* range for alpha-particles. Obtained by graphical integration of the specific ionization curve of Fig. 9 and matched to the known relation in the region of natural alphas. Accuracy: 5 kv from 0 to 0.5 Mev, 1 percent from 0.5 to 2.0 Mev, 20 kv from 2.0 to 4.0 Mev, 0.5 to 0.3 percent from 4.0 to 5.0 Mev, and 0.2 percent in range and 0.1 percent in energy from 5.0 to 8.0 Mev.

range where it is known to a good accuracy. The result, in the customary Mev units is shown in Fig. 11 on a sufficiently large scale to be used directly. The method used was to plot the ranges and energies of the natural alphas, corrected as indicated in the discussion to follow and given in Table II, and to extend it to energies below 5 Mev by the use of Mano's[6] data on the energies of retarded alphas (also corrected to the new standard range). When matched in absolute value the experimental curve also matched the natural alpha-curve accurately in slope over a considerable region, a partial justification of the assumption above. For if there had been any appreciable variation in the energy loss per ion pair at low energies the computed range ionization curve would not have had the same slope as the range energy curve.

Straggling

In Fig. 5 the low bias number distance curves are observed to have a common slope which is a measure of the total straggling. The difference between mean range (half-maximum) and the extrapolated range, under standard temperature and pressure conditions, shows an average value, s, of 0.070 cm. Another estimate of this total straggling is obtained from the slopes of the straight lines used in interpolating the values of half-maximum count which are plotted in Fig. 7. From an average value of slope in the low bias region we obtain an s of 0.079 cm. The first method has a statistical error due to smaller numbers of counts on each point (1 minute); the second has an error due to the long extrapolation through the two points near the half-value. They are probably of equivalent accuracy and the variation in s obtained is an indication of the errors. We use an average of 0.074 cm as the best estimate of the distance s. This results in a total straggling parameter, $\alpha_t = 0.074/(\frac{1}{2}\pi^{\frac{1}{2}}) = 0.084$ cm.

The observed straggling is the resultant of many separate straggling effects. We will list and discuss these in turn:

(*a*) *Range straggling.*—The experimental value of the range straggling parameter which we have chosen to use is that given by Lewis and Wynn-Williams[5] for Po ($\alpha_1=0.062$ cm), obtained from Briggs'[21] measurements of range straggling in mica and reduced to air. In the discussion to follow the experimental Bragg curves of Curie and Naidu are found to be in good agreement with this value.

(*b*) *Noise straggling.*—Analysis of the slopes of the number-bias curves of the amplifier calibration run gave an "s" of 0.020 cm; from this $\alpha_2=0.023$ cm.

(*c*) *Ionization straggling.*—The chamber used in these measurements has an electrical depth at standard conditions of only 1.31 mm. The number of ionization collisions occurring in this length of path can be estimated to be less than 5000 for particles with 1 mm or less residual range, allowing a statistical variation of bias in the various readings. Furthermore the statistical variation of energy loss per collision about the mean value (32 volts/ion pair) results in additional straggling. An approximate calculation of these two effects leads to a range equivalent of this ionization straggling, α_3 of 0.011 cm.

(*d*) *Angular straggling.*—The geometry of the collimation slits leads to a correction due to the fact that the average alpha-particle observed makes a slight angle with the normal (see below). The variation in angle about this average angle within the collimation limits introduces a straggling which is nearly symmetrical about the mean angle. The total correction for the average angle was only 0.0043 cm, so the angular straggling, α_4, will be only a small fraction of this, and may be neglected.

(*e*) *Chamber depth straggling.*—The method of taking the data results in bias readings determined by the chamber depth and specific ionization; the smooth curves plotted through the points and the methods of subtracting bias curves have essentially reduced the depth of the chamber to zero. However, the electrical face of the chamber as determined is an average value, and it will vary for particles entering the chamber adjacent to a grid wire or in the center of a grid aperture. This depends on the shapes of the equipotential lines near the face of the grid, which are not known. An estimate of the straggling can be obtained from the difference between the outer surface of the grid wires and the average electrical face, which is about 0.021 cm. Assuming this to represent the over-all straggling ($2s$) we obtain a $\alpha_5=0.012$ cm.

(*f*) *Source straggling.*—The straggling effects discussed above are essentially symmetrical, and would result in a distribution centered about the mean range. As such, they can have no effect on the measured value of mean range. However, there is at least one other effect which is not symmetrical, the straggling due to depth of source. This will not only increase the total straggling observed, but it will result in a smaller value of mean range. The best estimate of the source straggling comes from the observed difference in range of particles from the relatively thick source used in the range and ionization measurements, and the freshly prepared source which had no appreciable thickness. The observed difference in range of these two sources under identical conditions was 0.042 cm (see below). This is directly the correction to be applied to the mean range value obtained and from it we can deduce a $\alpha_6=0.048$ cm.

If our analysis of the various straggling factors is correct we should be able to deduce the total straggling parameter from the individual effects. We find for the collimated group of polonium alphas $\alpha_t=(0.062^2+0.023^2+0.011^2+0.012^2+0.048^2)^{\frac{1}{2}}=0.083$, in agreement with the observed $\alpha_t=0.084$ cm.

Determination of the Absolute Mean Range of Po Alphas

The mean range of 3.798 cm determined above and illustrated in Fig. 7 must be corrected for certain known factors, such as the angle of collimation, the thickness of source and the composition of the air (absolute ranges are for dry air at 15°C and 760 mm of Hg pressure).

The largest error in absolute range was that due to the finite thickness of source, and indicated by the straggling. The correction was obtained directly by observing the difference between the source used above and a freshly prepared source having no appreciable thickness. The fresh source was first checked for straggling, and was found to give essentially that expected from range and instrumental straggling alone. With a common

bias voltage of 50 volts, corresponding to 0.418 of the peak of the specific ionization curve, measurements were made of the positions for half-maximum counting rates for the two sources. The absolute measurements of distance from source to chamber face were taken and reduced to standard conditions; the distance for the new source was found to be 0.042 cm greater than for the old source. This is exactly the correction to be added to the end of range observed; it is the "s" of the source straggling and gives a α_6 of 0.048 cm.

The imperfect collimation of the beam would result in an apparent range less than the true range for perfect collimation. The collimation used allowed a maximum deviation from the direction normal to the chamber face of 6.8 degrees. The average particle observed corresponds to an average angle, and hence to a distance slightly less than the true range along the normal. This average angle, θ, can be determined following the procedure outlined by Bethe.[33] The distribution of particles with angle may be approximated by a Gaussian function: $g(\theta) \simeq \epsilon^{-(\sin^2\theta/\beta^2)}$; where $\beta^2=(1.27a^2/b^2)=0.0045$ and where a is the average radius of the collimating holes and b the distance between them. By integration we find the average $\langle\theta^2\rangle_{Av}=\frac{1}{2}\beta^2$. The correction to the observed range, for a particle of 3.84 cm range is $3.84((1/\cos\theta)-1)$ $=3.84(\frac{1}{4}\beta^2)=0.0043$ cm. On adding these two corrections to the observed value of the end of range of 3.798 ± 0.008 cm, we obtain a value for the absolute mean range of Po alphas of 3.840 ± 0.010 cm. This probable error includes an arbitrary error of ±0.006 cm which, because of the uncertainty in the corrections, we have added to the purely experimental errors.

The relative humidity of the air was about 20 percent at 25°C during the experiments, indicating a water vapor content of 0.6 percent of the observed pressure. Taking the stopping power of water vapor to be $\frac{3}{4}$ relative to air we find a correction in range of -0.007 cm. The CO_2 content of the air in the closed room was estimated to be 0.5 percent greater than normal, resulting in a positive correction of about the same magnitude. Since the resultant correction could not be determined accurately and would be smaller than the experimental error, no correction was applied. The standardization of the gravitational constant to 45° latitude was estimated and found to be trivial.

[33] Reference 9, p. 279.

Comparison with Results of Other Experiments

The best determinations of the ionization extrapolated range for alpha-particle groups are by Henderson.[3] He obtains for Th C′ and Ra C′, respectively, the values: 8.616 ± 0.004, and 6.953 ± 0.004 cm in dry air at 15°C and 760 mm of Hg pressure. Harper and Salaman[34] check the Th C′ result, with a larger error. Curie and Behounek[35] and Harper and Salaman[34] are in sufficient agreement for Ra C′, but Naidu[15] reports a low value. For Po three observers are in excellent agreement; Curie[4] gives $3.870(\pm0.006)$, Naidu[15] 3.868 ± 0.006 and Harper and Salaman[34] 3.870 ± 0.008 cm. Since no other method of measurement has resulted in such precise determinations, ionization measurements should be used in establishing the absolute range scale. We have chosen to use Henderson's values of Th C′ and Ra C′ and the average of Curie's and Naidu's results for Po as standards of ionization extrapolated range.

The most complete survey of the relative mean ranges of natural alpha-particle groups has been made in the Cavendish Laboratory with the differential ionization chamber.[1, 5] The measurements were all relative to Th C′ as a standard, and this standard was established by comparisons with Henderson's results. Lewis and Wynn-Williams[5] used the only single particle ionization curve available at that time, obtained by Feather and Nimmo[12] from the photographic density of alpha-particle tracks in a cloud chamber, and the data of Briggs[21] on the straggling parameters for the various groups, to construct an average ionization (Bragg) curve. With several assumed values of α they computed average ionization curves, and from the extrapolated intercepts they obtained an empirical relation for the difference between such extrapolated values and the mean range: $x=0.8\alpha-0.006$ cm. They then used this relation to determine the absolute scale for their relative mean range determinations, namely, that for which Th C′

[34] Harper and Salaman, Proc. Roy. Soc. **127**, 175 (1930).
[35] Curie and Behounek, J. de phys. et rad. **7**, 125 (1926).

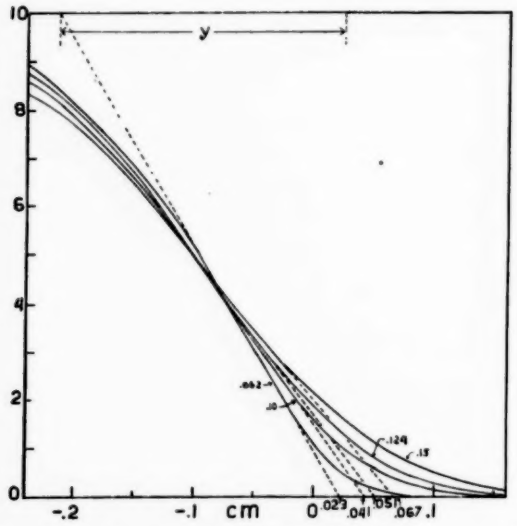

FIG. 12. Average ionization (Bragg) curves computed from the single particle ionization curve and the range distribution functions characterized by straggling parameters of 0.062, 0.100, 0.124 and 0.150 cm. The extrapolated intercepts are used to obtain an empirical relation between mean range and ionization extrapolated range. The slopes, expressed in terms of the intercept distance, y, provide a method of determining the straggling from experimental ionization curves.

alphas had a mean range of 8.533 cm. It is "the value such that the extrapolated ranges calculated from the mean ranges determined for Th C′, Ra C′ and (with less weight) Th C and Po, differ by a minimum amount from the most accurate absolute determinations of these extrapolated ranges." These minimum differences are +0.007, −0.008 and −0.021 cm for Th C′, Ra C′ and Po, greater than the stated errors in the measurements. This value for Th C′ has been accepted and used as a range standard. It should be pointed out that it is a derived value, based upon an incorrect specific ionization curve for a single alpha-particle.

The first single particle ionization curve reported was deduced by Curie[4] from an observed average ionization curve and a measured range straggling parameter for Po. Following the early work of Feather and Nimmo[12] others have attempted to measure the single particle curve, but their results were handicapped by instrumental straggling. Schulze[20] used a proportional amplifier and measured the average size of pulses due to the ionization produced in a short section of path; his results show a decided "tail" similar to the average ionization curve. Stetter and Jentschke[31] used two shallow chambers and linear pulse amplifiers and measured average heights of oscillographically recorded pulses. They obtain a steeper curve, in rough agreement with that obtained in these investigations.

With our more precise determination of the single particle ionization curve it is possible to make a better analysis of the Bragg curves. Using assumed Gaussian distributions with range straggling parameters of 0.062 (Po, illustrated in Fig. 1), 0.100, 0.124 and 0.150 cm we have computed the shapes of the average ionization curves.[36] They are illustrated in Fig. 12. From the indicated extrapolated intercepts we find that the empirical relation between x (the difference between mean and ionization extrapolated range) and α is essentially linear and can be expressed as: $x=0.47\alpha-0.006$ cm. Extreme lines drawn through the points suggest a probable error of 8 percent in the region of the natural alpha-particles, exclusive of the error in α. It is now possible to use this empirical relation in the manner of Lewis and Wynn-Williams to relate extrapolated ionization ranges and relative mean ranges. However, before doing this it is essential to consider that each experimental observation of extrapolated range includes possible straggling factors other than range straggling, and so may have an α differing from the range straggling parameter used by Lewis and Wynn-Williams.

The most definite quantity connected with the shape of a computed average ionization curve of Fig. 12 is the slope of the straight line used in the extrapolation. When the slopes are plotted against the corresponding values of α a relation is observed which is linear to a better accuracy than the empirical relation between x and α described above. If the slope is expressed in terms of the distance y between the upper and lower intercepts of this straight line (through the ordinates representing the peak of the curve and

[36] This was done following the procedure outlined by Lewis and Wynn-Williams in obtaining the average ionization, I: $I=\sum_{z=z}^{z=\infty} f(x)I(x-z)$, where $I(x-z)$ is the ionization produced by a single alpha-particle in a short interval at an average distance $x-z$ from the end of its track, and $f(x)$ is the distribution function characterized by the chosen value of α. The summation was performed with intervals of 0.02 cm, and the result normalized to fit the maximum to the peak of the Bragg curve.

zero ionization) we obtain a relation: $\alpha=0.917y-0.160$ cm$\pm$5 percent. A value for y may be obtained from any observed ionization curve, and this relation used to determine the α characteristic of the experiment.

Henderson's published curve for Th C′ has a value y of 0.304 cm, indicating an α of 0.119 cm, in good agreement with the Cavendish value of 0.120 cm. For his Ra C′ curve $y=0.292$ and $\alpha=0.108$, somewhat higher than the range straggling value 0.102 cm and indicating additional straggling in the experiment. For Po the curve by Curie shows $y=0.242$ and $\alpha=0.062$ while that of Naidu gives $y=0.246$ and $\alpha=0.066$ cm. The experimental values of α determined in this way are in general slightly higher than the Cavendish range straggling values, which is to be expected. The reasonably close checks indicate that the Cavendish tabulation of α is essentially correct and, furthermore, that our computed ionization curves are in satisfactory agreement with the experimentally observed curves in this essential feature of slope of the extrapolation line. When the experimental curves are compared point-by-point with the computed curves for the same α the agreement is not as satisfactory, the experimental curves in general falling below in the region of 0.7 to 0.9 of the peak, and also differing in the shape of the tail past the extrapolated limit. We assume that the slope of the front of the curve is less dependent upon variable experimental factors than the extreme regions.

We are now able to compute the mean ranges indicated by the ionization extrapolation measurements of the standards chosen. Using the relation $x=0.47\alpha-0.006$ cm, and values of α obtained above from the observed curves we obtain the values given in Table I. When the Lewis and Wynn-Williams values for relative mean ranges are increased by 0.037 cm we obtain for the standards 8.570, 6.907 and 3.842 cm, which differ by minimum amounts from the computed mean range values. These differences are now 0.004, -0.001 and -0.003 cm, less than the experimental errors in the ionization measurements and also less than the relative errors of Lewis and Wynn-Williams. In order to preserve the relative accuracy inherent in the differential ionization chamber data we have chosen to use as mean range standards the Lewis and Wynn-Williams values for Th C′, Ra C′ and Po, increased by 0.037 cm.

The validity of the various methods for determination of mean range is indicated in the case of Po. That computed from extrapolated ionization range (Bragg curves) is 3.845 cm; that obtained by correcting the Lewis and Wynn-Williams relative mean range is 3.842; the value obtained from the number distance bias method reported in this paper is 3.840 cm; and a direct cloud chamber study by Curie gives 3.85 cm. These four measurements, obtained by four different techniques, are in excellent agreement, well within the limits of error. A weighted average of these values gives a range of 3.843 $\pm$0.005 cm for Po. It is interesting to note that the cloud chamber determination of mean range checks the corrected mean ranges obtained from electrical measurements. Hence the apparent disagreement between ranges of nuclear disintegration particles observed in the cloud chamber and with ionization chamber and counter techniques was largely a result of the low range standards.

In Table II the corrected values for mean range, the probable error in the mean range, the straggling parameter, α, the ionization extrapolated range and the number distance extrapolated range are tabulated with the magnetically determined energies. The values in bold faced type in Table II are those chosen as standards, the starred values are those for which measurements were made relative to a standard. Unstarred values for the other types of range are derived. The computed extrapolated ranges are based upon the tabulated values of range straggling parameter, α. The set of values A are the corrected relative mean ranges of Lewis and Wynn-Williams;[5] the set B for the long range groups are from Rutherford, Wynn-Williams,

TABLE I. *Determination of mean range standards.*

	Ion. extr. range R_i:	Conv. factor ($x=.47\alpha-.006$) R_i-R_m:	Mean range std. (computed): R_m:	Rel. mean range std.: (L. & W. W. +0.037)
Th C′ (Hend.)	8.616±0.004	0.050±0.005	8.556±0.007	8.570
Ra C′ (Hend.)	6.953±0.004	0.045±0.004$_5$	6.908±0.006	6.907
Po				
(Curie)	3.870±(0.006)	0.023±0.002$_3$	3.847±0.007	
(Naidu)	3.868±0.006	0.025±0.002$_5$	3.843±0.007	
Po (Av.)			3.845±0.006	3.842

Lewis and Bowden;[1] the U values, C, are those reported by Rayton and Wilkins[14] relative to Po. The errors in mean ranges are obtained from the stated experimental errors plus the error involved in the conversion to mean range from ionization range. The values for α were taken directly from the tabulation by Lewis and Wynn-Williams[5] with the exception of the bracketed items which were extrapolated from the Cavendish relation of α and mean range.

The energies of the alphas in the various groups have been measured by the magnetic deflection method. The energy values in Table II are from tabulations by Lewis and Bowden,[37] Briggs,[2] and Rosenblum and Dupouy.[38] Lewis and Bowden base their energy scale upon a velocity of $(1.922_{00}\pm0.002)\times10^9$ cm/sec. for the alphas of the 9.907 cm group from Ra C′. Briggs, using improved apparatus and a better value of e/m for He, has redetermined this velocity and finds it to be $(1.92148\pm0.00009)\times10^9$ cm/sec. This latter velocity corresponds to an energy of $(7.6802\pm0.0006)\times10^9$ electron volts. On this basis Briggs has recomputed the energies of the alphas of several groups (Rn, Ra A, Ra C′, Tn, Th X, Th A, and Th C′) whose relative velocities he had measured. His energy values are the ones given in Table II for these groups. To get the energies of the alphas in the other groups the values of Lewis and Bowden and of Rosenblum and Dupouy are multiplied by the ratio, 7.6802/7.6830, between Briggs' new Ra C′ energy value and that of Lewis and Bowden. Of these latter groups the An and Ac C (short and long) were measured by Rosenblum,[38, 39] and the rest by the Cavendish group. The probable errors in the table are taken from the original papers.

TABLE II. *Ranges and energies of natural alpha-particles.*

		Mean range:	Acc:	Strag. par. α:	Extrap. ranges: Ioniz:	Extrap. ranges: N-dist:	Energy (Mev):	Energy Acc:
A:	An (short) (mean)	5.240*	±0.015	0.081	5.272	5.312		
	An (long)	5.692*	±0.015	0.087	5.727	5.769	6.8235	±0.014
	Ac A	6.457*	0.008	0.096	6.496	6.542		
	Ac C (short)	4.984*	0.015	0.078	5.015	5.053	6.272_7	0.012
	Ac C (long)	5.429*	0.015	0.083	5.462	5.503	6.618_6	0.013
	Ac C′	6.555*	0.015	0.097	6.595	6.641		
	Tn	5.001*	0.008	0.078	5.035	5.073	6.2818	0.0008
	Th A	5.638*	0.008	0.086	5.672	5.714	6.7744	0.0008
	Th C (mean)	4.730*	0.008	0.074	4.778	4.796	6.0537	0.0007
	Th C′	**8.570**	0.007	0.120	**8.616**	8.676	8.7759	0.0009
	Rn	4.051*	0.008	0.065	4.075	4.109	5.4860	0.0005
	Ra A	4.657*	0.008	0.073	4.685	4.722	5.9981	0.0005
	Ra C′	**6.907**	0.006	0.102	**6.953**	6.997	**7.6802**	0.0006
	Ra F (Po)	**3.842**	0.006	0.062	**3.870**	3.897	5.2984	0.0021
B:	Ra C′ (long)	7.792*	0.015	(0.112)	7.839	7.891	8.2769	0.0033
	Ra C′ (long)	9.04*	0.02	(0.125)	9.09	9.15	9.0655	0.0037
	Ra C′ (long)	11.51*	0.02	(0.15)	11.57	11.64	10.5052	0.0043
	Th C′ (long)	9.724*	0.008	(0.132)	9.780	9.841	9.4877	0.0038
	Th C′ (long)	11.580*	0.008	(0.15)	11.64_3	11.71_3	10.5379	0.0043
C:	U I	2.653*	0.007	(0.045)	2.669	2.693		
	U II	3.211*	0.007	(0.053)	3.230	3.258		

Bold face = standards.
* = Measured relative to a standard.

Geiger[40] has reported ionization measurements of some 20 alpha-particle groups, giving extrapolated ranges differing so widely from the Cavendish results that they are difficult to evaluate. For example, he reports extrapolated ranges for Th C′, Ra C′, and Po of 8.617±0.007, 6.971 ±0.004 and 3.925±0.004 cm, respectively, differing from the accepted values above by +0.001, +0.018 and +0.055 cm in the three cases. In the case of Ac A his value is 0.088 cm greater than that computed from the Cavendish results (Table II), yet he quotes an error of only ±0.010 cm. In attempting to find a reason for these discrepancies we have determined the straggling parameter from the slope of the extrapolation line of his published curve for Ra C′ through the method described above, and obtain a value of nearly 0.20 cm. This is essentially double the range straggling for Ra C′ and would result in a much larger extrapolated range than that obtained by Henderson. We must conclude that Geiger's high values are due to excessive straggling, seemingly differing widely from one group to another. The curves reported by Geiger contain groups and hence the straggling cannot be determined at all accurately. For this reason Geiger's curves are not subject to the analysis used above and so are not included in the tabulation.

The Range Energy Relation

The new values for mean range of the natural alphas require a small but significant correction

[37] Lewis and Bowden, Proc. Roy. Soc. **145**, 235 (1934).
[38] Rosenblum and Dupouy, J. de phys. et rad. **4**, 262 (1933).
[39] Curie and Rosenblum, Comptes rendus **196**, 1663 (1933).
[40] Geiger, Zeits. f. Physik **8**, 45 (1922).

to the range-energy relation, essentially increasing the range for all values of energy in this region by 0.037 cm. In Fig. 11 is plotted the complete corrected relation, based upon the natural alpha-particle ranges given in Table II. In this region the errors given for mean range and energy specify the accuracy of the curve, about 0.2 percent in range and 0.1 percent in energy. The extension through Mano's reduced range values in the region in which the experimental curve was matched (about 4 Mev) is of somewhat less accuracy, estimated to be about 0.5 percent at the point of matching. Errors in the single particle ionization curve are thought to be of the order of ± 1 volt in bias values; the range bias curve obtained by graphical integration will be somewhat more accurate due to the smoothing inherent in the graphical integration process. When matched at zero and at 4 Mev the maximum percentage error will be in the median region (about 2 Mev). We estimate ± 5 kv from zero to 0.5 Mev, 1 percent from 0.5 to 2 Mev, and 20 kv from 2 to 4 Mev. In addition to the experimental errors, a possible variation of the energy loss per ion pair may further increase the error in the low energy region.

The range energy relation described above[41] supercedes the Cornell relation of 1937.[9] The theoretically determined curve is in close agreement with the new experimental relation, however, agreeing to within its limits of error even in the low energy region. The theoretical relation for energies above 8 Mev must be corrected for the change in the alpha-particle standards. This requires the addition of 0.037 cm to the range values of the published curves.[9] In the extreme low energy region the experimental points of Blackett and Lees[8] match the curve with reasonable accuracy when corrected by 9 percent for the range energy relation used.[9] The unpublished data of Blewett and Blewett on the ranges and energies of retarded alphas are in reasonable agreement between 3.5 and 5 Mev when corrected to the revised Po range standard, but lie definitely above the curve at lower energies.

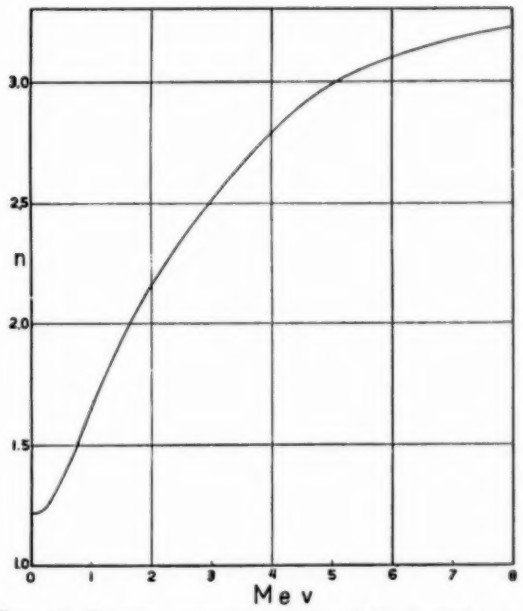

FIG. 13. Range exponent, n, for alpha-particles as a function of energy. n is defined in terms of the logarithmic derivative, $n = 2d \log R/d \log E$. Important for thick target and angular straggling corrections.

In computing the corrections to experimental range data due to thickness of target, angular straggling, etc., it is valuable to know the variation of range exponent with energy. Bethe[42] uses the logarithmic derivative of the range with respect to the energy: $n = 2d(\log R)/d(\log E) = 2(E/R)(dR/dE)$, and plots a curve of n *vs.* E obtained from the range energy relation available at that time. From our range energy and specific ionization curves we have determined this range exponent; the result is plotted in Fig. 13. The curve differs from the previously published curve considerably in shape and absolute value in the low energy region. The assumption of constant range exponent used in extrapolating to the end of range shows in the horizontal intercept at zero energy, partially justified by the trend of the curve within the last 3 mm.

The authors wish to express their appreciation to Professor H. A. Bethe for many helpful suggestions in the analysis and interpretation of the results. The work was partially supported by a grant from the Research Corporation.

[41] A limited number of large scale blue prints of this relation are available and may be obtained by addressing the senior author (M. S. L.).

[42] Reference 9, p. 271.

The Excitation Function for the Disintegration of Li^7 Under Bombardment by Low Energy Protons*

L. J. HAWORTH† AND L. D. P. KING‡
University of Wisconsin, Madison, Wisconsin
(Received March 18, 1938)

Accurate measurements were made of the yields of 8 cm alpha-particles from thick and thin films of lithium bombarded by homogeneous beams of protons in the energy range from 38 to 210 kv. Careful analyses are described whereby the thin film data were reduced to the values to be expected from films of infinitesimal thickness, thus allowing a relative calculation of the excitation function. From values of the stopping power by other observers the absolute cross section of the lithium nucleus for this process was calculated approximately as a function of the energy. The curves were extended to 400 kv by applying corrections to previously published data of Herb, Parkinson and Kerst.

MANY investigators[1–9] have studied the yield of 8.4 cm alpha-particles arising from the disintegration of Li^7 by protons in the reaction $Li^7+H^1 \rightarrow He^4+He^4$. At low energies, however, little work has been done with metallic lithium as a target material and practically none with thin films. A notable exception is the thick and thin film work of Herb, Parkinson and Kerst[5] in the energy range from 100 to 400 kv. Preliminary work, of which this is an extension, has been done on thick metallic films in the energy range 45 to 200 kv by Heydenburg, Zahn and King.[8] Other determinations at low energies mostly concern themselves with the yields from thick films of lithium compounds.

It is impossible to calculate the excitation function from thick film data alone since the law of penetration of the particles into the target material is not accurately known. Furthermore the yields from thick films of compounds cannot readily be converted into equivalent yields from thick metallic films since, as Mano,[10] Livingston and Bethe,[11] and others have shown, the ratio of the penetrations of the protons in two different materials is not independent of the energy.

APPARATUS

The protons used in these experiments obtained their energy by passing down a three foot vertical accelerating tube to which were applied potentials generated by a Cockcroft and Walton[12] type voltage quadrupler. Potentials were determined by measuring, with a standard resistance and potentiometer, the currents through a corona-free resistance unit similar to that described by Hafstad, Heydenburg and Tuve.[9] Detailed descriptions of the voltage generator, the proton source, the accelerating tube and the voltmeter (together with the method of calibrating it) are given elsewhere,[13] but a brief description of the capabilities of the apparatus will be included here.

A steady potential in excess of 300 kv is available. Small fluctuations (of the order of a few tenths of one percent) were continuously compensated by a manually operated rheostat in the primary circuit of the high voltage trans-

* Supported in part by a grant for apparatus from the Carnegie Institution at Washington and by a grant from the Penrose fund of the American Philosophical Society.
† Now at the Massachusetts Institute of Technology (Research Laboratory of Physical Chemistry).
‡ Now at Purdue University.
[1] J. D. Cockcroft and E. T. S. Walton, Proc. Roy. Soc. **A137**, 229 (1932).
[2] E. O. Lawrence, M. S. Livingston and M. G. White, Phys. Rev. **42**, 150 (1932).
[3] M. L. Oliphant and Lord Rutherford, Proc. Roy. Soc. **A141**, 259 (1933).
[4] M. C. Henderson, Phys. Rev. **43**, 98 (1933).
[5] R. G. Herb, D. B. Parkinson and D. W. Kerst, Phys. Rev. **48**, 118 (1935).
[6] L. R. Hafstad and M. A. Tuve, Phys. Rev. **48**, 306 (1935).
[7] H. D. Doolittle, Phys. Rev. **49**, 779 (1936).
[8] N. P. Heydenburg, C. T. Zahn and L. D. P. King, Phys. Rev. **49**, 100 (1936).
[9] L. R. Hafstad, N. P. Heydenburg and M. A. Tuve, Phys. Rev. **50**, 504 (1936).
[10] G. Mano, J. de phys. et rad. **5**, 628 (1934); Ann. d. Physik **1**, 407 (1934).
[11] M. S. Livingston and H. A. Bethe, Rev. Mod. Phys. **9**, 245 (1937).
[12] J. D. Cockcroft and E. T. S. Walton, Proc. Roy. Soc. **A136**, 619 (1932).
[13] L. J. Haworth, L. D. P. King, C. T. Zahn and N. P. Heydenburg, Rev. Sci. Inst. **8**, 486 (1937).

former so that the average deviation of the potential from the desired value was probably negligible. The 60-cycle ripple present is of the order of two percent between extremes.

Very steady, sharply focused, atomic ion beams are available in intensities up to 12 microamperes. By employing the molecular ion beams of mass 2 and mass 3, proton intensities equivalent to 40 and 60 microamperes respectively may be obtained. These relatively intense molecular ion beams are quite useful in disintegration experiments at low energies where the disintegration probability is very low. The inhomogeneity of the proton energies is somewhat increased by the fact, discussed in detail in reference 13, that they do not all originate at points of the same potential in the ion source. This effect is of importance, however, only when very intense beams of atomic ions are used and is negligible in the greater part of the present experiment.

For most of the observations the voltmeter multiplier consisted of a 15-section unit of resistance 3×10^9 ohms. However, in the case of the five points of lowest energy in the thin film studies a smaller unit of six sections was used. These multipliers have been carefully calibrated in various ways and are believed to be accurate to 0.1 percent relatively and perhaps 0.3 percent absolutely when proper corrections are made for temperature variations.[14]

Details of the disintegration chamber, etc. are shown in Fig. 1. The beam, after being deflected in the magnetic analyzer, is focused and aligned by observing the fluorescence on the quartz plate Q. After proper adjustment of the beam, Q is removed from its path by rotating the ground joint J and the beam is allowed to strike the target T. The latter consists of a film of lithium deposited by evaporation from the furnace F onto a thick nickel plate. T may be rotated by a second ground joint G, a stop being provided to assure the proper position for either evaporation or bombardment. Rotation of G after the target strikes the stop gives, by means of the screw S, a horizontal motion to T so that different parts of the nickel plate may be used for the target backing. The usable portion is 1.25 inches in length.

The system for recording the alpha-particles consists of the ionization chamber I, a Dunning[15] type linear amplifier, a scale of four thyratron counter and a mechanical counter. A cathode-ray oscilloscope and a loudspeaker are useful accessories. The solid angle included in the measurements is determined by the aperture d in the ionization chamber. Such an aperture 4.76 mm in diameter was carefully measured and the solid angle computed geometrically. A second, much larger, aperture covered with a wire grid was used when the counting rate was low. It was calibrated empirically by comparison with the small aperture.

Proton currents were measured by observing the deflection of a galvanometer attached to the target chamber which served as a Faraday cage. A visual average of the deflection was made and recorded over each thirty seconds. The escape of secondary electrons was prevented by a small

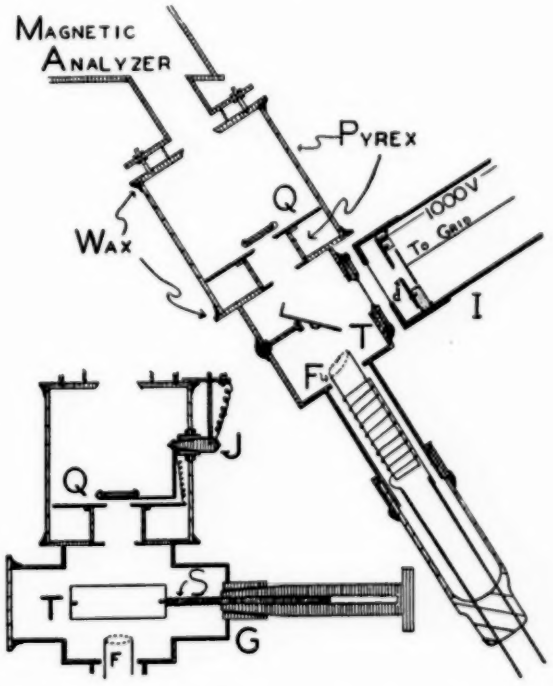

FIG. 1. The disintegration chamber, etc. Both views are normal to the proton beam.

[14] It should be mentioned that the data taken with the smaller resistance unit were obtained before it was realized that there was a dependence on temperature so that no temperatures were recorded. However, as will be shown later, it is believed that in this particular case any error arising from this source is negligible.

[15] Dunning, Rev. Sci. Inst. **5**, 387 (1934).

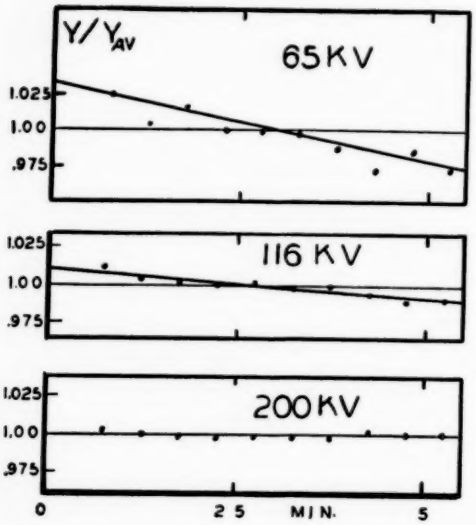

FIG. 2. Thick film fatigue curves. The individual yields have been divided by the average yield throughout the entire five minutes. The ordinate 1.00 represents the average yield.

electromagnet. In general the currents were very steady; the maximum fluctuation in a thirty second interval was usually not greater than one percent.

EXPERIMENTAL METHODS AND RESULTS

Thick film measurements

It was found, in agreement with other observers, that the yield from massive films showed a steady decrease with time after evaporation of the film. The relative effect was greatest at the lowest proton energies. This was interpreted as being due to the formation of a thin film of oil or other contamination which slowed down the protons so that their energy on reaching the lithium became less as the layer became thicker. After bombardment a brown spot appeared where the beam had struck the target, due, probably, to a carbonization of the surface impurity.[16] The fatigue in the yield did not seem, however, to be affected by the bombardment itself to any appreciable extent.

Because of this effect only very fresh lithium surfaces were used. The lithium furnace was kept hot continuously. At the beginning of a set of experiments several minutes were allowed for the deposition of a thick coating on the target. The target was then turned into position for bombardment, the beam turned on and, after thirty seconds allotted for making any minor adjustments, the measurements were begun. These continued for five minutes during which the counter and the current galvanometer were read every thirty seconds. A period of three or four minutes was then devoted to evaporating a new layer of lithium over the old. The proton beam was checked meanwhile and the voltage changed if desired. Another five minute run was then taken and so on.

It was necessary after a few days to remove and clean the target and, less often, the mica window. A careful washing in distilled water sufficed in both cases.

In addition to the precautions taken to ensure fresh surfaces, corrections were applied for the fatigue occurring during the five minutes required to take the data for each layer. At each energy the yields for each thirty second interval were calculated and plotted as a function of the time after evaporation (see Fig. 2). The resulting curve was extrapolated to zero time and the intercept taken as the true yield. Reference to Fig. 2 indicates that the fatigue effect is greater the lower the energy. It was determined graphically that the variation of the effect with energy was similar to that to be expected from a film of impurity of stopping power about 0.2 kv at 115 kv incident energy.

TABLE I. *Thick film yields $Y(E)$ and collision cross sections $\sigma(E)$. These values were read from smooth curves. See the text for a discussion of possible errors.*

E (kv)	$Y(E)$ (DISINTEGRATIONS PER PROTON)			$\sigma(E)$ (CM²)		
	H.K.	H.P.K. (UNCORR.)	H.P.K. (CORR.)	H.K.	H.P.K. (UNCORR.)	H.P.K. (CORR.)
36	1.46×10^{-13}			2.60×10^{-31}		
40	3.42×10^{-13}			5.64×10^{-31}		
50	1.87×10^{-12}			2.38×10^{-30}		
60	6.50×10^{-12}			6.61×10^{-30}		
70	1.77×10^{-11}			1.53×10^{-29}		
80	3.92×10^{-11}			2.91×10^{-29}		
90	7.71×10^{-11}			4.90×10^{-29}		
100	1.35×10^{-10}	1.10×10^{-10}	1.30×10^{-10}	7.50×10^{-29}	7.75×10^{-29}	8.20×10^{-29}
125	4.20×10^{-10}	3.73×10^{-10}	4.17×10^{-10}	1.68×10^{-28}	1.70×10^{-28}	1.77×10^{-28}
150	9.83×10^{-10}	9.0×10^{-10}	9.82×10^{-10}	3.00×10^{-28}	3.04×10^{-28}	3.08×10^{-28}
175	1.96×10^{-9}	1.84×10^{-9}*	1.97×10^{-9}	4.73×10^{-28}	4.73×10^{-28}	4.78×10^{-28}
200	3.46×10^{-9}	3.20×10^{-9}	3.42×10^{-9}	6.73×10^{-28}	6.78×10^{-28}	6.65×10^{-28}
250		8.15×10^{-9}	8.43×10^{-9}		1.10×10^{-27}	1.06×10^{-27}
300		1.67×10^{-8}	1.69×10^{-8}		1.51×10^{-27}	1.46×10^{-27}
350		2.90×10^{-8}	2.95×10^{-8}		1.94×10^{-27}	1.85×10^{-27}
400		4.64×10^{-8}	4.71×10^{-8}		2.35×10^{-27}	2.25×10^{-27}

* Dr. Herb has asked us to call attention to an error in this value as listed in the table in conjunction with Fig. 3 of their paper. The value given was much too high to be consistent with their data, the error having arisen when reading the value from a smooth curve.

[16] R. L. Stewart, Phys. Rev. **45**, 488 (1934).

The final thick film yields, after correction for probe voltage, fatigue, etc. are given in Table I and in Fig. 3, curves *A* and *B*, where the log of the yield[17] is plotted as a function of $E^{-\frac{1}{2}}$. Experimental points are plotted in the figure, but in the table are given values read at standard energies from a smooth curve. The results of other observers are also plotted for comparison. Those of Doolittle,[7] at energies below 75 kv, were obtained from a target believed to be LiOH. The observed values were multiplied by four in an attempt to compensate for the stopping power of the oxygen and hydrogen atoms. Such a method is not very accurate since the binding energies of the electrons as well as their number becomes of consequence at these very low energies. This probably accounts for the lack of agreement with our own results.

The high energy end of the curve is shown on a larger scale in curve *B* together with the results of Herb, Parkinson and Kerst[5] (hereafter referred to as H. P. K.). There is a marked disagreement with their values as published (circles) which is greatest at the lowest energies. However, in their work the lithium target was not usually used until some time (often a day or more) after evaporation so that there was ample time for the formation of a relatively thick impurity layer. The crosses represent an attempt to correct for this by assuming the presence of a foreign film of stopping power 3 kv at 175 kv incident energy. As in our own case adjustment was made for the variation with incident energy of the stopping power of the impurity film. The assumption made is not unreasonable in view of our own experience with old films.[18] Furthermore, a few experimental points taken by H. P. K. with very fresh surfaces are found to agree better with the corrected than with the original curve. The agreement of the corrected results with those of the present authors is very good over the whole range of energies in which they overlap; both the yield curves and their slopes agree to about one percent except at the very lowest energies, where H. P. K. do not consider their results very accurate. No explanation offers itself for the discrepancy, at the higher energies, between the results of H. P. K. and those of Hafstad, Heydenburg and Tuve[9] which are shown approximately by the dotted curve.

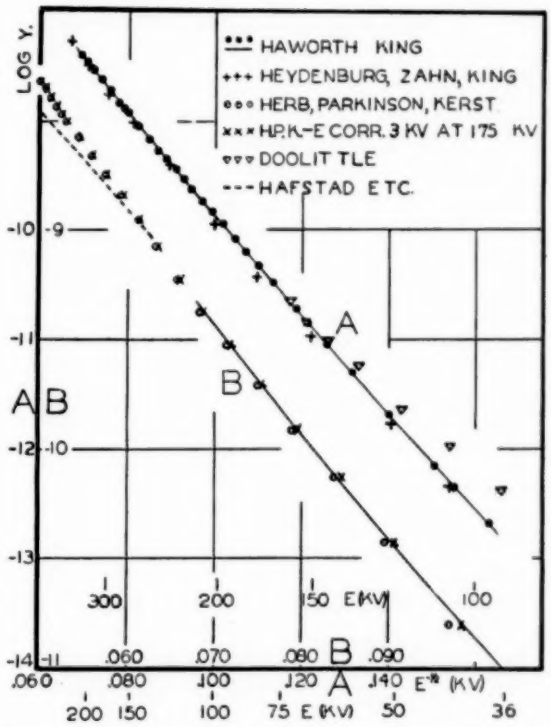

FIG. 3. Thick film yield curves. *Erratum:* In curve *B* the ordinates indicated are one unit too large negatively.

Thin film measurements

The requirement that the surface be relatively fresh necessitated the use of a great many thin films, about 400 in all. These were formed by evaporation onto the nickel backing for a fixed time (30 seconds) with a definite heating current through the winding of the lithium furnace. By moving the target horizontally it was possible to deposit and use four films before it became necessary to remove and clean the nickel.

In spite of the utmost precautions it was impossible to obtain equal thicknesses for all films. For this reason it was necessary to observe the yield from each film at some standard reference energy(116 kv was chosen) as well as at the voltage under consideration. The following procedure was adopted. Observations were taken for five minutes as in the case of the thick films. The voltage was then changed to the reference

[17] Throughout this paper the term "yield" is understood to refer to the number of disintegrations per incident proton.

[18] It should be mentioned that H. P. K. used a mercury diffusion pump and liquid-air trap, whereas an Apiezon oil pump without trap was used in the present work.

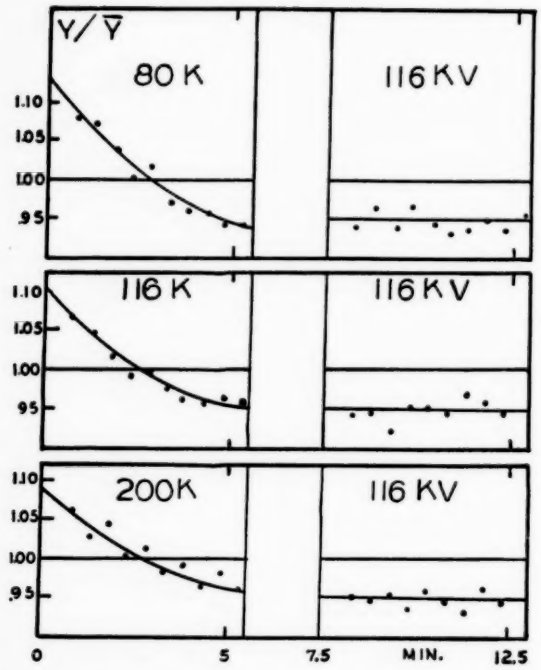

FIG. 4. Thin film fatigue curves. In each case $\bar{Y}$ represents the average yield, over the first five minutes, from a fresh film bombarded at the energy in question. The yields for the reference energy are plotted on the right.

value and the beam readjusted and refocused. Great care was necessary that the beam strike exactly the same spot on the target at both energies.[19] A small electromagnet at the top of the magnetic analyzer served to give lateral adjustment. Two minutes were alloted for the adjusting process, after which observations were made for five minutes at the reference energy.

The yields for a few characteristic energies are plotted as functions of time in thirty second intervals in Fig. 4. It may be seen that the yields decreased very rapidly during the first few minutes and assumed later a more nearly constant value. It is believed that this fatigue arose from two causes: (1) the surface impurity previously discussed and (2) an actual thinning of the film due to evaporation caused by the heating effect of the beam. To this evaporation is attributed the rapid decrease in yield during the first few minutes. That it did not continue indefinitely was doubtless due to the formation of the impurity layer on the surface. The surface impurity has its greatest relative effect at low energies, whereas a given change in thickness by evaporation should produce its greatest relative change in the yields at high energies (since the yield does not fall off so rapidly with penetration). A careful study was made in which the surface impurity was considered the same as in the case of thick films. The residual fatigue after correcting for the impurity was indeed found to be higher at the higher energies to an extent about that to be expected if the decrease in thickness were the same in all cases. (The beam intensity had been adjusted in such a way that the energy density on the surface was always approximately the same.) It was also found that the effect of the fatigue on the yield at the reference energy was essentially independent of the proton energy used during the first five minute period. This was established by the above described features of the fatigue and by the following additional facts. (1) Films evaporated successively and presumably of approximately the same thickness gave nearly equal yields at the reference energy regardless of the energy used during the first period. (2) Reversal of the usual order of bombardment yielded the same results as the regular method, when calculations to be described later were correctly carried out. (3) In a number of cases a film was bombarded for a short time at the reference energy, following which the regular procedure was carried out at a spot slightly removed from the first one. The ratio of the yields at the reference energy from the two spots was found to be independent of the energy used during the first five minutes on the second spot.

The combined effect of the impurity layer and the evaporation was such as to decrease the average yield at the reference point to a value five percent lower than it would have been had the film not been previously bombarded. It was found from thick film studies that the average absorbing power of the impurity film during a second five minute period was approximately 0.5 kv, or 0.3 kv greater than during the first period. This 0.3 kv change will account for about 1 percent in the 5 percent fatigue effect, leaving 4 percent to be attributed to evaporation.

The necessary corrections for fatigue thus

[19] Neglect of this precaution at one time gave rise to a spurious "hump" in the thin film yield curve. This effect was present at the time of a report given before a Chicago meeting of the American Physical Society, Nov., 1936.

consist of: (1) a 0.15 to 0.2 kv decrease in the energies at the experimental points; (2) a 4 percent increase in the yields and a 0.5 kv decrease in the energies at the reference point. The corrections applied to the reference point have, however, only a very slight effect on the relative thin film yields calculated from the data.

Evaluation of the thin film data

The purpose of a thin film yield curve is to make it possible to calculate the disintegration cross section of the atomic nucleus, at least relatively. A true thin film (or excitation) curve should have ordinates proportional to this cross section at each energy. If a beam of protons of incident energy E_0 passes through a film of thickness Δx, the yield $y(E_0)$ is given by

$$y(E_0)=N\int_0^{\Delta x}\sigma(E)dx, \qquad (1)$$

where N is the number of Li^7 nuclei per cm^3 and $\sigma(E)$ is the disintegration cross section. It is obvious that if the proton energy remained constant throughout the film the yield would be given by

$$y(E_0)=N\sigma(E_0)\Delta x.$$

In the case of infinitesimally thin films this would be true to a high degree of approximation and with such films a reduction to constant thickness could be made by dividing the various values of $y(E_0)$ by the corresponding yields $y(R_0)$ at the reference energy. Actually, however, the films used were of finite thickness and the reduction in energy in passing through them was appreciable. The above approximation is therefore not sufficiently accurate. Proper treatment of the data makes it possible, however, to obtain values for $\sigma(E)\times$ const. at each energy E as follows.

Let the energy loss of the protons in passing through the film be ΔE. Then we may say

$$y(E_0)=N\int_0^{\Delta x}\sigma(E)dx=N\sigma(E_e)\Delta x, \qquad (2)$$

where E_e is some energy in the interval E_0 to $E_0-\Delta E$. Then the various $y(E_0)$ will, when reduced to a constant film thickness, be proportional to the true cross section at the corresponding energies E_e.

As a first approximation to the true values for E_e it was decided to use the mean energy $\bar{E}=E_0-\Delta E/2$. In order to determine the values of ΔE it was necessary to resort to the thick film curve. Let the thick film yield at incident energy E_0 be $Y(E_0)$. Of this, an amount $y(E_0)$ is the yield from a surface layer of thickness Δx equal to that of a thin film which yields $y(E_0)$ at the same incident energy. The difference $Y(E_0)-y(E_0)$ is equal to the thick film yield at incident energy $E'=E_0-\Delta E$. In order to find ΔE it is only necessary to find, on the thick film yield curve, the energy E' at which $Y(E')=Y(E_0)-y(E_0)$ and obtain $\Delta E=E_0-E'$ by subtraction. This was done for all cases, including the reference point. The values of E_0 and $y(E_0)$ were obtained by averaging over the several films used at the experimental energy in question. The various effective energies E_e were then calculated to a first approximation from the relationship $E_e\cong\bar{E}=E_0-\Delta E/2$.

The yields were then corrected for film thickness. To a first approximation this could be done by simply dividing $y(E_0)$ by the corresponding yield $y(R_0)$ at the reference energy. However, the values of $\bar{R}$, the mean reference energy, were not all exactly the same for two reasons: (1) although the voltmeter current was always the same, R_0 varied slightly because of differences in temperature and probe voltage; (2) different film thicknesses affected $\bar{R}$ through ΔR. It was necessary, therefore to apply corrections to the various $y(R_0)$. Each $y(R_0)$ was reduced to the value it would have had at some standard $\bar{R}$. This was accomplished as follows. A number of films for which $\bar{R}$ was practically the same were selected and, a curve of $y(E_0)/y(R_0)$ against energy was plotted in the neighborhood of the reference point. One hundred fourteen kv was chosen as the standard value of $\bar{R}$ and each $y(R_0)$ was corrected to this standard by forming the product $y(R_0)\times z(114)/z(\bar{R})$ where $z(114)$ and $z(\bar{R})$ are the respective ordinates at 114 kv and $\bar{R}$ on the curve just described.

A standard film was chosen of such thickness that the absorbing power would be 4 kv (approximately the average for all films) at an incident energy of 116 kv. By inspection of the thick film yield curve it was found that such a film would give a yield of 4.65×10^{-11} disinte-

grations per proton at $E_0=116$ kv, $\bar{E}=114$ kv. The final corrected values of the yields were then given by

$$\bar{y}(\bar{E})=\frac{y(E_0)}{y(R_0)}\times\frac{z(\bar{R})}{z(114)}\times 4.65 \times 10^{-11} \text{ disintegrations per proton.} \quad (3)$$

A plot of $\bar{y}(\bar{E})$ against $\bar{E}$ gives a first approximation to the desired excitation curve. In order to determine the accuracy of the approximation it is necessary to investigate the extent to which $\bar{E}$ differs from E_e, the true effective energy. By Eq. (2) the true E_e will be the energy such that

$$\sigma(E_e)=\frac{\int_0^{\Delta x}\sigma(E)dx}{\Delta x}$$

or, in more usable form

$$\sigma(E_e)=\frac{\int_{E_0}^{E_0-\Delta E}\sigma(E)(dx/dE)dE}{\int_{E_0}^{E_0-\Delta E}(dx/dE)dE}. \quad (4)$$

Values of dx/dE were calculated in arbitrary units as follows. ΔE and the corresponding ΔR are measures of the stopping powers of a given thin film at incident energies E_0 and R_0 respectively, so that

$$\frac{\Delta E}{\Delta R}=\frac{\Delta E/\Delta x}{\Delta R/\Delta x}$$

is a measure of the stopping power of that film at incident energy E_0 in terms of the stopping power at incident energy R_0. The various values of $\Delta E/\Delta R$ (corrected for the variation in $\bar{R}$) are thus measures of $\Delta E/\Delta x$ in arbitrary units. Numerical and graphical tests were applied to the curve having $\Delta x/\Delta E$ as ordinates and $\bar{E}$ as abscissae which showed that to a high degree of approximation (much better than one percent)

$$\frac{\Delta R}{\Delta E}=k\frac{\Delta x}{\Delta E}=k\left(\frac{dx}{dE}\right)^{20} \text{ at } E=\bar{E}.$$

Curves of (dx/dE) at $E=\bar{E}$ and $\bar{y}(\bar{E})$ were then plotted as functions of $\bar{E}$ and were considered (except for proportionality constants) sufficiently good approximations to the true curves for dx/dE and $\sigma(E)$ to furnish a criterion for the accuracy of the relationship $\bar{E}\cong E_e$. Values at corresponding energies read from these curves were substituted in Eq. (4) and graphical and numerical calculations (in which the proportionality constants cancel) were performed which showed that $\bar{E}$ differs appreciably from E_e only at the very lowest energies. It is approximately 0.15 kv too low at 36 kv and practically correct at all energies above 70 kv.[21]

---

[20] That this approximation is a highly accurate one can be surmised in another way as follows. Assume that in the narrow energy range ΔE a sufficiently accurate approximation to the range law is given by the relationship $x=A+CE^n$ where A and C are constant over ΔE. Then

$$\Delta x=C[(\bar{E}+\Delta E/2)^n-(\bar{E}-\Delta E/2)^n]$$
$$=Cn\bar{E}^{n-1}\Delta E[1+(1/24)(n-1)(n-2)(\Delta E/\bar{E})^2+++],$$

whence at $E=\bar{E}$

$$(dx/dE)=[\Delta x/\Delta E][1-(1/24)(n-1)(n-2)\times(\Delta E/\bar{E})^2+++]=(\Delta x/\Delta E)(1-\delta+++).$$

Actually, in our case n varies between 1.5 and 0.5 at different parts of the curve. Thus $(1/24)(n-1)(n-2)$ lies between -0.01 and $+0.03$. The highest value in any case for $(\Delta E/\bar{E})^2$ was for the case $\bar{E}=36$, $\Delta E=4.3$ kv, or $(\Delta E/\bar{E})^2=0.01$ (approximately). Thus we see that δ is of the order of 10^{-4} or less and may be considered negligible.

[21] Professor Breit has suggested the following method of checking this point. From the curve for $\bar{y}(\bar{E})$ it is found that approximately $\sigma(E)=Ce^{-k/(E)^{\frac{1}{2}}}$ where, in the low energy range, k has the approximate value 88 when E is measured in kilovolts. Furthermore dx/dE varies so slowly in comparison with $\sigma(E)$ that we shall consider it constant over the thin film for purposes of this discussion. Then Eq. (4) becomes

$$\sigma(E)=\frac{\int_{\Delta E/2}^{\bar{E}+\Delta E/2}\sigma(E)dE.}{\Delta E}$$

Expanding about $\bar{E}$ and integrating, we obtain

$$\sigma(E_e)=\sigma(\bar{E})+\frac{(\Delta E)^2}{24}\sigma''(\bar{E})++\cdots.$$

Furthermore, letting $E_e=(\bar{E})+\delta E$ and expanding about $\bar{E}$ we obtain

$$\sigma(E_e)=\sigma(\bar{E})+\sigma'(\bar{E})\delta E++\cdots.$$

Comparison of the two above values for $\sigma(E_e)$ yields

$$\delta E=\frac{(\Delta E)^2}{24}\frac{\sigma''(\bar{E})}{\sigma'(\bar{E})}++\cdots.$$

Or, by substitution of the assumed expression for $\sigma(E)$

$$\delta E=\frac{(\Delta E)^2}{48\bar{E}}(K\bar{E}^{-\frac{1}{2}}-3).$$

In the case of the lowest energy which we used $\bar{E}=36$ kv, $\Delta E=4.3$ kv, whence

$$\delta E=0.11 \text{ kv},$$

in fairly good agreement (below experimental error from other sources at these energies) with the directly calculated correction.

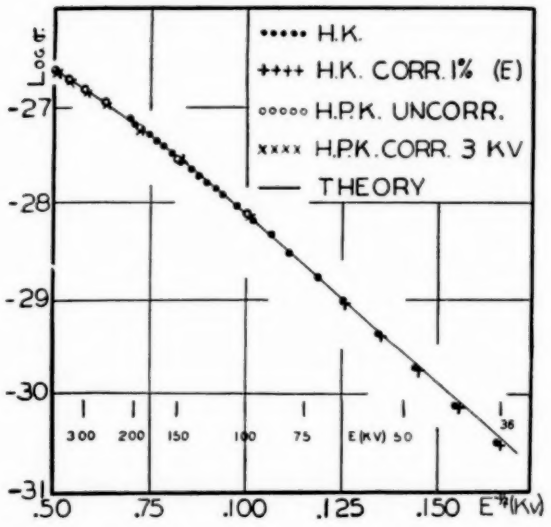

FIG. 5. The excitation cross section. All sets brought into agreement at 175 kv. The plus signs show the effect of lowering the voltage one percent at both the experimental and the reference energies. The theoretical curve is for the case $L=1$, $U=23$ kv.

The indicated corrections were applied to $\bar{E}$ to give the true E_e. A plot of $\bar{y}(E_e)$ then gave our final curve for the excitation function in terms of the yield from a film of stopping power 4 kv at 114 kv.

Disintegration cross section

An approximate calculation of the thickness of our standard film and hence of the absolute cross section was made as follows. Livingston and Bethe[11] give for σ_a, the stopping cross section of air, at 175 kv the value 14.9×10^{-18} kv cm^2. From figures given by Mano[10] it is estimated that the stopping cross section of Li relative to air at the same energy is 0.565. Thus the stopping power of Li at 175 kv is given approximately by

$$dE/dx=0.565\sigma_a N'=0.565\times14.9\times10^{-18}\times4.67\times10^{22}=3.94\times10^{5}\text{ kv/cm}$$

where N' is the *total* number of Li atoms per cm^3. From our curve of $\Delta E/\Delta R$ it is found that the energy absorbed in our standard film at 175 kv is 3.7 kv. Hence $\Delta x=3.7/(3.94\times10^5)=9.4\ 10^{-6}$ cm. As the stopping cross section of air and the ratio of Li to air are probably more accurately known at higher energies, the data of H. P. K. (the thin film curve was standardized to ours at 175 kv) were used at 400 kv to perform a similar calculation. This yielded the result $\Delta x=8.35\times10^{-6}$ cm.

A value of 8.8×10^{-6} cm was then chosen for use in future computations. From this thickness and the thin film excitation curve it is possible to calculate approximate absolute values of $\sigma(E)$ from the equation

$$\bar{y}(\bar{E}_e)=N\sigma(E_e)\Delta x.$$

In this case $N=4.31\times10^{22}$, the number of Li^7 nuclei per cm^3.

Experimental values of $\sigma(E)$ thus computed are plotted in Fig. 5[22] and listed in Table I.

The results of Herb, Parkinson and Kerst are also given. Two corrections to their data as published were considered. (1) The energies assigned to the respective yields were shifted so as to represent the average energy of the protons in the films rather than the incident energy. This was done in a manner analogous to that used on our own data. (2) The effect of a possible surface film was considered. Considerable uncertainty exists as to how large this second correction should be. Consequently the results are given for two cases. In the first no correction was applied. In the second the same correction as in the case of

[22] As previously mentioned the data for the five points of lowest energy in Fig. 5 were obtained when the small voltmeter multiplier was used without making temperature observations. Both thick and thin film measurements were made with this multiplier at all energies up to 115 kv. After the installation of the larger multiplier all of these were repeated with the exception of the five points in question. Because of the very large number of films required to obtain sufficient counts at these energies it was believed not to be worth while to repeat these. An average temperature was assumed, which was based on temperature observations in a great many cases after the effect was discovered. Any error involved is believed to be negligible for the following reasons. (1) Thick film measurements obtained more or less simultaneously with the thin film measurements in question agreed well with those obtained later with the larger multiplier in the energy range from 36 to 115 kv. The same was true of thin film measurements in the higher part of this energy range. (2) The maximum temperature variation observed was such as to allow a maximum uncertainty in the energy of only 0.5 percent. (3) Any voltage error due to temperature uncertainty was largely nullified by the use of a reference point. For example, at 36 kv any error present would be reduced by a factor of four on this account. It should be mentioned in this connection that these points were obtained by the use of molecular ion beams so that the voltmeter currents were of the same order at both experimental and reference points. In fact, at energies 36 and 55 kv they were exactly the same. The plus signs of Fig. 5 represent the effect of assuming a one percent error in voltage at both the experimental and the reference points. Such an error is believed to be outside the possible limits, at least in so far as temperature is concerned.

the thick films (3 kv at 175 kv) was applied. It is seen that the first gives results which seem to agree best with our own. However there was undoubtedly a film present and the seeming agreement without a correction is probably fortuitous. It is possible that the slight lack of agreement at the low energies when a correction is applied is the result of stray counts. Dr. Herb has informed us that they had considerable difficulty on this account. It should be mentioned that the two sets are separately adjusted to agree with our own at 175 kv.

Possible errors

The errors involved in the present experimental work may involve both the yields and the voltages. Errors in the counting process itself are believed to be negligible in so far as their effect on the smooth yield curves is concerned, although it is true that at the lowest energies the number of counts observed, particularly in the case of thin films was not great enough to prevent some statistical fluctuation in the individual points. The absolute scale of yields in the case of thick films is believed correct to one percent.

Of greater importance are the possible errors involving the voltage. The mean energy of the incident protons is believed to be known in every case to within two or three tenths of one percent (except, perhaps, in the case discussed in reference 22). However, some error is introduced by the inhomogeneity of the proton beam. In the case of a symmetrical distribution about the mean energy, the inhomogeneity would result in slightly too high values of the yields since the second derivatives of the yield curves are positive. This effect would be worst at the lowest energies. As mentioned earlier, the total inhomogeneity is of the order of two percent which at 40 kv results in a spread of 0.8 kv in the incident energies. By assuming as an extreme case that the beam consists of two equally intense components 0.8 kv apart it was calculated that this would introduce an error of less than one percent in the yields. This was not corrected for since it was within the limit of other experimental errors, corrections for which could not be computed.

Two additional possible sources of error are inherent in the use of films of finite thickness. Our development of the data was based on the assumptions that the films were of uniform thickness across the area struck by the beam and that there was no straggling of the protons in passing through the films. Nonuniformity of the individual films might introduce serious errors at low energies where the yield is a very rapid function of the energy. In this case nuclei in the lower layers of the thicker spots would contribute fewer disintegrations than those nearer the surface so that the yield from a given amount of lithium would be lower if it were "bunched" in a few spots than if it were uniformly distributed. At the reference point, on the other hand, this effect would be much less marked since the dependence of cross section on energy would not be so great. Thus the relative yields at the low energies would be too small. This effect would be magnified by the fact that too small a value for $y(E_n)$ results in an underestimation of ΔE and consequently too high a value for E_e. The magnitudes of the possible errors on this account are hard to estimate, but they may amount to several percent at the lowest energies and are probably the most important in the entire experiment.

The straggling of the protons in passing through the thin film will somewhat increase the value of $y(E_0)$. For, since the second derivative of $\sigma(E)$ is positive, the extra yield from those protons whose average energy through the film is greater than $\bar{E}$ will more than compensate for the deficit from those whose average energy is less than $\bar{E}$. There is, however, a compensating factor. There will be straggling to the same extent in the thick films as in the thin so that, after passing through a surface layer of thickness Δx equal to that of the thin film, there will be the same distribution in proton energies as on emergence from the thin film. Then we may say

$$Y(E_0)=y(E_0)+Y_0(E),$$

where $Y_0(E)$ is the thick film yield which would be produced by a beam having an energy distribution just that of the protons after passing through the layer Δx. Now, since $d^2Y/dE^2>0$,

$$Y(E'')=Y_0(E)>Y(E')$$

for a case of symmetrical straggling. Here E' is the mean energy of emergence from Δx and $Y(E')$ is the measured thick film yield at incident

energy E'. Then our measured value of ΔE is given by

$$\Delta E_{\text{meas.}} = E_0 - E'' < E_0 - E'$$

and is too small. Thus the measured E_e will be greater than had there been no straggling so that the increase in thin film yield introduced by the straggling is accompanied by a compensating increase in the energy assigned to that yield. By making various simple but exaggerated assumptions as to the straggling and graphically integrating $\sigma(E)(dx/dE)$ between the proper limits it was found that the two increases correspond almost exactly (the net effect on σ being less than 1 percent). In these integrations account must be taken of the fact that dx/dE is different for each degree of straggling.

We may summarize by stating our belief that the thick film yield curve (of the authors) is accurate to perhaps one or two percent (in the yields) over the entire range of energies covered; that the cross section curve (of the authors) is accurate relatively to about the same extent at the higher energies; but that errors of a few percent may enter in the latter at the lowest energies, principally because of the possibility of nonuniformity in the individual films. The absolute values of the cross section are, of course, only approximate.

The corrected values calculated from the data of H. P. K. may involve somewhat larger errors but it is difficult to make an estimation.

Comparison with theory

Ostrofsky, Breit and Johnson[23] have calculated theoretically the disintegration cross section of the lithium nucleus for this process for various values of the depth of the potential well. The smooth curve of Fig. 5 represents their calculations for the case $L=1$, $U=23$ Mev which seems to give the best agreement. Adjustment has been made arbitrarily to bring the values into agreement at 175 kv.

The absolute values of $\sigma(E)$ as here plotted are somewhat larger than those arrived at by Ostrofsky, Breit and Johnson who used the data of H. P. K. in a somewhat different manner. Assuming the $\frac{3}{2}$ power dependence of proton range on energy and a constant value of 0.547 for the stopping power of lithium relative to air they computed, from the range measurements given by Rutherford, Chadwick and Ellis on oxygen, air, etc., the value of k_1 in the equation $x=k_1E^{\frac{3}{2}}$ where x is the range. Inserting this in the equation

$$Y(400) = N\int_0^{400} \sigma(E)\frac{dx}{dE}dE = Nk_2\int_0^{400} y(E)\frac{dx}{dE}dE$$

and using for $Y(E)$ and $y(E)$ the experimental values of H. P. K. they computed numerically the right hand integral and evaluated k_2 by a comparison with $Y(400)$. Values of $\sigma(E)$ were then found through the relationship $\sigma(E) = k_2y(E)$. In this way they arrived at a value for $\sigma(400)$ some 30 percent lower than that of the present calculations. The difference is caused principally by their assumption of the law of range which, as they have pointed out, makes their computations somewhat in error. The corrections applied to the data of H. P. K. are of little moment in this connection, being, in fact, in such a direction as to reduce the difference in the absolute values.

It is seen that the relative agreement of experiment and theory is quite good except at the very lowest energies. The discrepancy is in the direction to be expected from errors in the data due to nonuniformity of the thin films.

It is a pleasure to express our gratitude to Professor G. Breit for much aid and encouragement and to Drs. Herb, Parkinson and Kerst for the use of their original data. We are also indebted to Professor H. B. Wahlin for helpful suggestions, to Messrs. G. Ragan and R. Syrdal for aid in the making of observations, and to Drs. N. P. Heydenburg and C. T. Zahn who began the research and constructed much of the apparatus.

We gratefully acknowledge the grants described at the beginning of this article.

[23] Ostrofsky, Breit and Johnson, Phys. Rev. **49**, 22 (1936).

The Stopping Power of Lithium for Low Energy Protons

L. J. HAWORTH* AND L. D. P. KING†
University of Wisconsin, Madison, Wisconsin

(Received March 18, 1938)

The stopping power of lithium for protons as a function of energy has been calculated in the energy range 35 to 400 kv from measurements by Herb, Parkinson and Kerst and by the authors of the yields of 8 cm alpha-particles from thick and thin films of lithium. The absolute scale of units is based on an extrapolation of values given by Mano for the stopping power at energies above 500 kv. Integration of the reciprocals of the stopping power provides, except for a constant of integration which may be estimated, a knowledge of the range law as a function of energy.

ALTHOUGH some work has been done,[1] little direct experimental information is available on the stopping power of substances for protons, etc. at energies much below 500 kv.

Consequently the authors have felt that calculations they have performed, based on the yields of 8 cm alpha-particles from thick and thin films of lithium might prove of interest. The data used were those of Herb, Parkinson and Kerst[2] and of the authors[3] and cover the energy range from 35 to 400 kv.

The number of disintegrations per incident proton from a massive target (thick film) at incident energy E_0 is given by the equation

$$Y(E_0)=N\int_{E_0}^{0}\sigma(E)\frac{dx}{dE}dE,$$

where N is the number of Li^7 nuclei per cm^3, $\sigma(E)$ is the disintegration cross section at energy E and dx/dE is the reciprocal of the stopping power. By differentiation, we obtain

$$\frac{dY}{dE}=N\sigma(E)\frac{dx}{dE} \quad \text{or} \quad \frac{dE}{dx}=\frac{N\sigma(E)}{dY/dE}.$$

$\sigma(E)$ has been computed over the entire energy range in the preceding paper from the experimental thin film yields. In order to calculate dY/dE, $\Delta Y/\Delta E$ was determined graphically from the thick film yield curve (by the use of a large scale log Y *versus* E^{-1} curve) for energy intervals of 4 kv. These values were found to represent sufficiently well the values of dY/dE at the midpoints of the energy intervals except at the very lowest energies where it was necessary to apply slight corrections similar to those made by Haworth and King in computing the effective energy of the protons which pass through the thin films. It should be mentioned that the absolute values of the calculated disintegration cross sections were dependent upon a knowledge of the thickness of the thin films used, which thickness was computed by extrapolating data given by Mano[4] on the stopping power of lithium at energies above 500 kv and by applying at a few points a process which was the reverse of that of the present paper.

The values of dE/dx thus obtained are plotted against the energy in Fig. 1, and listed for a few energies in Table I. As discussed in the preceding paper it was necessary to apply corrections to the data of Herb, Parkinson, and Kerst on account of the impurity film which collected on the film surfaces in the time which elapsed between evaporation and the making of the observations. In the case of thick films the stopping power of the impurity film could be estimated from the disagreement, in the absolute values of the yields, with our own observations which were made on fresh films. No such criterion was available, however, in the case of thin films. For this reason two sets of computations were

* Now at the Massachusetts Institute of Technology, Research Laboratory of Physical Chemistry.

† Now at Purdue University.

[1] The best is, perhaps, that of Blackett and Lees on air, Proc. Roy. Soc. **A134**, 658 (1932) and of Parkinson, Herb, Bellamy and Hudson on air and aluminum, Phys. Rev. **52**, 75 (1937).

[2] Herb, Parkinson and Kerst, Phys. Rev. **48**, 118 (1935).

[3] See the preceding paper.

[4] G. Mano, Ann. d. Physik **1**, 407 (1934).

made. In the first of these no correction whatever was made. In the second the same correction was applied as in the case of thick films (3 kv at 175 kv). As the values of $\sigma(E)$ seemed to agree with our own better in the first than in the second case it is probable that the true value lies somewhere between. The values of $\sigma(E)$ were adjusted to give agreement between all sets at 175 kv. The slight difference in the values of the stopping powers at this energy is due to a difference in the values of dY/dE between the two sets of observers.

The results were computed as though for a film of constant stopping power (ΔE constant). Included for comparison in Fig. 1 (squares) are values computed by King and Haworth for a film of constant thickness ($\Delta E/\Delta R$ of their paper). The staggering is due to the fact that they were calculated directly from the data without any smoothing, whereas the present calculations were based on values read from smoothed curves.

The dashed curve of Fig. 1 was obtained from that of Livingston and Bethe[5] for air, after approximate adjustment was made for the relative stopping power of lithium and air according to Mano.[4] The greater steepness of our curve at low energies may be, perhaps, the result of the effect of nonuniformity of the thin films used. As shown in the preceding paper this would result in too small values for $\sigma(E)$ to an increasing extent as the energy is lowered. The same effect would, of course, be exerted on the computed values of the stopping power.

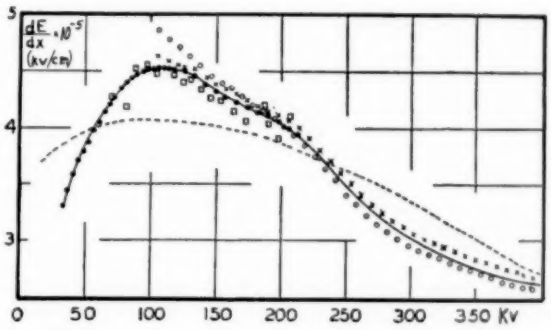

FIG. 1. The stopping power as a function of energy. Legend: Solid dots, Haworth-King, from smoothed yield curves; squares, Haworth-King, from measurement of $\Delta E/\Delta R$; crosses, H. P. K. no correction to thin film yields; circles, H. P. K. thin film voltages lowered (3 kv at 175 kv); dashed curve Livingston-Bethe, reduced to lithium according to Mano.

Another error producing the same sort of effect results from the straggling of the protons in passing through the lithium. In calculating ΔY we have used the relationship $\Delta Y = Y(E_0) - Y(E')$ where $E' = E_0 - \Delta E$ and we have assumed that ΔY is the yield produced by protons all of which lose energy ΔE in the process. Actually, however, when the mean energy loss is ΔE there is a distribution of energies so that the above equation should be replaced by $\Delta Y = Y(E_0) - Y_0(E)$ where $Y_0(E)$ is the yield that would be produced by an incident proton beam having just the distribution of energies that our beam has after suffering a mean energy loss ΔE. Now for symmetrical straggling $Y_0(E) > Y(E')$ since $d^2Y/dE^2 > 0$. Then

$$Y(E_0) - Y(E') > Y(E_0) - Y_0(E)$$

and we have overestimated ΔY and consequently underestimated dE/dx. This effect will be pronounced only at the lowest energies.

In order to calculate the order of magnitude of this effect let us consider as a simple example that when the mean energy loss is ΔE there are two equally intense groups of protons of energies $E_0 - \Delta E + \delta E$ and $E_0 - \Delta E - \delta E$, respectively. Then

$$Y_0(E) = \tfrac{1}{2}[Y(E_0 - \Delta E + \delta E) + Y(E_0 - \Delta E - \delta E)].$$

TABLE I. *Our own values have been used up to 200 kv and above that energy the mean of the two sets from Herb, Parkinson and Kerst. The last figure in each case is added only for the sake of internal consistency.*

E (KV)	dE/dx (KV/CM $\times 10^{-5}$)	RANGE (CM $\times 10^{4}$)
36	3.40	1.80
40	3.57	1.93
50	3.86	2.19
60	4.02	2.44
70	4.20	2.68
80	4.32	2.93
90	4.47	3.16
100	4.54	3.38
125	4.51	3.92
150	4.34	4.50
175	4.18	5.06
200	4.05	5.68
250	3.46	7.00
300	3.02	8.56
350	2.79	10.38
400	2.62	12.28

[5] M. S. Livingston and H. A. Bethe, Rev. Mod. Phys. **9**, 245 (1937).

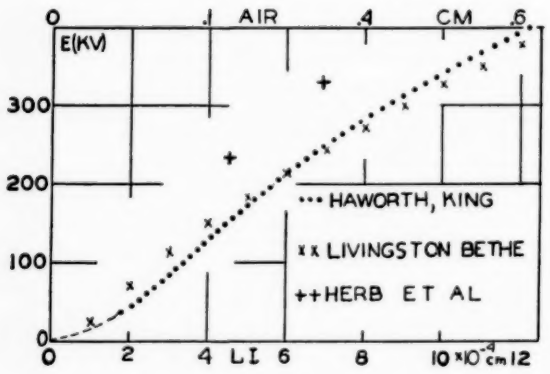

FIG. 2. Range-energy curve.

From an equation of Livingston and Bethe[6] it is calculated that the mean square deviation from the mean energy loss for the case $E_0=42$ kv, $\Delta E=4$ kv is approximately 3 kv^2 or δE is 1.7 kv. As an extreme case we will use $\delta E=2$ kv. Then $E'=38$ kv; $E_0-\Delta E+\delta E=40$ kv; $E_0-\Delta E-\delta E=36$ kv. To obtain the various Y's it is sufficiently accurate for this purpose to use our thick film yield curve. We find, in units of 10^{-12} disintegrations per incident proton: $Y(36)=1.46$; $Y(38)=2.27$; $Y(40)=3.42$; $Y(42)=5.01$. Then

$$Y(42)-Y(38)=5.01-2.27=2.74,$$
$$Y(42)-Y_0(E)=5.01-\tfrac{1}{2}(3.42-1.46)=2.57$$

or a difference of about six percent. A similar calculation at 70 kv shows a difference of 2.5 percent, etc.

[6] Reference 5, Eq (788).

Because of the indefiniteness no corrections were applied for this effect. It seems safe to say, however, that the errors on this account cannot at the most exceed five or six percent even at the very lowest voltages and that they decrease rapidly as the voltage is increased.

In Fig. 2 is plotted a range-energy curve obtained by numerical integration of a smooth curve of dx/dE against E. For this purpose calculations were made from the solid curve of Fig. 1. The unknown integration constant, representing the range below 36 kv, was approximated by extrapolating the stopping power curve to zero energies before taking the reciprocals. This checked well with values arrived at by extrapolating the range curve itself without any assignment of the integration constant.

For comparison the curve of Blackett and Lees[1] (as corrected by Livingston and Bethe[5]) for air has also been plotted. It is seen that this curve, as does the dashed curve of Fig. 1 indicates a maximum stopping power at a somewhat lower energy than in our own case. Measurements of Parkinson, Herb, Bellamy and Hudson[1] are also included. Their data show a somewhat shorter range than do those of Blackett and Lees.

The authors are deeply grateful to Professor G. Breit for much valuable advice. We are also indebted to Messrs. G. Ragan and R. Syrdal for assistance in some of the numerical calculations. One of us (L. J. H.) acknowledges with gratitude the receipt of a grant from the Wisconsin Alumni Research Foundation during part of the time that the work was being done.

Radioactive Isotopes of Iron

J. J. LIVINGOOD, *Radiation Laboratory, Department of Physics, University of California*

AND

G. T. SEABORG, *Department of Chemistry, University of California, Berkeley, California*

(Received May 10, 1938)

Radioactive Fe^{59} has been produced through the reactions $Fe^{58}(d, p)Fe^{59}$ and $Co^{59}(n, p)Fe^{59}$; the half-life is 47 ± 3 days. The emitted particles are negative electrons, most of which have a range of 0.09 grams/cm² Al, while a small number extend to 0.35 grams/cm² Al. The gamma-ray shows a half-thickness of 10 grams/cm² Pb. Radioactive Fe^{53} is formed by the two processes $Fe^{54}(n, 2n)Fe^{53}$ and $Cr^{50}(\alpha, n)Fe^{53}$; positrons are ejected with a half-life of 8.9 ± 0.2 minutes. No subsequent decay of Mn^{53} to Cr^{53} has been observed. No activity corresponding to Fe^{55} has been detected, although Cr, Mn, Fe, Co and Ni have been bombarded with protons, neutrons, deuterons and alpha-particles in all the combinations that might be expected to produce this isotope; it is concluded that Fe^{55} is either stable or has a very long or a very short life.

INTRODUCTION

EVIDENCE is here presented for the production of a new negative electron emitting radio isotope of 47 ± 3 days half-life ascribed to Fe^{59}, which is made by the reactions $Fe^{58}(d, p)Fe^{59}$ and $Co^{59}(n, p)Fe^{59}$, and for a positron emitter of 8.9 ± 0.2 minutes half-life assigned to Fe^{53}, produced by the process $Fe^{54}(n, 2n)Fe^{53}$, with confirmation of the alternative mode $Cr^{50}(\alpha, n)Fe^{53}$.

APPARATUS

Activations were made with the Berkeley cyclotron, with deuteron currents of 100 to 20 microamperes at 5 to 8 Mev, proton currents of 100 microamperes at 3.2 Mev and alpha-particle currents of 0.5 microampere at 16 Mev. Sheet iron of known purity from various sources was used; this was often simply screwed to the water-cooled target holder, but for the more energetic bombardments the periphery of the iron was directly soldered to a cooling pipe. C.P. oxides of manganese, cobalt and chromium were supported generally behind a 0.0005-inch foil of commercial aluminum; more recently (to avoid recoil impurities from the foil) these powders have been sprinkled onto a sloping corrugated block of carbon. The radioactivities were measured with a quartz fiber electroscope equipped with a window of 0.0001 inch aluminum. An activity of 1 division per second corresponds roughly to 1 microcurie. The background activity, equal to about 0.001 divisions per second, has been subtracted in all the data shown.

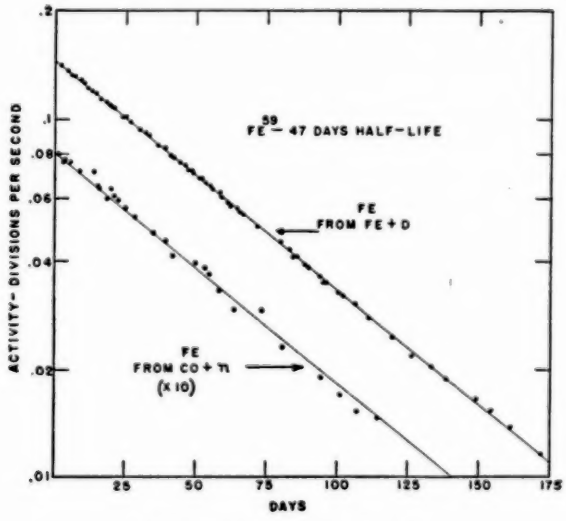

FIG. 1. Decay curves of Fe^{59}.

IRON ACTIVITY OF 47 DAYS HALF-LIFE FROM Fe+D

Figure 1 shows the decay curve of iron chemically separated from iron bombarded with 5.5 Mev deuterons for about 170 microampere hours. The half-life is 47 ± 3 days, this value superseding the 40-day figure given in a preliminary communication.[1]

The bombarded iron was dissolved in a mixture of HCl and HNO_3, and small amounts of $MnCl_2$

[1] Livingood, Seaborg and Fairbrother, Phys. Rev. **52**, 135 (1937).

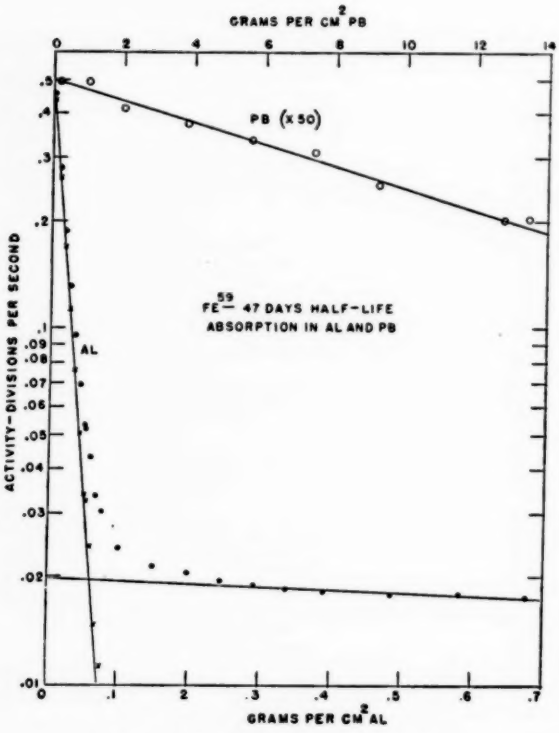

FIG. 2. Absorption curves of Fe^{59}.

and $CoCl_2$ were added to serve as carriers for the transmutation products. NaH_2PO_4 was also included to take care of the radio-sodium and radio-phosphorus generally present. The solution was made 6*N* in HCl and the iron was extracted as $FeCl_3$ by shaking with an equal volume of ether, according to the method of Noyes and Bray.[2] The ether containing the $FeCl_3$ was then always shaken with four or five successive portions of equal volumes of 6*N* HCl in order to remove all traces of radio Mn and Co. The complete absence of the very strong 18-hour Co and 2.6-hour Mn activities[1] in the iron fraction showed that this method offered a very good separation.

In some cases the $FeCl_3$ was converted into Fe_2O_3 after the separation, since it was found that Fe_2O_3 suffered fewer physical and chemical changes over a long period of time and so afforded better decay curves.

The iron was separated by an entirely different method on several occasions. $Fe(OH)_3$ was precipitated (after the removal of the manganese as MnO_2) by the addition of NH_4OH to a solution which contained a high concentration of ammonium ion. With this technique it was necessary to redissolve and reprecipitate the $Fe(OH)_3$ four or five times in order to effect a complete separation from cobalt. The iron fraction obtained in this manner showed the same 47-day activity as obtained in the ether extractions.

The absorption in aluminum of the 47-day activity is shown in Fig. 2. (These data were taken with a much stronger sample than that shown in Fig. 1.) The majority of the electrons have a range of about 0.09 grams/cm², while a weak tail extends out to 0.35 grams/cm². By the use of Feather's relation[3] ($E=R+0.091/0.511$ where the energy E is in Mev and the range R is in grams/cm²) the energies of the two groups are found to be 0.4 Mev and 0.9 Mev. With the range-energy relation of Widdowson and Champion[4] (wherein the two constants of Feather's equation are altered to 0.165 and 0.536) the energies are about 0.5 and 1.0 Mev.

The gamma-ray absorption is also shown in Fig. 2, indicating a half-thickness of 10 grams/cm² Pb, which corresponds to an energy of about 1 Mev from the data of Gentner.[5]

The sign of the particles has been observed to be negative, by the use of simple magnetic deflection through air and also by a cloud chamber with magnetic field and by a trochoid analyzer, for which we are indebted to Dr. F. N. D. Kurie and Dr. E. Lyman.

IRON ACTIVITY OF 47 DAYS HALF-LIFE FROM Co+*n*

Several grams of C.P. cobalt oxide were left for three months in close proximity to the target chamber of the cyclotron in order to receive the neutrons released from the bombardment with deuterons of beryllium or other targets. A chemical separation for manganese, iron and cobalt was made, and an activity of approximately 47 days half-life was found in the iron fraction, as previously reported.[1] It was not possible to check the sign of the particles in this

[2] Noyes and Bray, *Qualitative Analysis for the Rare Elements* (Macmillan Company, 1927).

[3] Feather, Phys. Rev. **35**, 1559 (1930).

[4] Widdowson and Champion, Proc. Phys. Soc. **50**, 192 (1938).

[5] Gentner, J. de phys. et rad. **6**, 274 (1935).

weak sample. The decay curve is shown in Fig. 1. That the activity is really due to a transmutation of cobalt and not to iron impurity in the cobalt oxide, is attested to by the fact that the 47-day period has not been obtained from direct bombardment of iron with neutrons (see below).

Identification of the 47 Day Activity with Fe^{59}

Figure 3 shows the percent abundance of the stable Cr, Mn, Fe, Co and Ni isotopes as quoted by Livingston and Bethe.[6] It is at once apparent that only Fe^{59} can be negative electron active. Furthermore, the only radio-iron that can be made from cobalt with neutrons is Fe^{59}, so that we are justified in ascribing the 47-day activity to this isotope. The two transmutations are

$$_{26}Fe^{58}+{}_1D^2\rightarrow{}_{26}Fe^{59}+{}_1H^1$$

and

$$_{27}Co^{59}+{}_0n^1\rightarrow{}_{26}Fe^{59}+{}_1H^1.$$

Each is followed by

$$_{26}Fe^{59}\rightarrow{}_{27}Co^{59}+{}_{-1}e^0 \quad (47\text{ days}).$$

It might reasonably be expected that this activity should also occur after neutron bombardment of iron through $Fe^{58}(n,\gamma)Fe^{59}$, but we have been unable to detect the effect, even when borings were taken from the iron pole pieces of the cyclotron which had received neutron bombardment for many months. This may be understood from the very small abundance of Fe^{58} (0.5 percent) and the relatively small number of neutrons compared to deuterons.

Andersen[7] has reported a 3-day activity, following neutron irradiation of cobalt, said to be chemically identified with iron. We have not

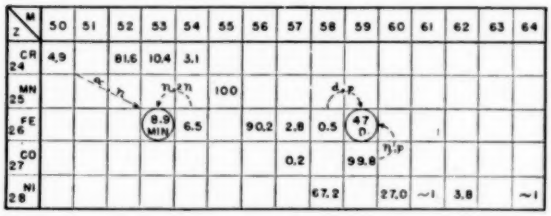

FIG. 3. Percent abundance of isotopes in the neighborhood of iron. Radioactive isotopes, with their half-lives, are encircled, the broken lines indicating the reactions by which they are produced.

[6] Livingston and Bethe, Rev. Mod. Phys. **9**, 380 (1938).
[7] Andersen, Nature **138**, 76 (1936).

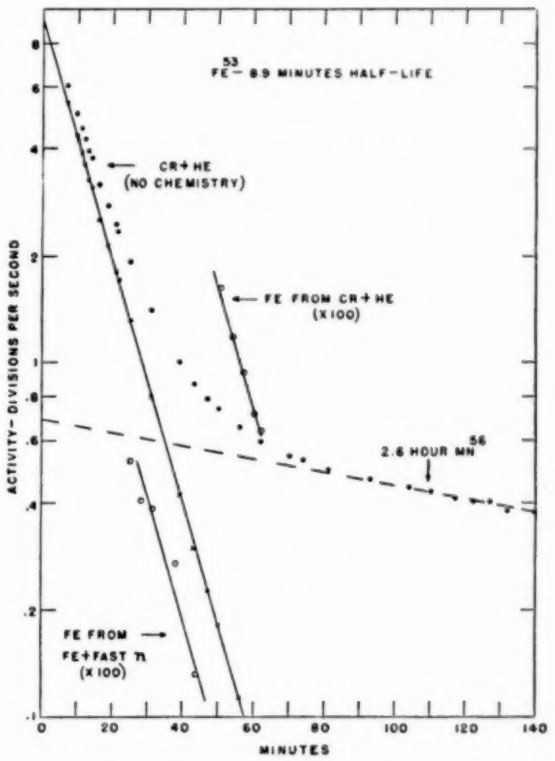
53 FE – 8.9 MINUTES HALF-LIFE
CR+HE (NO CHEMISTRY)
FE FROM CR+HE (X100)
2.6 HOUR MN 56
FE FROM FE+FAST n (X100)
ACTIVITY – DIVISIONS PER SECOND
MINUTES
0 20 40 60 80 100 120 140

FIG. 4. Decay curves of Fe^{53}.

detected this period on any occasion and are inclined to believe it to represent a poor determination of the 47-day activity, probably because of the weakness of the source.

The bombardment of nickel with neutrons has thus far failed to produce the 47-day period, although the reaction $Ni^{62}(n,\alpha)Fe^{59}$ might be expected. Ni^{62} is present to only 3.8 percent, which may account for this failure.

Iron Activity of 9 Minutes Half-Life from Cr+He

Henderson and Ridenour[8] have reported a radioactive iron of 8.9 ± 0.3 minutes half-life, which emits positrons, and which is produced by bombarding chromium with electrically accelerated alpha-particles of 9 Mev energy. They also find an electron emitting manganese isotope of 2.66 ± 0.25 hours half-life as a result of the same bombardment and ascribe it to the well-known Mn^{56} isotope, according to the reaction $Cr^{53}(\alpha,p)Mn^{56}$.

[8] Henderson and Ridenour, Phys. Rev. **52**, 889 (1937).

We have repeated this experiment with 16 Mev alpha-particles and confirm their results in every essential particular. Our values for the half-lives are 8.9±0.2 minutes and 2.60±0.05 hours. The decay curves are shown in Fig. 4, both for chemically separated iron and for an untreated sample which shows both the iron and manganese periods.

Iron Activity of 9 Minutes Half-Life from Fe+Fast Neutrons

We have not observed any activities ascribable to iron when bombarding this metal with neutrons from Be+D, but when the fast neutrons from Li+D are used, the 9-minute decay is obtained. If no chemical separation is made, the activity is composite, the 9-minute period is superimposed on the 2.6 hour Mn^{56} period. The Mn^{56} is formed on this occasion by $Fe^{56}(n, p)Mn^{56}$. The decay of the separated iron is shown in Fig. 3.

Identification of the 9-Minute Activity with Fe^{53}

Henderson and Ridenour assigned the 9-minute positron emitting isotope to either Fe^{53} or Fe^{55} through the two alternatives $Cr^{50, 52}(\alpha, n)Fe^{53, 55}$. With the former choice, the difficulty arises as to the fate of the radio-Mn^{53} which must be formed by the decay of Fe^{53}, since no second period was observed. We also have been unable to find any evidence of the decay of Mn^{53}, but in spite of this we believe the 9-minute activity to be due to Fe^{53} rather than to Fe^{55} because:

(1) it is not produced by deuteron or slow neutron bombardment of Fe,

(2) it is produced by fast neutrons on Fe,

(3) attempts to produce Fe^{55} by other reactions have not disclosed a 9 minute activity (see below).

We therefore conclude that the 9-minute period is formed by

$$_{24}Cr^{50}+{}_{2}He^{4}\rightarrow{}_{26}Fe^{53}+{}_{0}n^{1}$$

and by $$_{26}Fe^{54}+{}_{0}n^{1}\rightarrow{}_{26}Fe^{53}+2{}_{0}n^{1},$$

followed by

$$_{26}Fe^{53}\rightarrow{}_{25}Mn^{53}+{}_{1}e^{0} \quad (8.9 \text{ minutes}),$$

while the decay of Mn^{53} to stable Cr^{53} is still undetected.

It is interesting to note that this fast neutron effect on iron has a half-life almost identical with the 8 to 10 minutes given by Clay and his associates when reporting[9, 10] an activity induced in iron by cosmic rays. Recently Ramsey and the Montgomerys[11] have endeavored to repeat this cosmic-ray experiment, but were unable to confirm the effect.

Search for Fe^{55}

We have not found any iron activity after bombarding iron with protons at 3.6 Mev, although the transmutation $Mn^{55}(p, n)Fe^{55}$ might be expected. DuBridge and his associates have also made this experiment using 4 Mev protons and also report negative results.[12]

Only the reaction $Mn^{55}(d, 2n)Fe^{55}$ could lead to radioactive iron if manganese is exposed to deuterons. We have made this attempt on several occasions, but have not obtained any activities definitely attributable to iron.

The bombardment of chromium with alpha-particles could give $Cr^{52}(\alpha, n)Fe^{55}$, but the only iron period we have observed is the 9-minute one which has been assigned to Fe^{53} (see above).

Activation of cobalt with deuterons might be expected to produce Fe^{55} by the reaction $Co^{57}(d, \alpha)Fe^{55}$, but no iron activity has been found after a number of such attempts.

We have not found any iron periods after irradiating iron with slow neutrons and only the 9-minute period is disclosed when using fast neutrons. On one occasion the iron separated from a deuteron bombardment of iron was placed directly inside the electroscope, in case the radiations from Fe^{55} should not be able to penetrate the 0.0001-inch aluminum window; nothing but the 47-day period was observed.

Darling, Curtis and Cork[13] and ourselves[1] have found an 18-hour positron emitting cobalt isotope produced by deuterons on iron. This has been

[9] Clay and Van Tijn, Physica **4**, 909 (1937).
[10] Clay and Jonker, Physica **5**, 171 (1938).
[11] Ramsey, C. G. and D. D. Montgomery, Phys. Rev. **53**, 196 (1938).
[12] DuBridge, Barnes, Buck and Strain, Phys. Rev. **53**, 447 (1938).
[13] Darling, Curtis and Cork, Phys. Rev. **51**, 1011 (1937).

presumed to be Co^{55}, formed by $Fe^{54}(d, n)Co^{55}$. A second activity growing in the cobalt should be observed, if this is the case, as Co^{55} decays to Fe^{55} and this in turn to stable Mn^{55}. We have made very rapid separations of iron from radio-cobalt when the 18-hour activity was exceedingly strong, hoping to detect a shorter lived iron, but nothing was found. This procedure has been repeated at a much later time, in case Fe^{55} had a considerably longer life which would require more time for it to grow to an observable amount, but again with negative results.

The existence of a positron emitting cobalt of several months half-life (formed from deuterons on iron) has been announced.[1] The possibility was considered that this isotope might be Co^{55} and hence might be the source of Fe^{55}. Iron has been separated from such cobalt samples of various ages, from a few days to several months, but again without disclosing any evidence for Fe^{55}.

We must therefore fall back on the usual conclusions in such cases: Fe^{55} is stable, or it has a very short or a very long lifetime. (We are continuing to follow some of our iron samples, in case an activity longer than 47 days should ultimately appear.)

Detection of Gallium Impurity in Iron

During the course of the deuteron bombardments of iron, there were repeatedly obtained in the ether extract of $FeCl_3$ not only the 47-day period but also weak activities of 18 to 25 minutes and 14 to 20 hours half-lives, both emitting negative electrons. These activities were so feeble as to make it extremely unlikely that they should be ascribed to iron. Therefore possible impurities in the iron were considered which could give these periods and whose chlorides would be extracted in the ether. $GaCl_3$ would be so extracted, and the periods of gallium under slow neutron bombardment have been given by Amaldi[14] as 20 minutes and 23 hours.

A chemical separation of gallium and iron was made after another deuteron bombardment of iron. A little gallium was added to the acid solution of activated iron, as well as the usual manganese and cobalt. Since $FeCl_2$ is not soluble in ether, the iron was reduced to this form by the addition of mercury, and the $GaCl_3$ was then extracted with ether from a solution $6N$ in HCl. The $FeCl_2$ was then oxidized to $FeCl_3$ with HNO_3, and the $FeCl_3$ was separated from the Mn and Co by extraction with ether. The iron fraction showed only the 47-day period, while the gallium exhibited periods of 23 minutes and 14 hours. In as much as this was not in total accord with the results of Amaldi, we felt it desirable to activate gallium with slow neutrons for an independent check. This was done and a chemical separation for gallium, zinc and copper was made. The gallium fraction showed half-lives of 23 minutes and 14 hours. These figures are in close agreement with the 20 minutes and 14.1 hours quoted by Sagane,[15] who activated gallium with slow neutrons but without benefit of chemical identification.

The relative intensities of these gallium and 47-day iron activities, together with the known isotopic abundances and the duration and intensity of the bombardments, allows an estimate to be made of the amount of gallium present in the iron, on the assumption that the cross section for capturing the neutron out of the deuteron is the same for gallium as for iron. For example, one iron sample showed a gallium content of 6 parts in 10^6. One tenth this much could have been detected readily.

A number of other weak activities, due to impurities, have been found in some of the other bombardments discussed above. In certain cases identification has been possible, while in others no positive assignment has as yet been made.

Acknowledgments

This research has been materially aided by the support of the Chemical Foundation, the Research Corporation and the Josiah Macy Jr. Foundation, to which we express our greatest appreciation.

[14] Amaldi, D'Agostino, Fermi, Pontecorvo, Rasetti and Segrè, Proc. Roy. Soc. **A149**, 522 (1935).

[15] Sagane, Phys. Rev. **53**, 212 (1938).

Note on the Theory of the Neutral Particle

W. H. FURRY
Physics Research Laboratory, Harvard University, Cambridge, Massachusetts
(Received March 28, 1938)

Majorana has recently shown by using a special set of Dirac matrices that the symmetry properties of the Dirac equations make possible the elimination of the negative energy states in the case of a free particle. We present here a further investigation of this possibility, in a treatment based on an arbitrary Hermitian representation of the Dirac matrices instead of Majorana's special representation. The new procedure is compared with Schroedinger's early attempt to eliminate the negative energy states. The question of Lorentz invariance is discussed, and also the possibility of subjecting the particle to forces; it is found that the only sort of force having a classical analogue which is consistent with Majorana's way of eliminating the negative energy states is the nonelectric force of a scalar potential. The theory is worked through for this case, and it is pointed out that, in spite of the fact that the exclusion of negative energy states is accomplished without the introduction of antiparticles, the formalism still shows the stigmata associated with subtraction theories of the positron: the presence of otiose infinite terms which should be removed by subtraction, and the creation and destruction of pairs of particles. The application of Majorana's formalism to the theory of β-radioactivity is discussed at the end of the paper. Here the physical interpretation is quite different from that of the ordinary theory, since only neutrinos appear instead of the neutrinos and antineutrinos of the usual picture. The results predicted for all observed processes are nevertheless identical with those of the ordinary theory. An experimental decision between the formulation using neutrinos and antineutrinos and that using only neutrinos will apparently be even more difficult than the direct demonstration of the existence of the neutrino.

I. INTRODUCTION

IN a recent paper[1] Majorana has presented a derivation of a symmetrical theory of the electron and positron from a new type of variation principle whose use depends essentially on the fact that the quantities involved are q-numbers. In spite of this novel approach, the positron theory he obtains is essentially just a subtraction theory of the simplest type; but Majorana also showed how his ideas can be applied in the theory of the neutral particle to obtain a formalism essentially different from that of the ordinary Dirac theory. Qualitatively the difference appears in the number of states having the same momentum. In the Dirac theory as used at present there are four such states, corresponding to two alternatives for the spin orientation and to the possible existence of both the particles in question and their "antiparticles"—e.g., neutrinos and antineutrinos. In the Majorana theory there are just two states for a given momentum, corresponding to the two possibilities for the spin: there are no "antiparticles" and, in the final formulation, no mention of negative energy states.

As has been remarked by Racah,[2] a theory of Majorana's type cannot very reasonably be supposed to hold for neutrons because of their unsymmetrical relation to the two signs of charge and their possession of a magnetic moment. For the neutrino, however, the Majorana theory is *a priori* just as acceptable as the ordinary Dirac theory. It is interesting to find that it is possible to accomplish all the purposes for which the neutrino theory was devised, including the discussion of both electron emission and positron emission, without the introduction of antineutrinos. This point will be discussed further in the concluding section.

The main formal developments of the present paper are concerned with the generalization of the theory to allow the use of an arbitrary Hermitian representation of the Dirac matrices, instead of the special sort of representation to which Majorana's original treatment is restricted, and with the extension of the theory to include the action on the particles of the nonelectric field of a scalar potential.[3] Although such fields have not had to be postulated in any of the existing applications of the neutrino theory, their introduction into the present dis-

[1] E. Majorana, Nuovo Cimento **14**, 171 (1937).

[2] G. Racah, Nuovo Cimento **14**, 322 (1937).

[3] W. H. Furry, Phys. Rev. **50**, 784 (1936).

cussion is not without interest for two reasons: First, we are enabled to see that the Majorana theory still shows a strong resemblance to the usual Dirac theory, since in spite of the absence of antineutrinos we find that particles are produced in pairs; and second, it helps to bring clearly to light the spin behavior of the particles by showing the existence of a spin-orbit coupling.[4]

The emphasis will here be placed, not on Majorana's interesting new type of variation principle, concerning which we have nothing new to add, but on the application of a symmetry property of the Dirac equations by means of which Majorana accomplishes the elimination of the negative energy states. Before proceeding to the developments of the following sections, we wish to give a general discussion of this idea, comparing it especially with Schroedinger's early suggestion[5] for the elimination of the negative energy states of the electron.

In both cases we may take as the essential problem that of projecting the function space of the Dirac wave functions into one of two equal subspaces. But our use in this connection of the terms "projection" and "subspace" must at once be accompanied by a warning: In the Schroedinger case we are actually concerned with projection into a linear subspace according to the accepted definition[6] of these words, but this is not so in the Majorana case. In Section II we shall discuss in detail the unorthodox and rather artificial sense in which such terms may be used about Majorana's procedure. It is interesting that the procedure which is more artificial is also much more successful.

In the Schroedinger case the two subspaces are those of the positive energy and negative energy wave functions of a free particle, and the projection is to consist in omitting the negative energy components of any given wave function. That is, if

$$\psi=\psi^{(+)}+\psi^{(-)}, \tag{I 1}$$

where $\psi^{(+)}$ consists of positive energy functions of a free particle and $\psi^{(-)}$ of negative energy functions, then the projection is given by

$$\psi\rightarrow\psi^{(+)}. \tag{I 2}$$

This can be formulated in general by using the operator[7] given in the p-representation by

$$\Lambda=(-\boldsymbol{\alpha}\cdot\mathbf{p}-\beta mc)(m^2c^2+p^2)^{-\frac{1}{2}}, \tag{I 3}$$

which has the property

$$\Lambda\psi^{(+)}=\psi^{(+)};\quad \Lambda\psi^{(-)}=-\psi^{(-)}. \tag{I 4}$$

Schroedinger's projection is then simply

$$\psi\rightarrow\tfrac{1}{2}(1+\Lambda)\psi. \tag{I 5}$$

It is well known that an essential difficulty with Schroedinger's suggestion is that it is not relativistically invariant. A Lorentz transformation of ψ is accomplished by an operator $L(a^{\nu}{}_{\mu})$:

$$\begin{aligned}\psi'(x'^{\sigma})&=L(a^{\nu}{}_{\mu})\psi(x^{\lambda})=S(a^{\nu}{}_{\mu})A(a^{\nu}{}_{\mu})\psi(x^{\lambda})\\&=S(a^{\nu}{}_{\mu})\psi(a^{\nu}{}_{\mu}x'^{\mu}).\end{aligned} \tag{I 6}$$

Here $a^{\nu}{}_{\mu}$ is the Lorentz transformation of the coordinates, and $S(a^{\nu}{}_{\mu})$ is the corresponding four-rowed matrix operating on the components of the Dirac wave function.[8] The noninvariance of (I 5) then results from the fact that Λ and L do not commute:

$$\Lambda L-L\Lambda\neq 0. \tag{I 7}$$

The projection (I 5) also has the disadvantage that after a wave function has been projected into the positive-energy subspace it will not remain confined to that subspace if the particle is subject to forces of any ordinary sort. This is because Λ does not commute with the Dirac Hamiltonian for a bound particle. Schroedinger accordingly suggested that the terms admitted to the Hamiltonian be restricted to "even" operators, i.e., those which do not connect the two subspaces, or in other words those which commute with Λ. It is well known that this procedure leads to difficulties not only with invariance but also with the physical results of the theory.

It is interesting to note that although the operator $\Lambda L-L\Lambda$ is not equal to zero, it gives

[4] Cf. D. R. Inglis, Phys. Rev. **50**, 783 (1936).
[5] E. Schroedinger, Berl. Ber. p. 63, 1931.
[6] Cf. J. von Neumann, *Math. Grundlagen der Quantenmechanick*, p. 40.
[7] Cf. W. Pauli, *Handbuch der Physik*, Vol. 24, pp. 230–231.
[8] Cf. reference 7, p. 221.

the result zero when applied to any *free particle* wave function. This assertion may at first sight seem to be inconsistent with the possibility of analyzing an arbitrary wave function in terms of free particle wave functions, which is postulated in (I 1). But the analysis (I 1) and the projection (I 5) make use only of the instantaneous values of ψ throughout space, and it is only for such three-dimensional purposes that the free particle wave functions form a complete set. It is, however, obviously impossible either to make the Lorentz transformation (I 6) or to tell whether or not ψ is actually just a free particle function unless one makes use of the time dependence of ψ as well as its instantaneous values. If ψ_f is any wave function whose time dependence is that given by the Dirac equation without field, then on using this time dependence in making the Lorentz transformation, one indeed finds that

$$(\Lambda L - L\Lambda)\psi_f = 0. \qquad \text{(I 7')}$$

It is this fact which makes it possible to use the wave functions of a free electron as a basis for constructing a positron theory which is at least formally Lorentz invariant, although in practice the invariance is destroyed by divergence difficulties. In using the method of second quantization to set up the formalism of positron theory one of course uses wave functions with the time factors removed; but Lorentz transformations may be made correctly by using the p-representation and regarding p as the space part of a four-vector whose time component is $\pm(m^2c^2+p^2)^{\frac{1}{2}}$. Thus without explicit reference to the time factor one can still verify that $\Lambda L - L\Lambda$ gives zero when applied to such a function.[9]

The projection used by Majorana may be defined for an arbitrary representation of the Dirac matrices by using an operator A which was previously used by the writer to prove a symmetry theorem in the positron theory.[10] The existence of this operator and its unique determination apart from a phase factor have been proved by Pauli.[11] The operator A is a constant unitary four-rowed matrix, and has the property that if ψ is any pure positive energy free particle wave function, then $A\psi$ is the complex conjugate of a pure negative energy function; and if ψ is any pure negative function, $A\psi$ is the complex conjugate of a pure positive function. Majorana's projection is given by

$$\psi \rightarrow \tfrac{1}{2}\{\psi + (A\psi)^*\}, \qquad \text{(I 8)}$$

where $(A\psi)^*$ is the complex conjugate of $A\psi$.

In the next section we shall show that the operation indicated in (I 8) has the important property of being idempotent, which enables us to regard it in a certain sense[12] as a projection operator; that the projection into the other of the two equal subspaces is given by

$$\psi \rightarrow \tfrac{1}{2}\{\psi - (A\psi)^*\}; \qquad \text{(I 9)}$$

that the projection (I 8) is relativistically invariant; and that the wave function will remain confined to the subspace if the wave equation is that of a free particle or a particle subject to a nonelectric force,[3] but not if the particle has an electric charge or a magnetic moment introduced as suggested by Pauli.[13]

It is seen from the stated properties of A and the form of (I 8) that instead of discarding the negative energy states Majorana's projection may in a sense be regarded as symmetrizing the wave function with respect to positive and negative states. The fact that the phase of A is not fixed by its definition in terms of its properties shows, however, that one has no right to attach the terms "symmetric" and "antisymmetric" to the functions given by (I 8) and (I 9), respectively.

II. Properties of Majorana's Projection

Notation. In the Dirac theory of a single particle there occur four-row square matrices such as α_i and A, four-row one-column matrices such as the wave function ψ, and one-row four-

[9] It may be remarked that this same circumstance makes Schroedinger's procedure work just as well as Majorana's for the case of a *free particle*, which is the only case Majorana discusses for the neutral particle. The extension to the case of a nonelectric force (Section III) and the application to β-radioactivity (Section IV) are, however, impossible in the Schroedinger case.

[10] W. H. Furry, Phys. Rev. **51**, 125 (1937).

[11] W. Pauli, Ann. Inst. Henri Poincare **6**, 130 (1936). The matrix in question is there denoted by C.

[12] But not at all in the usual sense—cf. Section II and reference 6.

[13] Reference 7, p. 233.

column matrices such as the Hermitian adjoint of ψ. In dealing with such matrices we shall use an asterisk (*) to indicate the complex conjugate matrix, a prime (′) to indicate the transposed matrix, and a dagger (†) to indicate the Hermitian adjoint matrix. Similar notations hold for the two-row and/or two-column matrices which are introduced in the latter part of Section III.

It is important to note carefully how the notation is to be interpreted when we come to apply the method of second quantization, and regard the components of the wave function as q-numbers. Since when the ψ's are c numbers $\psi_i+\psi_i^*$ is a real number, when the ψ's are q-numbers $\psi_i+\psi_i^*$ must be a real q number, or in other words a self-adjoint operator. Thus *when the ψ's are operators, ψ_i^* must be the Hermitian adjoint operator to ψ_i.* By ψ we mean the one-column matrix with the components ψ_1, ψ_2, ψ_3, ψ_4, and by ψ' the one-row matrix with the same components; by ψ^* we mean the one-column matrix with the components ψ_1^*, ψ_2^*, ψ_3^*, ψ_4^*, and by $\psi^\dagger$ the one-row matrix with these components. Such symbols as ψ_i' and $\psi_i^\dagger$ will never be used. The concept of transposition is indeed not a suitable one to be introduced with regard to operators in general, since it is not invariant under canonical transformations and its meaning depends on the representation used. Its use in the case of the matrices of the Dirac theory is, however, free from ambiguity and offers well-known advantages in the way of shortening the formulas.

The matrix A and the projections. We shall develop the theory for an arbitrary Hermitian representation of the Dirac matrices, and we shall denote this set of matrices by α_i, β or by $\boldsymbol{\alpha}$, β. Corresponding to this representation of the Dirac matrices there is a certain matrix A, uniquely determined except for phase, which has the properties described in the introduction. The conditions on this matrix are[14]

$$A^\dagger A=1. \tag{1}$$

$$\begin{aligned}\alpha_i' A &= A\alpha_i,\\ \beta' A &= -A\beta.\end{aligned} \tag{2}$$

Pauli has shown[15] that A also satisfies

$$A^*A=1. \tag{3}$$

From (1) and (3) we see that

$$A'=A. \tag{4}$$

We now represent the projections (I 8) and (I 9) by $\psi\rightarrow P\psi$ and $\psi\rightarrow I\psi$, respectively, with

$$P\psi=\tfrac{1}{2}(\psi+A^*\psi^*), \tag{5}$$

$$I\psi=\tfrac{1}{2}(\psi-A^*\psi^*). \tag{5′}$$

The operators P and I obviously satisfy

$$P+I=1 \tag{6}$$

and we can readily show that they also satisfy

$$P^2=P, \qquad I^2=I \tag{7}$$

and

$$PI=IP=0. \tag{8}$$

The meaning of such equations is of course that the application of the left member to an arbitrary ψ gives the same result as the application of the right member. To prove (7) and (8), we have only to substitute from (5) and (5′) and use (3). For instance,

$$\begin{aligned}P^2\psi &= P\cdot\tfrac{1}{2}(\psi+A^*\psi^*)\\ &= \tfrac{1}{2}\{\tfrac{1}{2}(\psi+A^*\psi^*)+A^*\cdot\tfrac{1}{2}(\psi+A^*\psi^*)^*\}\\ &= \tfrac{1}{2}(\psi+A^*\psi^*)=P\psi. \qquad \text{Q.E.D.}\end{aligned}$$

Equation (7) expresses the fact that the operators P and I are idempotent, a property which a projection operator must possess, and (6) and (8) indicate that the "subspaces" into which the two operators project are collectively exhaustive and mutually exclusive.

In order, however, for an operator to be a projection operator associated with a linear subspace, it must be not only idempotent but linear and Hermitian;[6] and it is obvious from (5) and (5′) that our operators P and I are *not linear*. What we have called the "subspaces" defined by these operators are accordingly not subspaces in the usual sense, i.e., not *linear subspaces;* for from

$$\begin{aligned}P\psi&=\psi, \qquad I\psi=0,\\ P\varphi&=\varphi, \qquad I\varphi=0\end{aligned}$$

[14] Reference 10, Eq. (10) and (14).

[15] Reference 11, Eq. (33a).

we cannot conclude that

$$P(a\psi+b\varphi)=a\psi+b\varphi, \qquad I(a\psi+b\varphi)=0,$$

unless a and b are real numbers. The subspaces of the Majorana projection are invariant under Lorentz transformation and under time displacement as determined by the Dirac equations of a particle subject to a nonelectric force, as we shall show below, but they are not invariant under simple multiplication by a complex constant. This makes the theory look rather artificial, but does not interfere with its success, because such multiplication plays no part in it.

Lorentz invariance. The projection is Lorentz invariant because it makes no difference whether one makes a Lorentz transformation before or after the projection operator is applied:

$$L(a^{\nu}{}_{\mu})P\psi=PL(a^{\nu}{}_{\mu})\psi. \tag{9}$$

Proof: Since the operations involved in applying P have nothing to do with the dependence of ψ on the x^{μ}, (9) is equivalent to

$$S(a^{\nu}{}_{\mu})P\psi=PS(a^{\nu}{}_{\mu})\psi. \tag{10}$$

By (5), (10) becomes

$$S(a^{\nu}{}_{\mu})\cdot\tfrac{1}{2}(\psi+A^*\psi^*)=\tfrac{1}{2}\{S(a^{\nu}{}_{\mu})\psi+A^*S^*(a^{\nu}{}_{\mu})\psi^*\}$$

and this is true for an arbitrary ψ if

$$S(a^{\nu}{}_{\mu})A^*=A^*S^*(a^{\nu}{}_{\mu}). \tag{11}$$

Now $S(a^{\nu}{}_{\mu})$ can be represented as a product of factors of the following types:

Rotation in (i, j) plane:

$$S=e^{(\theta/2)\alpha_i\alpha_j}$$

Velocity along j axis:

$$S=e^{(\theta/2)\alpha_j} \tag{12}$$

Reflection of the i axis:

$$S=i\alpha_j\alpha_k\beta,\ j\neq i\neq k\neq j$$

Reflection of the time axis:

$$S=i\alpha_1\alpha_2\alpha_3\beta.$$

On making use of (2) and of the Hermitian character of α and β, one finds that (11) is satisfied by any product of factors of the forms (12), so that the truth of (10) is established.

Because of the noninvariance of the projection P under change of phase, the phase factors in $S(a^{\nu}{}_{\mu})$ must be kept the same as specified in (12), apart from a possible factor -1. The necessity of fixing these phase factors in a definite way in order for (11) to hold has been pointed out by Racah,[2] who calls attention to the fact that these factors have a significance for the choice of the interaction operator in Fermi's original theory of β-decay.

Persistance of the projection in time. The Dirac equations are

$$\partial\psi/\partial t=D\psi, \tag{13}$$

where D is an operator whose various possible forms are listed below. According to (13), if ψ had the value ψ_0 at $t=0$, its value at a later time is

$$\psi=e^{Dt}\psi_0. \tag{14}$$

We now want to investigate whether

$$P\psi_0=\psi_0, \qquad I\psi_0=0,$$

together with (14), implies that

$$P\psi=\psi, \qquad I\psi=0.$$

This will be so if P and I commute with e^{Dt}, or in other words if

$$PD\psi=DP\psi, \qquad ID\psi=DI\psi \tag{15}$$

for arbitrary ψ. Substituting from (5) and (6), we find that (15) will hold for arbitrary ψ if and only if

$$DA^*=A^*D^*. \tag{16}$$

Now D is just $(i\hbar)^{-1}$ times the Dirac Hamiltonian for the particle. Thus it must contain the terms

$$D_0=(i\hbar)^{-1}\{i\hbar c(\boldsymbol{\alpha}\cdot\nabla)-\beta mc^2\} \tag{17}$$

for a free particle, together with terms representing any interactions of the particle with fields of force. The known possibilities for forces having classical analogs are:

$$\begin{aligned}
&D_1=(i\hbar)^{-1}\{e(\boldsymbol{\alpha}\cdot\mathbf{A})+e\varphi\}\\
&\qquad\text{(charge } e \text{ on particle)},\\
&D_2=(i\hbar)^{-1}\{-\mu(\beta\boldsymbol{\sigma}\cdot\mathbf{H})-i\mu(\beta\boldsymbol{\alpha}\cdot\mathbf{E})\}\\
&\qquad\text{(magnetic moment } \mu),\\
&D_3=(i\hbar)^{-1}\{-\beta\Phi\}\\
&\qquad\text{(nonelectric potential energy } \Phi).
\end{aligned} \tag{18}$$

By use of (2), we find that (16) is satisfied for

$$D=D_0+D_3 \tag{19}$$

but not if D_1 or D_2 is included in D. Thus if the wave function is to remain confined to one Majorana subspace the only one of these three kinds of force that can act on the particle is the nonelectric force.

Commutation relations. Hitherto we have been concerned only with certain linear conditions satisfied by the wave function before and after projection. In what follows we shall have to introduce bilinear expressions, and use the technique of second quantization, so that it will be necessary to know the commutation rules obeyed by the components of the projected wave function. Assuming the four components of ψ to satisfy the usual Jordan-Wigner[16] relations

$$\begin{aligned}\psi_i^*(\mathbf{r})\psi_j(\mathbf{r}')+\psi_j(\mathbf{r}')\psi_i^*(\mathbf{r})&=\delta_{ij}\delta(\mathbf{r}-\mathbf{r}'),\\ \psi_i(\mathbf{r})\psi_j(\mathbf{r}')+\psi_j(\mathbf{r}')\psi_i(\mathbf{r})&=0,\\ \psi_i^*(\mathbf{r})\psi_j^*(\mathbf{r}')+\psi_j^*(\mathbf{r}')\psi_i^*(\mathbf{r})&=0.\end{aligned}\tag{20}$$

We find on using (5) that the four components of the function U defined by

$$U=P\psi \tag{21}$$

satisfy the relations

$$\begin{aligned}U_i^*(\mathbf{r})U_j(\mathbf{r}')+U_j(\mathbf{r}')U_i^*(\mathbf{r})&=\tfrac{1}{2}\delta_{ij}\delta(\mathbf{r}-\mathbf{r}'),\\ U_i(\mathbf{r})U_j(\mathbf{r}')+U_j(\mathbf{r}')U_i(\mathbf{r})&=\tfrac{1}{2}A_{ij}{}^*\delta(\mathbf{r}-\mathbf{r}'),\\ U_i^*(\mathbf{r})U_j^*(\mathbf{r}')+U_j^*(\mathbf{r}')U_i^*(\mathbf{r})&=\tfrac{1}{2}A_{ij}\delta(\mathbf{r}-\mathbf{r}')\end{aligned}\tag{22}$$

III. Transformation of the Hamiltonian Function

The inclusion of a nonelectric potential energy represented, for a single particle, by the scalar function $\Phi(\mathbf{r})$ makes no difference whatever in Majorana's derivation of his Hamiltonian from his special variation principle. With this modification, his result is

$$H=\int U_M'(\mathbf{r})\mathfrak{H}_M U_M(\mathbf{r})dt=\int U_M'(\mathbf{r})$$
$$\times\{i\hbar c(\boldsymbol{\alpha}_M\cdot\nabla)-\beta_M(mc^2+\Phi(\mathbf{r}))\}U_M(\mathbf{r})d\tau. \tag{23}$$

Here U_M is a purely real four-component function, or, more strictly, a set of four self-adjoint operators which are functions of $\mathbf{r}$. $\mathfrak{H}_M$ is the Dirac Hamiltonian for a single particle, expressed in terms of a specially chosen representation of the Dirac matrices, denoted by α_M, β_M, which satisfy

$$\boldsymbol{\alpha}_M{}^*=\boldsymbol{\alpha}_M{}'=\boldsymbol{\alpha}_M;\quad \beta_M{}^*=\beta_M{}'=-\beta_M. \tag{24}$$

For this representation, a suitable form of the operator A is

$$A_M=1, \tag{25}$$

as is seen by comparing (24) with (2). Then $P_M\psi_M$ is simply the real part of ψ_M—more strictly the "self-adjoint part"—and this is indeed what Majorana took as U_M.

Majorana's Hamiltonian (23) differs from the Hamiltonian of the ordinary Dirac theory,

$$\int\psi_M{}^\dagger(\mathbf{r})\mathfrak{H}_M\psi_M(\mathbf{r})d\tau, \tag{23'}$$

only by the omission of the term

$$\int V_M'(\mathbf{r})\mathfrak{H}_M V_M(\mathbf{r})d\tau, \tag{23''}$$

where $V_M=-iI_M\psi_M$, $\psi_M=U_M+iV_M$. The components of V_M all anticommute with all the components of U_M, so that any function of V_M commutes with the Hamiltonian (23). If terms of the types $i\hbar D_1$ and $i\hbar D_2$ defined in Eq. (18) were included in $\mathfrak{H}_M$, the expression (23') would contain not only the terms (23) and (23''), but also cross terms in U_M and V_M. Majorana's way of treating the Hamiltonian (23') by separating ψ_M into the two terms U_M and iV_M then leads directly to a simple subtraction theory of the electron and positron.

We shall now show in detail how the Hamiltonian (23) forms the basis of a theory in which there is just one type of particle, with two states for a given momentum, corresponding to two different spin orientations. First we shall free ourselves from the restriction to the special representation $\boldsymbol{\alpha}_M$, β_M for the Dirac matrices.

By a well-known general theorem,[17] the representation $\boldsymbol{\alpha}_M$, β_M is connected with our represen-

[16] P. Jordan and E. Wigner, Zeits. f. Physik **47**, 631 (1928).

[17] Cf. reference 11, p. 109. The representations of the Dirac matrices used there are not subject to the restriction that they be Hermitian, so that the transformation matrix need not be unitary.

tation α, β by a unitary transformation:

$$\alpha_M = T^\dagger \alpha T, \quad \beta_M = T^\dagger \beta T, \quad T^\dagger T = 1. \tag{26}$$

These relations suggest that we should subject (23) to the substitution

$$U_M = T^\dagger U, \quad U_M' = U^\dagger T \tag{27}$$

and regard the result as the Hamiltonian expressed in terms of our function U which satisfies the commutation relations (22).

To justify this procedure we shall show that (27) establishes a one-to-one correspondence between the set of all possible quantities satisfying

$$PU = U, \qquad IU = 0 \tag{21'}$$

and all possible real four-component quanties U_M. This is most readily proved by noting that according to (24) and (26) all of the conditions (1)–(4) on A are satisfied by

$$A = T^* T^\dagger. \tag{28}$$

Then $IU=0$ means $U = A^* U^*$, and $T^\dagger U = T^\dagger A^* U^* = T' U^* = (T^\dagger U)^*$, so that if U satisfies (21'), $T^\dagger U$ is real. Conversely, if U_M is real, $A^*(TU_M)^* = TT'T^* U_M = TU_M$, so that TU_M satisfies (21'). The fact that the phase of A is arbitrary is exactly taken care of by the arbitrariness of the phase of T, which makes no difference in the final result of substituting (27) in (23).

Majorana establishes the Lorentz invariance of his formalism by relating it to the general results of applying the Jordan-Wigner method to the Dirac theory. That the invariance is not damaged by the substitution (27) follows from the fact that corresponding Lorentz transformation matrices in the two formalisms are connected by the similarity transformation (26):

$$S_M = T^\dagger S T, \quad \text{so that} \quad U_M = T^\dagger U$$

implies $$S_M U_M = T^\dagger S U.$$

On substituting (27) in (23) and using (26), we have

$$H = \int U^\dagger(\mathbf{r}) \{ ihc(\boldsymbol{\alpha}\cdot\nabla) - \beta(mc^2 + \Phi(\mathbf{r})) \} U(\mathbf{r}) d\tau. \tag{29}$$

We now set

$$U(\mathbf{r}) = \Sigma(\mathbf{k})(\mathbf{r}|\mathbf{k}) a(\mathbf{k}), \tag{30}$$

where

$$(\mathbf{r}|\mathbf{k}) = (\mathbf{k}|\mathbf{r})^* = V^{-\frac{1}{2}} \exp\{ i(mc/\hbar)\mathbf{k}\cdot\mathbf{r} \} \tag{31}$$

and $a(\mathbf{k})$ is a four-component quantity; we suppose the allowed values of $\mathbf{k}$ made denumerable by imposition of the usual periodic boundary condition in a box of volume V, and the integral in (29) extended over this volume. Then

$$H = mc^2 \Sigma(\mathbf{k}) a^\dagger(\mathbf{k}) \{ -(\boldsymbol{\alpha}\cdot\mathbf{k}) - \beta \} a(\mathbf{k}) - \Sigma(\mathbf{k}, \mathbf{k}') a^\dagger(\mathbf{k}) (\mathbf{k}|\Phi|\mathbf{k}') \beta a(\mathbf{k}'), \tag{32}$$

where $$(\mathbf{k}|\Phi|\mathbf{k}') = \int_V (\mathbf{k}|\mathbf{r}) \Phi(\mathbf{r}) (\mathbf{r}|\mathbf{k}') d\tau. \tag{33}$$

Relations satisfied by $a_i(\mathbf{k})$ and $a_i^*(\mathbf{k})$. From (22) and (31) it follows that the commutation relations for these quantities are:

$$\begin{aligned} &a_i^*(\mathbf{k}) a_j(\mathbf{k}') + a_j(\mathbf{k}') a_i^*(\mathbf{k}) = \tfrac{1}{2}\delta_{ij}\delta(\mathbf{k}', \mathbf{k}), \\ &a_i(\mathbf{k}) a_j(\mathbf{k}') + a_j(\mathbf{k}') a_i(\mathbf{k}) = \tfrac{1}{2} A_{ij}^* \delta(-\mathbf{k}', \mathbf{k}), \\ &a_i^*(\mathbf{k}) a_j^*(\mathbf{k}') + a_j^*(\mathbf{k}') a_i^*(\mathbf{k}) = \tfrac{1}{2} A_{ij} \delta(-\mathbf{k}', \mathbf{k}). \end{aligned} \tag{34}$$

By substituting (5) and (30) into (21'), multiplying by $(\mathbf{k}|\mathbf{r})$ and integrating, one finds the linear relations

$$\begin{aligned} a(\mathbf{k}) &= A^* a^*(-\mathbf{k}), \\ a^*(\mathbf{k}) &= A a(-\mathbf{k}). \end{aligned} \tag{35}$$

It is readily verified that (34) and (35) are consistent with each other.

We now make a linear substitution on the $a(\mathbf{k})$ and $a^*(\mathbf{k})$, in order to diagonalize the free-particle terms in (32). Set

$$\begin{aligned} a(\mathbf{k}) &= S(\mathbf{k}) b(\mathbf{k}), \\ a^\dagger(\mathbf{k}) &= b^\dagger(\mathbf{k}) S^\dagger(\mathbf{k}). \end{aligned} \tag{36}$$

Here $S(\mathbf{k})$ is required to satisfy the conditions

$$S^\dagger(\mathbf{k}) S(\mathbf{k}) = 1, \tag{37}$$

$$S^\dagger(\mathbf{k}) \{ -(\boldsymbol{\alpha}\cdot\mathbf{k}) - \beta \} S(\mathbf{k}) = \epsilon\rho_3 = (1+k^2)^{\frac{1}{2}} \rho_3. \tag{38}$$

ρ_3 is one of the matrices originally defined by Dirac:[18]

$$\rho_3 = \begin{pmatrix} 1 & 0 \\ 0 & -1 \end{pmatrix}, \tag{39}$$

[18] P. A. M. Dirac, Proc. Roy. Soc. **A117**, 614 (1928).

the 0's and 1's being two-rowed matrices. Thus by (38) the free-particle terms are diagonalized, the four eigenvalues for a given $\mathbf{k}$ being ϵ, ϵ, $-\epsilon$, $-\epsilon$.

The existence of a matrix which satisfies (37) and (38) is most easily shown by exhibiting one, as we shall do later. Here we shall show that if $S_1(\mathbf{k})$ and $S_2(\mathbf{k})$ both satisfy (37) and (38), then

$$S_2(\mathbf{k}) = S_1(\mathbf{k}) \begin{pmatrix} \mathbf{u}_1(\mathbf{k}) & \mathbf{0} \\ \mathbf{0} & \mathbf{u}_2(\mathbf{k}) \end{pmatrix}, \tag{40}$$

where $\mathbf{u}_1$ and $\mathbf{u}_2$ are two-rowed unitary matrices. Proof: By (37) and (38),

$$S_1\rho_3 S_1^\dagger = S_2\rho_3 S_2^\dagger = \epsilon^{-1}\{-(\boldsymbol{\alpha}\cdot\mathbf{k}) - \beta\}.$$

Then
$$\rho_3 S_1^\dagger S_2 = S_1^\dagger S_2 \rho_3$$

and by an elementary result in matrix theory[19] it follows from (39) that

$$S_1^\dagger S_2 = \begin{pmatrix} \mathbf{u}_1 & \mathbf{0} \\ \mathbf{0} & \mathbf{u}_2 \end{pmatrix}.$$

The unitary character of $\mathbf{u}_1$ and $\mathbf{u}_2$, and (40) itself, then follow from (37).

The result of substituting (36) in (32) is

$$H = \Sigma(\mathbf{k})\epsilon mc^2 b^\dagger(\mathbf{k})\rho_3 b(\mathbf{k})$$
$$- \Sigma(\mathbf{k}, \mathbf{k}')b^\dagger(\mathbf{k})S^\dagger(\mathbf{k})(\mathbf{k}|\Phi|\mathbf{k}')\beta S(\mathbf{k}')b(\mathbf{k}'). \tag{41}$$

Relations satisfied by $b_i(\mathbf{k})$ and $b_i^*(\mathbf{k})$. From (34) and (36) we obtain the commutation relations

$$b_i^*(\mathbf{k})b_j(\mathbf{k}') + b_j(\mathbf{k}')b_i^*(\mathbf{k}) = \tfrac{1}{2}\delta_{ij}\delta(\mathbf{k}', \mathbf{k}),$$
$$b_i(\mathbf{k})b_j(\mathbf{k}') + b_j(\mathbf{k}')b_i(\mathbf{k}) = \tfrac{1}{2}T_{ij}^*(\mathbf{k})\delta(-\mathbf{k}', \mathbf{k}), \tag{42}$$
$$b_i^*(\mathbf{k})b_j^*(\mathbf{k}') + b_j^*(\mathbf{k}')b_i^*(\mathbf{k}) = \tfrac{1}{2}T_{ij}(\mathbf{k})\delta(-\mathbf{k}', \mathbf{k}),$$

where
$$T(\mathbf{k}) = S'(\mathbf{k})AS(-\mathbf{k}). \tag{43}$$

From (35) and (36) we get the linear relations

$$b(\mathbf{k}) = T^*(\mathbf{k})b^*(-\mathbf{k}),$$
$$b^*(\mathbf{k}) = T(\mathbf{k})b(-\mathbf{k}), \tag{44}$$

(42) and (44) are of course consistent.

The elimination from (41) of any reference to the negative energy states is made possible by the nature of the relations (44). We shall show that

$$T(\mathbf{k}) = \begin{pmatrix} \mathbf{0} & \mathbf{u}(\mathbf{k}) \\ \mathbf{v}(\mathbf{k}) & \mathbf{0} \end{pmatrix}, \tag{45}$$

where $\mathbf{u}(\mathbf{k})$ and $\mathbf{v}(\mathbf{k})$ are two-rowed unitary matrices. The proof is similar to that of (40). By (38) we have, since $\boldsymbol{\alpha}$, β are Hermitian,

$$S(-\mathbf{k})\rho_3 S^\dagger(-\mathbf{k}) = \epsilon^{-1}\{(\boldsymbol{\alpha}\cdot\mathbf{k}) - \beta\} \tag{46}$$

and
$$S^*(\mathbf{k})\rho_3 S'(\mathbf{k}) = \epsilon^{-1}\{-(\boldsymbol{\alpha}'\cdot\mathbf{k}) - \beta'\}. \tag{47}$$

Now by (2), if we multiply (46) by A from the left and (47) by A from the right, the right-hand members become equal and opposite. Thus we have

$$AS(-\mathbf{k})\rho_3 S^\dagger(-\mathbf{k}) = -S^*(\mathbf{k})\rho_3 S'(\mathbf{k})A.$$

On multiplying this from the left by $S'(\mathbf{k})$ and from the right by $S(-\mathbf{k})$, we have

$$T(\mathbf{k})\rho_3 = -\rho_3 T(\mathbf{k}) \tag{48}$$

and it is readily seen from (39) that a unitary matrix which anticommutes with ρ_3 must be of the form (45).

Accordingly we have

$$b(\mathbf{k}) = \begin{pmatrix} \mathbf{0} & \mathbf{u}^*(\mathbf{k}) \\ \mathbf{v}^*(\mathbf{k}) & \mathbf{0} \end{pmatrix} b^*(-\mathbf{k}). \tag{49}$$

In order to eliminate $b_3(\mathbf{k})$ and $b_4(\mathbf{k})$ from H we want to use for the one-column matrix $b(\mathbf{k})$ the expression

$$b(\mathbf{k}) = \begin{vmatrix} b_1(\mathbf{k}) \\ b_2(\mathbf{k}) \\ v_{11}^* b_1^*(-\mathbf{k}) + v_{12}^* b_2^*(-\mathbf{k}) \\ v_{21}^* b_1^*(-\mathbf{k}) + v_{22}^* b_2^*(-\mathbf{k}) \end{vmatrix}. \tag{50}$$

The actual use of the expression (50) and of an analogous expression for the one-row matrix $b^\dagger(\mathbf{k})$ is not at all difficult, but involves a considerable amount of writing. A simple way to get the same result is to make the substitutions

$$b(\mathbf{k}) \to b(\mathbf{k}) + T^*(\mathbf{k})b^*(-\mathbf{k}),$$
$$b^\dagger(\mathbf{k}) \to b^\dagger(\mathbf{k}) + b'(-\mathbf{k})T'(\mathbf{k}) \tag{51}$$

[19] Cf. E. Wigner, *Gruppentheorie*, p. 10.

in (41), and then discard all terms involving $b_3(\mathbf{k})$, $b_4(\mathbf{k})$, $b_3^*(\mathbf{k})$ and $b_4^*(\mathbf{k})$. The result is

$$\begin{aligned}H=&\tfrac{1}{2}\Sigma(\mathbf{k})\epsilon mc^2\{B^\dagger(\mathbf{k})[\rho_3]^0B(\mathbf{k})\\&+B^\dagger(\mathbf{k})[\rho_3T^*(\mathbf{k})]^0B^*(-\mathbf{k})\\&+B'(-\mathbf{k})[T'(\mathbf{k})\rho_3]^0B(\mathbf{k})\\&+B'(-\mathbf{k})[T'(\mathbf{k})\rho_3T^*(\mathbf{k})]^0B^*(-\mathbf{k})\}\\&-\tfrac{1}{2}\Sigma(\mathbf{k},\mathbf{k}')(\mathbf{k}|\Phi|\mathbf{k}')\{B^\dagger(\mathbf{k})[S^\dagger(\mathbf{k})\beta S(\mathbf{k}')]^0B(\mathbf{k}')\\&+B^\dagger(\mathbf{k})[S^\dagger(\mathbf{k})\beta S(\mathbf{k}')T^*(\mathbf{k}')]^0B^*(-\mathbf{k}')\\&+B'(-\mathbf{k})[T'(\mathbf{k})S^\dagger(\mathbf{k})\beta S(\mathbf{k}')]^0B(\mathbf{k}')\\&+B'(-\mathbf{k})[T'(\mathbf{k})S^\dagger(\mathbf{k})\beta S(\mathbf{k}')T^*(\mathbf{k}')]^0\\&\times B^*(-\mathbf{k}')\},\end{aligned}\tag{52}$$

where $[M]^0$ means the two-rowed matrix obtained from the four-rowed matrix M by taking the upper left hand quadrant, and

$$\begin{aligned}B_1(\mathbf{k})&=\sqrt{2}b_1(\mathbf{k}),\quad B_2(\mathbf{k})=\sqrt{2}b_2(\mathbf{k}),\\B_1^*(\mathbf{k})&=\sqrt{2}b_1^*(\mathbf{k}),\quad B_2^*(\mathbf{k})=\sqrt{2}b_2^*(\mathbf{k}).\end{aligned}\tag{53}$$

It is important to note that the subscript on B or B^* can take only two values instead of four.

The expression (52) can be simplified considerably by means of the relations (48), (45), (43), (39), (4), (3), and (2). One obtains:

$$\begin{aligned}H=&\tfrac{1}{2}\sum(\mathbf{k})\epsilon mc^2\{B^\dagger(\mathbf{k})B(\mathbf{k})-B'(\mathbf{k})B^*(\mathbf{k})\}\\&-\tfrac{1}{2}\Sigma(\mathbf{k},\mathbf{k}')(\mathbf{k}|\Phi|\mathbf{k}')\{B^\dagger(\mathbf{k})[S^\dagger(\mathbf{k})\beta S(\mathbf{k}')]^0B(\mathbf{k}')\\&+B^\dagger(\mathbf{k})[S^\dagger(\mathbf{k})\beta A^*S^*(-\mathbf{k}')]^0B^*(-\mathbf{k}')\\&+B'(-\mathbf{k})[S'(-\mathbf{k})A\beta S(\mathbf{k}')]^0B(\mathbf{k}')\\&-B'(-\mathbf{k})[S'(-\mathbf{k})\beta'S^*(-\mathbf{k}')]^0B^*(-\mathbf{k}')\}.\end{aligned}\tag{54}$$

Now from (53), (42), and (45) we find that the commutation relations on the B's and B^*'s are

$$\begin{aligned}B_i^*(\mathbf{k})B_j(\mathbf{k}')+B_j(\mathbf{k}')B_i^*(\mathbf{k})&=\delta_{ij}\delta(\mathbf{k}',\mathbf{k}),\\B_i(\mathbf{k})B_j(\mathbf{k}')+B_j(\mathbf{k}')B_i(\mathbf{k})&=0,\\B_i^*(\mathbf{k})B_j^*(\mathbf{k}')+B_j^*(\mathbf{k}')B_i^*(\mathbf{k})&=0,\end{aligned}\tag{55}$$

which are just the standard Jordan-Wigner relations. On using (55) in (54) and remembering that by (31) and (33) $(-\mathbf{k}|\Phi|-\mathbf{k}')=(\mathbf{k}'|\Phi|\mathbf{k})$, we get

$$\begin{aligned}H=&\Sigma(\mathbf{k})\epsilon mc^2\{\sum_{r=1}^{2}N_r(\mathbf{k})-1\}\\&-\Sigma(\mathbf{k},\mathbf{k}')(\mathbf{k}|\Phi|\mathbf{k}')\{B^\dagger(\mathbf{k})[S^\dagger(\mathbf{k})\beta S(\mathbf{k}')]^0B(\mathbf{k}')\\&-\tfrac{1}{2}\delta(\mathbf{k},\mathbf{k}')\sum_{r=1}^{2}[S^\dagger(\mathbf{k})\beta S(\mathbf{k})]_{rr}{}^0\}\\&-\tfrac{1}{2}\Sigma(\mathbf{k},\mathbf{k}')\{(\mathbf{k}|\Phi|-\mathbf{k}')B^\dagger(\mathbf{k})\\&\times[S^\dagger(\mathbf{k})\beta A^*S^*(\mathbf{k}')]^0B^*(\mathbf{k}')+(-\mathbf{k}|\Phi|\mathbf{k}')B'(\mathbf{k})\\&\times[S'(\mathbf{k})A\beta S(\mathbf{k}')]^0B(\mathbf{k}')\},\end{aligned}\tag{56}$$

where

$$N_r(\mathbf{k})=B_r^*(\mathbf{k})B_r(\mathbf{k}).\tag{57}$$

We now wish to give (56) a more explicit form by introducing special forms of the matrices β, A, and $S(\mathbf{k})$. Before doing so let us establish conclusively that the results are essentially independent of the choice of these forms. We shall prove that any change in this choice is equivalent to at most a two-rowed unitary transformation

$$\begin{aligned}B(\mathbf{k})&\rightarrow t(\mathbf{k})B(\mathbf{k}),\quad B'(\mathbf{k})\rightarrow B'(\mathbf{k})t'(\mathbf{k}),\\B^*(\mathbf{k})&\rightarrow t^*(\mathbf{k})B^*(\mathbf{k}),\quad B^\dagger(\mathbf{k})\rightarrow B^\dagger(\mathbf{k})t^\dagger(\mathbf{k}).\end{aligned}\tag{58}$$

In the first place, it is at once evident from (40) that a change in $S(\mathbf{k})$ for fixed $\boldsymbol{\alpha}$, β is equivalent to a transformation of the type (58). Also, for fixed $\boldsymbol{\alpha}$, β the only change we can make in A is a phase factor, which corresponds to a transformation of the type (58) with $t(\mathbf{k})$ a mere phase factor. These results permit us to discuss the case in which the representation of $\boldsymbol{\alpha}$, β is changed by prescribing particular corresponding changes of $S(\mathbf{k})$ and A. From (37), (38), and (1), (2), (3) it is evident that if the new Dirac matrices are

$$\bar{\alpha}_i=R^\dagger\alpha_iR,\quad \bar{\beta}=R^\dagger\beta R,\quad R^\dagger R=1,$$

one may use with them the matrices

$$\bar{S}(\mathbf{k})=R^\dagger S(\mathbf{k}),\quad \bar{A}=R'AR.$$

On substituting in (56) one finds that all the matrices $[M]^0$ which occur in that equation have the same value whether α_i, β, $S(\mathbf{k})$, A or $\bar{\alpha}_i$, $\bar{\beta}$, $\bar{S}(\mathbf{k})$, $\bar{A}$ are used.

We now fix the Dirac matrices in the form originally used by Dirac:[18]

$$\alpha_i=\begin{pmatrix}0 & \sigma_i\\ \sigma_i & 0\end{pmatrix},\quad \beta=\rho_3=\begin{pmatrix}1 & 0\\ 0 & -1\end{pmatrix}, \tag{59}$$

where $\mathbf{0}$, $\mathbf{1}$, and σ_i are two-rowed matrices, the last being the Pauli matrices. Since σ_x and σ_z are symmetric and σ_y antisymmetric, we can satisfy (1), (2), (3) by setting

$$A=i\alpha_y\beta. \tag{60}$$

It is readily verified that (37) and (38) are satisfied by

$$S(\mathbf{k})=C(k)\{(\epsilon+1)\rho_1-\rho_3(\boldsymbol{\sigma}\cdot\mathbf{k})\}, \tag{61}$$

where

$$C(k)=\{2\epsilon(\epsilon+1)\}^{-\frac{1}{2}},$$
$$\rho_1=\begin{pmatrix}0 & 1\\ 1 & 0\end{pmatrix},\quad \sigma_i=\begin{pmatrix}\sigma_i & 0\\ 0 & \sigma_i\end{pmatrix} \tag{62}$$

On substituting (59)–(62) into (56) one readily obtains

$$\begin{aligned}H=&\Sigma(\mathbf{k})\epsilon mc^2\{\sum_{r=1}^{2}N_r(\mathbf{k})-1\}-(0|\Phi|0)\Sigma(\mathbf{k})\epsilon^{-1}\\&+\Sigma(\mathbf{k},\mathbf{k}')B^\dagger(\mathbf{k})(\mathbf{k}|V|\mathbf{k}')B(\mathbf{k}')\\&+\Sigma(\mathbf{k},\mathbf{k}')B^\dagger(\mathbf{k})(\mathbf{k},\mathbf{k}'|C|)B^*(\mathbf{k}')\\&+\Sigma(\mathbf{k},\mathbf{k}')B'(\mathbf{k})(|D|\mathbf{k},\mathbf{k}')B(\mathbf{k}'),\end{aligned} \tag{63}$$

$$\begin{aligned}(\mathbf{k}|V|\mathbf{k}')=&(\mathbf{k}|\Phi|\mathbf{k}')\{(\epsilon+1)(\epsilon'+1)\\&-(\boldsymbol{\sigma}\cdot\mathbf{k})(\boldsymbol{\sigma}\cdot\mathbf{k}')\}\{4\epsilon\epsilon'(\epsilon+1)(\epsilon'+1)\}^{-\frac{1}{2}}\\(\mathbf{k},\mathbf{k}'|C|)=&(\mathbf{k}|\Phi|-\mathbf{k}')\{(\epsilon+1)(\boldsymbol{\sigma}\cdot\mathbf{k}')\\&-(\epsilon'+1)(\boldsymbol{\sigma}\cdot\mathbf{k})\}\{16\epsilon\epsilon'(\epsilon+1)(\epsilon'+1)\}^{-\frac{1}{2}}\cdot i\sigma_y\\(|D|\mathbf{k},\mathbf{k}')=&(-\mathbf{k}|\Phi|\mathbf{k}')\cdot i\sigma_y\{(\epsilon+1)(\boldsymbol{\sigma}\cdot\mathbf{k}')\\&-(\epsilon'+1)(\boldsymbol{\sigma}\cdot\mathbf{k})\}\{16\epsilon\epsilon'(\epsilon+1)(\epsilon'+1)\}^{-\frac{1}{2}}.\end{aligned} \tag{64}$$

The general significance of (63) is clear, since according to (55) and (57) the meanings of $B_r(\mathbf{k})$ and $B_r^*(\mathbf{k})$ can be taken to be those usually given to Jordan-Wigner operators: $B_r(\mathbf{k})$ corresponds to the transition of a particle *out of* the state characterized by the momentum $\mathbf{k}mc$ and the spin index r, and $B_r^*(\mathbf{k})$ corresponds to a transition *into* that state. Thus the terms in $(\mathbf{k}|V|\mathbf{k}')$ correspond to *transitions* between such states, those in $(\mathbf{k},\mathbf{k}'|C|)$ to the *creation* of pairs of particles, and those in $(|D|\mathbf{k},\mathbf{k}')$ to *destruction* of pairs. Further remarks about formulas (63) and (64) are given in the next section.

IV. Discussion

Although the above procedure based on the ideas of Majorana succeeds formally in eliminating the negative energy states without the introduction of corresponding "holes" or antiparticles, the results still show much more resemblance to the positron theory than to a theory based on Schroedinger's early suggestions. This resemblance appears not only in the presence in (63) of terms corresponding to the creation and destruction of pairs of particles, but also in the presence of infinite terms independent of the $B(\mathbf{k})$ and $B^*(\mathbf{k})$. These terms, namely

$$-\Sigma(\mathbf{k})\epsilon mc^2-(0|\Phi|0)\Sigma(\mathbf{k})\epsilon^{-1}$$

can play no part in calculations, and hence may be regarded as typical "subtraction terms," such as appear in the positron theory.

As is the case with much of the formalism of quantum electrodynamics and of positron theory, our final expressions are in a form highly unsymmetrical as regards space and time, so that direct investigation of their Lorentz invariance would be a complicated task. It is scarcely to be doubted that, just as in the positron theory, the Lorentz invariance of the final formulas has become illusory through divergence difficulties associated with the presence of the subtraction terms. It seems, however, not without interest to mention here the question of ordinary rotation invariance, since the unsymmetrical appearance of the expressions (64) might lead one at first glance to suppose that even this invariance is lacking. We can readily show that this is not so, and that the expressions (64) have exactly the sort of form required for the theory to be rotation invariant.

The theory of the spinning electron provides us with the following rule for transforming the two components $B_1(\mathbf{k})$ and $B_2(\mathbf{k})$ on rotation of axes: Corresponding to rotation through the angle θ around an axis in the direction $\mathbf{n}_1$, one subjects

the B_r to the unitary transformation

$$B \rightarrow u(\mathbf{n}_1; \theta)B,$$

$$u(\mathbf{n}_1; \theta) = \cos(\theta/2) + i(\boldsymbol{\sigma}\cdot\mathbf{n}_1)\sin(\theta/2) \quad (65)$$

and also

$$B' \rightarrow B'u'(\mathbf{n}_1; \theta), \quad B^* \rightarrow u^*(\mathbf{n}_1; \theta)B^*, \quad (65')$$

$$B^\dagger \rightarrow B^\dagger u^\dagger(\mathbf{n}_1; \theta).$$

Then if the matrix M involves σ only in products $(\boldsymbol{\sigma}\cdot\mathbf{A})$, the product $\bar{B}^\dagger MB$ is invariant under rotation of $\mathbf{A}$ according to ordinary geometry and transformation of B and $\bar{B}^\dagger$ by (65) and (65'). This is the familiar way of establishing the invariance of the "even" terms involving $(\mathbf{k}|V|\mathbf{k}')$. But since $(\mathbf{k}, \mathbf{k}'|C|)$ and $(|D|\mathbf{k}, \mathbf{k}')$ are of the forms $M\sigma_y$ and $\sigma_y M$, respectively, we find that $\bar{B}^\dagger CB^*$ and $\bar{B}'DB$ are invariant under these same rules of transformation, because

$$\sigma_y u^*(\mathbf{n}_1; \theta) = u(\mathbf{n}_1; \theta)\sigma_y;$$
$$u'(\mathbf{n}_1; \theta)\sigma_y = \sigma_y u^\dagger(\mathbf{n}_1; \theta). \quad (66)$$

These relations follow directly from the commutation rules of the σ's together with the fact that σ_y is imaginary antisymmetric and σ_x and σ_z are real symmetric. The unsymmetrical looking appearance of σ_y in (64) is thus precisely what is required to secure the actual rotation invariance of the formalism. It is evident that this factor should not be regarded as a spin matrix at all, but simply as the antisymmetric unit matrix which plays a part in spinor analysis.[20]

It is evident that the formalism here obtained cannot be regarded as equivalent to a definite wave equation for a single particle, both because of the presence of the "odd" terms, which show that the number of particles is not constant, and because of the highly irrational dependence on $\mathbf{k}$, which would be represented by the operator $(-i\hbar/mc)\nabla$. Apparently the only case in which an approximate treatment by means of a single particle wave equation can readily be given is that of a slowly moving particle in a weak field free of high frequency components. For such a field pairs will not be produced, and the only contributions to the energy from the odd terms will be of the order of $|(\mathbf{k}|\Phi|\mathbf{k}')|^2$, which, since the field is weak, can be neglected compared to the even terms. Also the irrationalities can be removed by expansion in powers of k and k', since for a slow particle these are small of order v/c; one may conveniently work to the order k^2. In this approximation the even matrix elements contained in (63) are, apart from the "subtraction terms" equivalent by partial integration to those of

$$H_1 = mc^2 - (\hbar^2/2m)\nabla^2 + \Phi - (\hbar^2/8m^2c^2)(\nabla^2\Phi) + (\hbar\boldsymbol{\sigma}/4c^2)\cdot[(\nabla\Phi/m)\times(\mathbf{p}/m)]. \quad (67)$$

Here the first three terms are, respectively, proper energy, nonrelativistic kinetic energy, and potential energy, and the last term gives precisely the spin orbit coupling corresponding to the Thomas precession.[21] Just as in the case of the nonrelativistic approximation obtained from the usual Dirac equations for a single particle there appears still another term, which in the present instance is Hermitian.

The matrix elements occurring in (64) are just those which appear in the simple subtraction theory in which both particles and antiparticles occur. The physical interpretation is, however, rather different; the events of creation and annihilation may here involve any two particles which occur at all in the theory, instead of having to involve one particle from each of two distinct kinds.

As was mentioned in the introduction, the neutrino theory of β-radioactivity either with electron emission or with positron emission can be based on this theory of the neutrino quite as well as on the usual formalism in which antineutrinos occur. As Racah[2] has pointed out, the procedure is, schematically, just to replace the neutrino wave function φ by $\frac{1}{2}(\varphi + A^*\varphi^*)$ and replace φ^* by $\frac{1}{2}(\varphi^* + A\varphi)$ throughout whatever formula for the interaction energy it is desired to use. In our present language this means replacing φ by U and φ^* by U^*, after which one may use the formulas of Section III to express the interaction in terms of the operators $B_r^*(\mathbf{k})$ and $B_r(\mathbf{k})(r = 1, 2)$, which refer to the emission and

[20] B. L. van der Waerden, *Gruppentheoretische Methode in der Quantenmechanik*, p. 79; O. Laporte and G. E. Uhlenbeck, Phys. Rev. **37**, 1383 (1931).

[21] Cf. references 4 and 3.

absorption of neutrinos. Using (30), (36), (50) and (53), we have

$$\varphi \rightarrow U = 2^{-\frac{1}{2}}\Sigma(\mathbf{k})(\mathbf{r}|\mathbf{k})S(\mathbf{k}) \cdot \begin{pmatrix} B_1(\mathbf{k}) \\ B_2(\mathbf{k}) \\ v_{11}{}^*B_1{}^*(-\mathbf{k})+v_{12}{}^*B_2{}^*(-\mathbf{k}) \\ v_{21}{}^*B_1{}^*(-\mathbf{k})+v_{22}{}^*B_2{}^*(-\mathbf{k}) \end{pmatrix}.$$

This differs from the corresponding expression for φ used in the ordinary theory only in the following ways: (a) A factor $2^{-\frac{1}{2}}$ occurs, which can be absorbed into the disposable constant coefficient of the interaction energy; (b) A spin transformation $\mathbf{v}^*$ appears, but this makes no difference in the total transition probabilities summed over both spins for the neutrino. (c) The role which in the ordinary theory is played by operators representing the emission of an antineutrino is here played by the $B_r{}^*$, which represent the emission of a neutrino. The actual four-component amplitudes used in calculating matrix elements are the same in both cases, the columns of $S(\mathbf{k})$. Thus in all cases in which the only part taken by the light neutral particles consists in one of them being emitted, there is no difference in the calculated intensities,[22] and the only difference between the two theories consists in our mental picture of what happens: In the ordinary theory one type of β-decay involves the emission of neutrinos and the other the emission of antineutrinos, but in the Majorana theory use is made of neutrinos only.

It should be possible to settle which theory is preferable by considering processes in which neutrinos are absorbed as well as emitted, but actually this does not seem feasible at present. Differences would presumably appear in the results of using the light particle fields to account for the forces between heavy particles, but this part of the subject is in such an unsatisfactory state owing to divergence difficulties that it seems to offer no hope of a decision, and indeed it seems quite doubtful that nuclear forces are to be explained in this way. Another possibility of deciding between the two theories is offered in principle by the phenomenon of β-decay with *absorption of* a light neutral particle instead of its *emission*, the β-ray accordingly having *more* energy than the limit of the spectrum instead of *less*. Here, as Racah has remarked, there is an obvious qualitative difference between the two theories. On the ordinary Dirac theory, a positron emitter can be "stimulated" only by an electron emitter, and vice versa, but on the Majorana theory any emission may "stimulate" any other emission, whether of the same or of opposite type. But since the cross section[23] of a radioactive nucleus for capture of a neutrino is of order of magnitude between 10^{-40} and 10^{-50} cm^2, it seems unlikely that this effect, which would not only serve to decide the question of the existence of antineutrinos but would provide experimental evidence of the best sort for the neutrino hypothesis itself, can ever be observed.

[22] This assertion may seem to contradict a statement made by Racah (reference 2), that differences can be obtained unless the rest mass of the neutrino is zero. Our present assertion holds, however, for the comparison between the Majorana theory and any neutrino theory in which the interaction energy involves the electron wave function ψ and the neutrino function φ through expressions of the form $\psi\dagger M\varphi$ and $\varphi\dagger M\dagger\psi$. For such theories the phases of the Lorentz transformation matrices (Eq. (12)) are arbitrary, but the way in which they are chosen has no effect on the form of the quantities $\psi\dagger M\varphi$ and $\varphi\dagger M\dagger\psi$ used in expressing the interaction energy; so that the phases may be taken to be those given in Eq. (12), and our arguments about the connection with the Majorana theory are at once applicable. This way of forming the interaction energy was used by Uhlenbeck and Konopinski, and is now the most commonly used. Fermi's original way of forming the interaction energy, however, involved expressions of the form $\psi\dagger M\varphi^*$ and $\varphi' M\dagger\psi$, and here the phases of the transformation matrices are not without effect on the way one must choose the form of the expression for the interaction energy in order to obtain Lorentz invariance. As Racah points out, the phases given in (12) are not consistent with Fermi's actual choice of the interaction energy expression, so that his original formalism could not be carried over into the Majorana theory. This lack of exact correspondence between the two points of view is to be regarded as due to objectionably artificial characteristics of the Fermi type of expression, which are avoided in the now generally accepted Konopinski-Uhlenbeck type.

[23] H. Bethe and R. Peierls, Nature **133**, 532 (1934).

Emission Bands in the $3p^1\Pi_{cd}-1s^1\Sigma$ System of the Hydrogen Molecule

C. RULON JEPPESEN
Department of Physics, University of California, Berkeley, California

(Received May 5, 1938)

The $3p^1\Pi_{cd}-1s^1\Sigma$ band system of the hydrogen molecule, heretofore observed only in absorption, has been discovered in emission. Ten bands from the first three vibrational levels of the excited state are analyzed and the rotational and vibrational constants are derived. The d component levels of the Λ type doubling are found to be strongly perturbed whereas the c components appear to be quite regular. The most significant of the constants derived are as follows: $T_e=113908$ cm^{-1}, $B_e=30.56$ cm^{-1} and $\omega_e=2353$ cm^{-1}.

INTRODUCTION

THIS paper is concerned with the identification and analysis of a number of emission bands in the $3p^1\Pi_{cd}-1s^1\Sigma$ system of H_2 and with the molecular constants derived therefrom. This band system was discovered by Hopfield[1] who found a v' progression in absorption lying in the extreme ultraviolet between 830 and 770A. Before the present study this system had not been observed in emission. Beutler, Deubner and Junger[2] and Beutler and Junger,[3] by means of the isotope effect showed that the absorption progression began with the $v=3$ level of the upper state. The $v=0$, 1 and 2 vibrational levels are missing. This had previously been suggested by Richardson[4] as a possible explanation of the bands, since the heat of dissociation and Rydberg denominator indicated by this progression were not compatible with other known data on H_2, if the first member of the progression were the 0−0 band.

Beutler, Deubner and Junger's thorough study of this absorption spectrum fixed the identification of the excited electronic level as the $3p^1\Pi_{cd}$ state and this conclusion is further substantiated by the results of the present study. These authors found also that the absorption bands were broadened and diffuse because of predissociation beginning at the $v=3$ level and autoionization beginning at the $v=6$ level. The presence of these phenomena explains the previous failure to find this band system in emission. The vibrational levels $v=0$, 1 and 2 should, however, give rise to emission bands and a number of these have now been found and are described in the following paragraphs. It is not possible however, as just noted, to obtain emission bands from higher vibrational levels than the third, hence our data are not so complete as might be desirable.

EXPERIMENTAL METHODS

The procedure used for excitation of the hydrogen spectrum has been described in an earlier paper[5] and the experimental results of this former study have been used in the present investigation. Additional data have been secured, however, in the region of the short wave-length end of the spectrum. This has been made possible through the use of a new spectrograph built in the shop of the University of California physics department. This spectrograph contains a grating ruled at the Johns Hopkins University, with 11,800 lines per cm and with a radius of 42 cm. The grating mounted at normal incidence is very fast and gives spectra relatively free from background. Most of the data of the present work were obtained with the 2 meter spectrograph described earlier[5] and hence the dispersion obtained on the plates is about 3.5A per mm. The small spectrograph mentioned above gives a dispersion of about 20A per mm and so for the very faint lines photographed only with this instrument, the probable error is perhaps as much as 0.05A. In this later study hydrogen lines from the former work have been used as standards.

ROTATIONAL ANALYSIS

The intervals between vibrational levels (ΔG_v values) in the $3p^1\Pi_{cd}$ state may be determined

[1] J. J. Hopfield, Nature **125**, 927 (1930).
[2] Beutler, Deubner and Junger, Zeits. f. Physik **98**, 181 (1935).
[3] Beutler and Junger, Zeits. f. Physik **100**, 80 (1936).
[4] O. W. Richardson, *Molecular Hydrogen and its Spectrum* (Yale University Press, 1934), p. 303.
[5] C. R. Jeppesen, Phys. Rev. **44**, 165 (1933).

directly for $v>3$ from the absorption progression previously mentioned. For $v<3$ approximate ΔG_v values may be obtained from the same data by extrapolation. Since a rather complete analysis of the lower $1s^1\Sigma$ state is known[5] we can then find the approximate position of each expected emission band in our system. The rotational analysis may then be carried out by the usual methods. The chief difficulty with such analysis lies in the extensive overlapping of bands, so that chance coincidences are very frequent. This is especially troublesome when, as in the present instance, the bands under consideration are comparatively low in intensity and are overlapped by other systems of greater strength. For this reason the tentative assignments given to a number of lines are quite doubtful and are not included in the data given here. The bands for which the assignments appear to be fairly certain are given in Table I. Since all of the numerical results deduced from the ten bands given in the table are consistent and are compatible with previously known results, it would appear that the essential correctness of the identifications cannot be doubted. Table I gives

TABLE I. *Emission bands of the* $3p^1\Pi_{cd}-1s^1\Sigma$ *system.*

K	I	R Branch	I	P Branch	I	Q Branch
0–1 band $\nu_0=108715$						
0	1	108773.1				
1	3	784.9			2	108655.4
2	0	744.8	1	108437.4	1	549.6
3	2	655.4*	3	227.2	2	391.8
4	1	523.8?	1	107972.5	0	182.8
5			6	666.2*	1*b*	107929.1
0–2 band $\nu_0=104791$						
0	3	104849.3				
1	4	865.8			4	104738.0
2	—	—	2*d*	104528.5	2	642.5
3	3	764.6	3	336.9	3	501.9
4	2	657.6	1	104.1	2	317.8
5			1	103831.4	1	093.2
0–3 band $\nu_0=101092$						
0	1	101151.3				
1	4	174.5			6	101045.5
2	0	159.0	2	100850.2	3	100963.0
3	1*b*	102.3	4	673.0*	3	838.2
4			1*d*	463.8	4	673.0*
5			1	215.5	3	475.3
1–1 band $\nu_0=110939$						
0						
1	2	110989.8			3	110875.1
2	1	934.7	1*bd*	110646.6*	2	763.1
3	1	820.4	4	433.5	3	596.2
4	1*bd*	646.6*	2	162.4	1	376.3
5	1	387.6?	2	109840.2	1*d*	104.6
1–3 band $\nu_0=103322$						
0	1*d*	103374.5				
1	3	386.4			4	103272.4*
2	1	355.9	2	103072.1	3*d*	180.5
3	4	272.4*	3	102886.4	3	048.5
4			1	659.7	—	—
5			2*b*	392.4	0	102675.6

K	I	R Branch	I	P Branch	I	Q Branch
1–4 band $\nu_0=99848$						
0	3*b*	99899.7*				
1	5	918.8			6	99803.6
2	3*b*	899.7*	2*d*	99617.4	3	725.5*
3	2	834.4	3	447.3	4	609.6
4	3	725.5*	2	243.4	3*b*	462.3
5			4	004.9	2	265.6
1–5 band $\nu_0=96605$						
0	2	96659.5				
1	4	684.2			5	96567.9
2	5	668.9	1	96390.3	4	500.3
3	3	626.5	3	237.4	2	401.0
4			1	054.7	—	—
5			2	843.0	1	108.1
2–2 band $\nu_0=109113$						
0	2	109161.6				
1	2	166.7			3	109051.8
2	0	119.6	3	108844.1	1	108945.2
3	0*b*	012.3	2	638.7	3	784.9
4	2*d*	108858.0	0	384.6		
5			3	084.5		
2–3 band $\nu_0=105421$						
0	1	105471.7				
1	3	480.4			4	105365.2
2	1	442.5	2	105168.8	2	269.3
3	1	356.6	2	104980.6	1	127.3
4			3	750.0	1	104940.9
5			1	474.4	0	711.1
2–5 band $\nu_0=98703$						
0	—	—				
1	4	98778.1*			5	98660.8
2	1	756.3	1	98488.6*	5	591.6
3	2	709.8	4	335.5*	3	481.5
4	1	621.0	1	148.2	4	335.5
5			1	97930.5	00	159.3

the origin of each band and the wave number of each line in the band together with an eye estimate of its intensity. Lines indicated by an asterisk are known blends. The letter "*d*" or "*b*" following the intensity estimate of a line indicates that it is either diffuse or broad as the case may be.

Derivation of Constants

As has been found previously[5] the rotational energy function for a state having the characteristics of the present $3p^1\Pi_{cd}$ level may be written:

$$F=B_i^x[K(K+1)-\Lambda^2] +D_i^xK^2(k+1)^2+F_i^xK^3(K+1)^3. \quad (1)$$

The subscript i indicates the double valued nature of the function, one set of rotational constants being necessary for the c component levels and another for the d components of the Λ type doubling. The superscript x indicates that these are the so-called "effective" values of the constants. In analogy to the $2p^1\Pi_{cd}$ level discussed earlier[5] it should be emphasized that in our case the "true" rotational constants are equal to the effective values given by the c component levels (our B_e^x, D_e^x etc.).

The values of B_e^x as a function of v determined directly from the wave numbers are given in the first column of Table II. In the second column of this table are given the smoothed values from the following linear equation:

$$(B_e^x)_v=30.56-1.643(v+\tfrac{1}{2}). \quad (2)$$

The third column of Table II records the observed $(B_d^x)_v$ values. In the case of the d component levels we find that the Δ_2F values, from which the rotational constants are determined, are quite irregular. It is therefore not possible to determine accurate values of $(B_d^x)_v$ and the values given in the table are to be considered only as approximations. They were determined by the graphical method described by Birge.[6] The last column in Table II gives the values of $(B_d^x)_v$ determined graphically from a straight line drawn through the data of column three. This last column is included only to indicate the futility of any attempt to represent these data by a simple function that will give a reasonable extrapolated value of $(B_d^x)_e$. The values of $(B_i^x)_v$ are shown graphically in Fig. 1.

Table II. *Values of* $(B_i^x)_v$ *in* cm^{-1} *units.*

v	Obs. $(B_e^x)_v$	Calc. $(B_e^x)_v$	Obs. $(B_d^x)_v$	Calc. $(B_d^x)_v$
0	29.73	29.74	31.22	30.92
1	28.11	28.10	28.65	29.17
2	26.43	26.45	27.62	27.43

[6] R. T. Birge, National Research Council Bulletin, No. 57, *Molecular Spectra in Gases* (1937), p. 172.

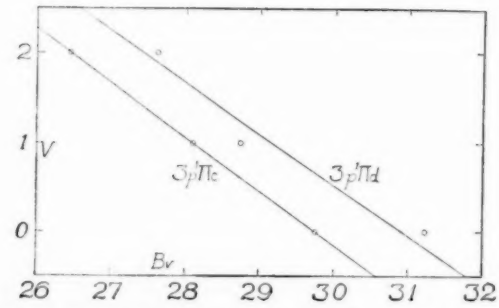

Fig. 1. Graphical representation of B_e^x and B_d^x as functions of v.

While the given values of $(B_d^x)_v$ have relatively large probable errors (by comparison with the $(B_e^x)_v$ values which are accurately determined by analytic methods) they deviate from a straight line by amounts many times greater than their individual probable errors. It is apparent from Fig. 1 that if the B_d^x values should be represented by the same type of function that fits the B_e^x data so well, the rotational levels of the $v=1$ state are crowded together more closely than they should be and the levels of the $v=0$ and $v=2$ states are spread more widely apart. Thus

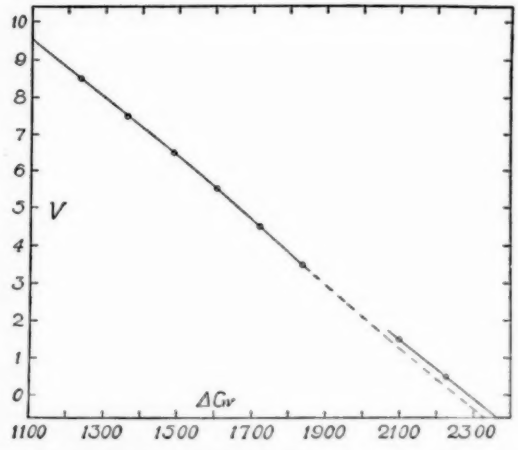

Fig. 2. Graphical representation of $\Delta G : v$. Data for $v>3$ are from the absorption spectrum (Beutler, Deubner and Junger) and for $v<2$ are from the present study of the emission spectrum.

the evidence that the d component levels of the $3p^1\Pi_{cd}$ state are perturbed is quite conclusive. The c component levels, on the other hand, appear to be entirely regular. This is the same situation as that which exists in the case of the $2p^1\Pi_{cd}$ state and which has been discussed in a previous paper.[5]

The vibrational term differences have already been obtained[1, 2] from the data of the absorption spectrum. These data however do not give as accurate a value of ΔG_e as can be obtained from the present work. In the first place the $v=0$, 1 and 2 levels are missing in the absorption spectrum and in the second place the origins of the bands cannot be closely determined until the rotational structure is analyzed. In Fig. 2 is indicated graphically the ΔG_v values obtained from the emission spectrum (low values of v) and from the absorption spectrum (high values of v). The directly determined ΔG_v values from the present study are $\Delta G_{\frac{1}{2}}=2226$ and $\Delta G_{1\frac{1}{2}}=2099$ cm^{-1} respectively. The extrapolated value of ΔG_e is then 2353 ± 10 cm^{-1} as compared with 2316 ± 20 cm^{-1}, derived[2] from the absorption spectrum.

TABLE III. *Constants of the $3p^1\Pi_{cd}$ state.*

T_e	113908 ± 10 cm^{-1}	r_e	1.044A
B_e	30.56 ± 0.04 cm^{-1}	α_e	1.643 cm^{-1}
ΔG_e	2353 ± 10 cm^{-1}	$2x_e\omega_e$	227 cm^{-1}
I_e	0.9051×10^{-40} g cm^2		

A summary of the values of the important constants is given in Table III.

It may be remarked that in the calculation of T_e as given in Table III the presence of Λ in the rotational energy function (Eq. (1)) was taken into consideration.

A search for the $3p^1\Pi_{cd}-1s^1\Sigma$ band system in the emission spectrum of D_2 has been made, but because of the very small intensity of the D_2 spectra on the photographs thus far obtained and measured, the result of this study is inconclusive.

JULY 1, 1938 PHYSICAL REVIEW VOLUME 54

The Classification of the Spectrum of Singly Ionized Tin. Sn II

W. W. McCORMICK AND R. A. SAWYER
University of Michigan, Ann Arbor, Michigan

(Received May 7, 1938)

The spectrum of Sn II, as excited in a hollow cathode discharge in helium, has been photographed from 800A to 10,000A. Some 70 new lines have been classified and 28 new levels established. A few changes have been made in the levels and classifications previously made by Green and Loring, Narayan, and Lang. The $5s^2ms$, $-mp$, $-md$ and $-mf$ series have been extended, and the ^2F levels have been resolved for the first time. Six members of the $5s^2mg\ ^2G$ series have been located and used to make a new determination of the ionization potential of Sn II as $118{,}017\pm3$ cm^{-1}. The classification has been checked by series relations, Zeeman patterns, and by comparison with the isoelectronic spectra In I and Sb III. Irregularities in the ^2S and ^2D terms are explained qualitatively by consideration of interactions with perturbing terms from the configuration sp^2.

THE first classifications of Sn II were made independently by Green and Loring[1] and by Narayan and Rao[2] and were in substantial agreement. Green and Loring, using vacuum arc data, supplemented by data of R. J. Lang in the extreme ultraviolet, and with the help of a few Zeeman effects, classified thirty of the stronger lines, fixing nineteen low levels. Two levels each were found in the low normal ^2S, ^2P, ^2D and ^2F series, and the ^2D and ^2S levels from the configuration sp^2 were located. Lang[3] later rephotographed the spectrum with a hollow cathode discharge, and made a few corrections and additions, notably the ^4P terms from sp^2. No high terms were found in these researches and the ionization potential was determined only roughly by Green and Loring, who fixed it

[1] Green and Loring, Phys. Rev. **30**, 574 (1927).
[2] Narayan and Rao, Zeits. f. Physik **45**, 350 (1927).
[3] Lang, Phys. Rev. **35**, 445 (1930).

TABLE I. *Unresolved Zeeman patterns of Green and Loring, and computed centers of intensity according to Shenstone and Blair's formula. The observed pattern for each line is given first, the computed pattern is immediately below.*

λ	PATTERN	CLASSIFICATION
3283	(0) 0.91	$p^2\,{}^2D_{3/2}-4^2F_{5/2}$
	0.90	
3352	(0) 1.06	$p^2\,{}^2D_{5/2}-4^2F_{7/2}$
	1.07	
5332	(0) 0.835	$6^2P_{1/2}-6^2D_{3/2}$
	0.833	
5562	(0) 1.04	$6^2P_{3/2}-6^2D_{5/2}$
	1.10	
5589	(0) 0.90	$5^2D_{3/2}-4^2F_{5/2}$
	0.90	
5799	(0) 1.07	$5^2D_{5/2}-4^2F_{7/2}$
	1.07	

by assuming equal effective quantum numbers for the first two members of the ${}^2F$ term sequence.

The lowest state of singly ionized lead is $5s^25p\,{}^2P_{1/2}$. Excitation of the $5p$ electron to higher states gives rise to the usual doublet series ${}^2S$, ${}^2P$, ${}^2D$, ${}^2F$—, all of which have as a limit the $5s^2\,{}^1S_0$ term of Sn III. Excitation of one of the two $5s$ electrons leads to configurations of the types $5s5p^2$, $5s5p5d$, $5s5d^2$, etc., with higher limits in the Sn III spectrum. However, a consideration of the energy values in Sn III, corresponding to the excitation of a $5s$ electron to $5p$, $5d$, etc., states, permits a rough calculation of such energies in Sn II. It is easily seen that the only configuration arising from an excited $5s$ electron in Sn II which will lie below the $5s^2$ ionization limits is $5s5p^2$. From this configuration are expected the eight levels ${}^4P_{1/2,\,3/2,\,5/2}$, ${}^2D_{3/2,\,5/2}$, ${}^2P_{1/2,\,3/2}$ and ${}^2S_{1/2}$. As noted above, six of these terms were found by earlier investigators, in addition to a few low terms in the normal series.

EXPERIMENTAL

The light source chosen for the present investigation was the hollow cathode discharge in an atmosphere of helium. The excitation in this discharge tends to be limited by the reactions between the metal atoms or ions and the metastable or ionized rare gas atoms.[4] The energy of ionization of helium is about 198,000 cm^{-1} while that of Sn I is roughly 59,000 cm^{-1}. Thus there is left available nearly 139,000 cm^{-1} from this reaction for the excitation of the Sn II levels. Since the ionization potential of Sn II is approximately 118,000 cm^{-1}, it is apparent that the Sn II spectrum should be completely excited in this discharge, while the residual energy above that required to doubly ionize tin is not sufficient to excite even the lowest Sn III levels, which lie about 55,000 cm^{-1} higher. The only difficulty in obtaining satisfactory spectra from the discharge arose from the low vapor pressure of tin (boiling point 2260°C), which tends to keep the tin pressure in the discharge too low for the best intensity in the higher excited states of Sn II.

The gas purifying system and excitation conditions have been sufficiently described elsewhere.[5] In the present set-up, the helium was circulated continuously by a mercury vapor pump through a purifying system consisting of suitable traps in liquid air. Current was furnished by a vacuum tube rectifier, the discharge drawing nearly 350 milliamperes. Pure tin was cut into small pieces and placed inside a tungsten cathode, whence it entered the discharge both by temperature evaporation and by bombardment.

The spectrum of the discharge was photographed from 800A to 9000A, a region sufficient to cover all the important lines of the tin spark spectrum. The region of wave-lengths shorter than λ2200 was photographed with a concave grating vacuum spectrograph.[6] The grating (1 m radius, 14,400 lines per inch) gave a dispersion of about 17A/mm. Satisfactory standards of wave-length were found among the O, He, and Hg lines which appeared in the discharge. The region from 2200A to 2700A was photographed with a Hilger E2 quartz spectrograph, while for the regions 2500A to 4500A and 4500A to 10,000A, a Hilger E1 quartz and a glass spectrograph of comparable dimensions were used. Iron arc comparison spectra were placed on all plates through the quartz and glass regions up to 8000A. Above 8000A a neon comparison spectrum was used. All plates were measured on a Gaertner comparator. The calculated wave-lengths in air were reduced to wave numbers in vacuum with the help of Kayser's table. For wave-lengths greater than 2200A, the wave number values are probably correct, in most cases, to about one wave per centimeter;

[4] Sawyer, Phys. Rev. **36**, 44 (1930).

[5] Sawyer and Paschen, Ann. d. Physik **84**, 1 (1927).

[6] Sawyer, J. Opt. Soc. Am. **15**, 305 (1927).

for the wave-lengths from the vacuum spectrograph, the error is somewhat greater and may be as high as 10 cm^{-1} for the shortest wave-lengths and weakest lines.

Data and Classification

Green and Loring,[1] in their work on the tin spectra, determined the Zeeman effects of eight Sn II lines. Only two of the pat-

Table II. *Classified lines in* Sn II.

I	λ Vac.	ν Vac.	Classification	$\Delta\nu$	Notes	I	λ Air	ν Vac.	Classification	$\Delta\nu$	Notes
0	888.38	112,564	$5^2P_{1/2}-11^2D_{3/2}$	7		1	2912.80	34,321	$5^2D_{5/2}-9^2P_{3/2}$	0	
1	899.92	111,121	$5^2P_{1/2}-10^2D_{3/2}$	−1		6	2919.82	34,239	$6^2P_{1/2}-8^2D_{3/2}$	1	
2	917.40	109,004	$5^2P_{1/2}-9^2D_{3/2}$	−1		0	2943.60	33,962	$5^2D_{3/2}-6^2F_{5/2}$	0	
0	923.07	108,334	$5^2P_{3/2}-11^2D_{5/2}$	−2		3	2991.00	33,424	$p^2\,{}^2D_{3/2}-7^2P_{3/2}$	0	
1	935.63	106,880	$5^2P_{3/2}-10^2D_{5/2}$	4		7	2994.44	33,386	$6^2P_{3/2}-8^2D_{5/2}$	0	
3	945.83	105,728	$5^2P_{1/2}-8^2D_{3/2}$	2		0	2997.13	33,356	$6^2P_{3/2}-8^2D_{3/2}$	0	
4	954.50	104,767	$5^2P_{3/2}-9^2D_{5/2}$	4		1	3012.18	33,189	$6^2P_{1/2}-9^2S_{1/2}$	0	
7	985.13	101,508	$5^2P_{3/2}-8^2D_{5/2}$	0		8	3023.94	33,060	$p^2\,{}^2D_{3/2}-7^2P_{1/2}$	−1	
0	995.77	100,425	$5^2P_{3/2}-9^2S_{1/2}$	2		12	3047.50	32,804	$p^2\,{}^2D_{5/2}-7^2P_{3/2}$	0	
4	997.21	100,280	$5^2P_{1/2}-7^2D_{3/2}$	0		6	3094.69	32,304	$6^2P_{3/2}-9^2S_{1/2}$	1	*g*
2	1016.26	98,400	$5^2P_{1/2}-8^2S_{1/2}$	−1		50	3283.21	30,449	$p^2\,{}^2D_{3/2}-4^2F_{5/2}$	−1	*x*
4	1040.78	96,082	$5^2P_{3/2}-7^2D_{5/2}$	0		60	3351.97	29,824	$p^2\,{}^2D_{5/2}-4^2F_{7/2}$	0	*x, l*
1	1041.32	96,032	$5^2P_{3/2}-7^2D_{3/2}$	−4		0	3355.55	29,793	$5^2D_{3/2}-8^2P_{1/2}$	2	
3	1062.10	94,153	$5^2P_{3/2}-8^2S_{1/2}$	−6		2	3407.48	29,339	$5^2D_{5/2}-8^2P_{3/2}$	−1	
8	1108.19	90,237	$5^2P_{1/2}-6^2D_{3/2}$	1	*x*	10	3472.46	28,790	$6^2P_{1/2}-7^2D_{3/2}$	0	
4	1159.05	86,277	$5^2P_{1/2}-7^2S_{1/2}$	−1	*y, a*	7	3537.57	28,260	$5^2D_{3/2}-5^2F_{5/2}$	2	*y, i*
10	1161.43	86,101	$5^2P_{3/2}-6^2D_{5/2}$	−5	*x*	11	3575.45	27,960	$6^2P_{3/2}-7^2D_{5/2}$	0	*y, k*
3	1162.94	85,989	$5^2P_{3/2}-6^2D_{3/2}$	−3	*x*	3	3582.39	27,906	$6^2P_{3/2}-7^2D_{3/2}$	0	
4	1180.51	84,709	$5^2P_{1/2}-p^2\,{}^2P_{3/2}$	−3	*x, b*	*c*	3587.33	27,867	$p^2\,{}^4P_{1/2}-6^2P_{3/2}$		*h*
9	1219.07	82,030	$5^2P_{3/2}-7^2S_{1/2}$	−6	*y, a*	2	3620.08	27,616	$5^2D_{5/2}-5^2F_{5/2}$	0	*i*
13	1223.70	81,719	$5^2P_{1/2}-p^2\,{}^2S_{1/2}$	0	*x, y*	6	3620.54	27,612	$5^2D_{5/2}-5^2F_{7/2}$	0	*y, i*
11	1243.00	80,450	$5^2P_{3/2}-p^2\,{}^2P_{3/2}$	4	*x, y, b*	*c*	3705.10	26,981	$p^2\,{}^4P_{1/2}-6^2P_{1/2}$		*h*
20	1290.86	77,467	$5^2P_{3/2}-p^2\,{}^2S_{1/2}$	0	*x, y*	6	3715.23	26,909	$6^2P_{1/2}-8^2S_{1/2}$	0	
20	1316.59	75,953	$5^2P_{3/2}-p^2\,{}^2P_{1/2}$	0		4	3841.44	26,024	$6^2P_{3/2}-8^2S_{1/2}$	1	
25	1400.52	71,402	$5^2P_{1/2}-5^2D_{3/2}$	3	*x*	0	3984.77	25,088	$4^2F_{7/2}-11^2G$	0	
20	1475.15	67,795	$5^2P_{3/2}-5^2D_{5/2}$	0	*x*	0	3994.51	25,027	$p^2\,{}^4P_{3/2}-6^2P_{1/2}$	0	
9	1489.22	67,149	$5^2P_{3/2}-5^2D_{3/2}$	4	*x*	0	4110.51	24,321	$4^2F_{7/2}-10^2G$	0	
7	1699.47	58,842	$5^2P_{1/2}-p^2\,{}^2D_{3/2}$	0	*x, y, c*	0	4111.59	24,315	$4^2F_{5/2}-10^2G$	0	
7	1758.00	56,883	$5^2P_{1/2}-6^2S_{1/2}$	0	*x*	0	4293.61	23,284	$4^2F_{7/2}-9^2G$	0	
15	1811.34	55,208	$5^2P_{3/2}-p^2\,{}^2D_{5/2}$	2	*x*	1	4294.65	23,278	$4^2F_{5/2}-9^2G$	0	
9	1831.89	54,588	$5^2P_{3/2}-p^2\,{}^2D_{3/2}$	2	*x, c*	1	4579.13	21,832	$4^2F_{7/2}-8^2G$	0	
12	1899.91	52,634	$5^2P_{3/2}-6^2S_{1/2}$	−3	*x*	1	4580.29	21,826	$4^2F_{5/2}-8^2G$	0	
1	2149.31	46,527	$p^2\,{}^2D_{3/2}-6^2F_{5/2}$	2		0	4792.22	20,861	$5^2D_{3/2}-7^2P_{3/2}$	0	
30	2152.22	46,464	$5^2P_{1/2}-p^2\,{}^4P_{3/2}$	−1	*y*	2	4877.22	20,498	$5^2D_{3/2}-7^2P_{1/2}$	0	
	λ Air	ν Vac.				3	4944.31	20,219	$5^2D_{5/2}-7^2P_{3/2}$	0	
						2	5071.14	19,714	$4^2F_{7/2}-7^2G$	0	
4	2209.67	45,241	$5^2P_{3/2}-p^2\,{}^4P_{5/2}$	0	*y*	2	5072.67	19,708	$4^2F_{5/2}-7^2G$	0	
6	2246.07	44,509	$5^2P_{1/2}-p^2\,{}^4P_{1/2}$	0	*y*	10	5332.36	18,748	$6^2P_{1/2}-6^2D_{3/2}$	0	*x, l*
3	2360.34	42,354	$p^2\,{}^2D_{3/2}-8^2P_{1/2}$	0		20	5561.95	17,974	$6^2P_{3/2}-6^2D_{5/2}$	0	*x, l*
22	2368.33	42,211	$5^2P_{3/2}-p^2\,{}^4P_{3/2}$	0	*y*	25	5588.92	17,887	$5^2D_{3/2}-4^2F_{5/2}$	0	*x, l*
4	2384.54	41,924	$p^2\,{}^2D_{5/2}-8^2P_{3/2}$	−1		2	5596.20	17,864	$6^2P_{3/2}-6^2D_{3/2}$	0	*x, l*
1	2433.52	41,080	$6^2P_{1/2}-11^2D_{3/2}$	1	*d*	1	5797.20	17,245	$5^2D_{5/2}-4^2F_{5/2}$	0	
15	2448.98	40,821	$p^2\,{}^2D_{3/2}-5^2F_{5/2}$	0	*y, e*	15	5799.18	17,239	$5^2D_{5/2}-4^2F_{7/2}$	0	*x, l*
13	2483.48	40,254	$5^2P_{3/2}-p^2\,{}^4P_{1/2}$	3	*y*	0	5965.69	16,758	$7^2P_{3/2}-9^2D_{5/2}$	−1	
10	2486.99	40,197	$p^2\,{}^2D_{5/2}-5^2F_{7/2}$	0	*y, e*	6	6077.48	16,449	$4^2F_{7/2}-6^2G$	0	
5	2522.61	39,630	$6^2P_{1/2}-10^2D_{3/2}$	0		5	6079.70	16,443	$4^2F_{5/2}-6^2G$	0	
0	2579.08	38,762	$6^2P_{3/2}-10^2D_{5/2}$	0		70	6453.50	15,491	$6^2S_{1/2}-6^2P_{3/2}$	0	*x*
0	2608.67	38,322	$6^2P_{3/2}-11^2S_{1/2}$	0		8	6761.45	14,786	$6^2P_{1/2}-7^2S_{1/2}$	0	
2	2664.93	37,513	$6^2P_{1/2}-9^2D_{3/2}$	0		25	6844.05	14,608	$6^2S_{1/2}-6^2P_{1/2}$	1	*x*
0	2711.74	36,866	$6^2P_{1/2}-10^2S_{1/2}$	0		20	7191.40	13,902	$6^2P_{3/2}-7^2S_{1/2}$	0	
2	2727.82	36,648	$6^2P_{5/2}-9^2D_{5/2}$	1		10	7387.79	13,532	$p^2\,{}^2D_{3/2}-6^2P_{3/2}$	0	
0	2778.34	35,982	$6^2P_{3/2}-10^2S_{1/2}$	0		1	7408.62	13,494	$7^2P_{3/2}-8^2D_{5/2}$	0	
2	2825.52	35,381	$6^2S_{1/2}-7^2P_{3/2}$	−2	*f*	13	7741.80	12,913	$p^2\,{}^2D_{5/2}-6^2P_{3/2}$	1	
1	2846.42	35,121	$6^2S_{1/2}-7^2P_{1/2}$	1	*f*	3	7904.00	12,648	$p^2\,{}^2D_{3/2}-6^2P_{1/2}$	0	

x, Classified by Green and Loring.
y, Classified by Lang.
a, Our measurements are about an angstrom higher than Lang's.
b, Green and Loring classified as $5^2P_{1/2,\ 3/2}-7^2S_{1/2}$.
c, Lang's classification has the *j* values interchanged.
d, May be the line 2433.473 classified in Sn I by Green and Loring.
e, Green and Loring gave λ2849.8 and λ2488 for this pair.
f, Green and Loring used λ2789.32 and λ2761.78 for this pair.
g, An OH line falls on the tin line.
h, These lines are covered by rather strong helium lines.
i, Green and Loring used λ3624.6 and λ3540.0 for this pair.
k, Lang classified as $6^2P_{1/2}-7^2D_{1/2}$.
l, Our measurements on these strong lines are lower than those of Green and Loring by 0.5 to 0.9A, perhaps because of the greater sharpness of the lines from the hollow cathode.

terns were resolved, λ6453 $6^2P_{3/2}-6^2S_{1/2}$ and λ5596 $6^2D_{1/2}-6^2P_{3/2}$, and gave patterns in complete agreement with the assignments. However, the later work of Shenstone and Blair[7] permits the calculation of the center of intensity of unresolved patterns. Table I shows the results of such a calculation for the remaining magnetic measurements of Green and Loring on Sn II lines. In this table, for each line, is given the separation observed by Green and Loring and, immediately below it, that to be expected from the formula of Shenstone and Blair for the classification given by Green and Loring. The correctness of the assignments is established by the good agreement. The 6^2P, 5^2D, 5^2D and $p^2\,{}^2D$ differences are thus established and these differences, together with the 5^2P difference of Green and Loring, which was assumed to be correct, formed a starting point for further classification.

It was found possible to extend all the doublet series beyond the two members already known. The 4^2F and 5^2F terms were resolved for the first time and found to be inverted. The 4^2F-m^2G series were discovered and six terms measured, and the $p^2\,{}^2P$ term located. In all, over 100 lines were classified and are given in Table II. Lines classified by other experimenters and changes made by the authors in previous classifications are indicated in the notes. The classified lines determine 48 terms, which are given in Table III, together with the separations and effective quantum numbers of the doublet series members. The term values here given are based on a new value of the ionization potential (118,017±3 cm^{-1}). This value was determined by adjusting the term values of the ^2G series until the quantum defects approached constancy, which could be done with an uncertainty of about one wave number. The accuracy of the determination of the ionization potential is then limited by the uncertainty in fixing the $5^2P_{1/2}$ level on the basis of the vacuum data for transitions to this term. Since there are several such transitions the uncertainty is much less than in a single measurement and is probably about ±3 cm^{-1}.

The $p^2\,{}^2P$ terms had not been located previously, but Lang's suggestion that the pair λλ1180.51 and 1243.00 formed part of the $^2P\,{}^2P'$ multiplet was adopted and the remaining pair searched for. A strong line at 1316.59A is probably one line of this pair but its companion, $p^2\,{}^2P_{1/2}-5^2P_{1/2}$, was not found. The location of these terms may be checked approximately by the relation given by Bacher and Goudsmit[8] which states that, for Russell-Saunders coupling, the interval between the terms ^4P and ^2P from the configuration sp^2 should be three halves the interval between the ^3P and ^1P terms of the corresponding configuration of the once more ionized atom when the intervals are measured between the centers of gravity of the terms. The $5s5p^2(^4P-{}^2P)$ difference in Sn II is about 35,000 cm^{-1} while the $5s5p(^3P-{}^1P)$ interval in Sn III is 22,600 cm^{-1}. The ratio is, then, 1.57.

TABLE III. *Term values in* Sn II, *with separations and effective quantum numbers. Previously determined terms are italicized. All others are new.*

	4	5	6	7	8	9	10	11
$^2S_{1/2}$			*61134*	*31741*	19618	13338	9661	7321
n^*			2.680	3.719	4.730	5.737	6.741	7.743
$^2P_{1/2}$		*118017*	*46527*	26114	16821			
n^*		1.929	3.072	4.100	5.108			
		4252	884	363	191			
$^2P_{3/2}$		*113765*	*45643*	25751	16630	11649		
n^*		1.965	3.101	4.129	5.138	6.139		
$^2D_{3/2}$		*46612*	*27779*	17737	12287	9014	6897	5446
n^*		3.069	3.975	4.975	5.977	6.978	7.978	8.978
		642	110	54	30	20	16	13
$^2D_{5/2}$		*45970*	*27669*	17683	12257	8994	6881	5433
n^*		3.090	3.983	4.982	5.984	6.986	7.987	8.988
$^2F_{5/2}$	*28725*	*18354*	12650					
n^*	3.909	4.891	5.891					
	−6	−4						
$^2F_{7/2}$	28731	18358						
n^*	3.909	4.890						
$^2G_{7/2,\ 9/2}$			12282	9017	6899	5447	4410	3643
n^*			5.978	6.977	7.977	8.977	9.977	10.977
	$^4P_{1/2}$	*73508*						
$6s6p^2$	$^4P_{3/2}$	*71554*	$^2D_{3/2}$	*59175*	$^2P_{1/2}$	37812		
	$^4P_{5/2}$	*68524*	$^2D_{5/2}$	*58555*	$^2P_{3/2}$	33311	$^2S_{1/2}$	*36298*

TABLE IV. *Unclassified lines of tin. The lines given by Arnolds are marked with an asterisk. The other lines are new.*

Intensity	λ Air	ν Vac.	Intensity	λ Air	ν Vac.
* 9	2265.98	44,116	*13	3413.03	29,291
9	2419.49	41,318	10	3102.23	32,226
*10	2445.01	40,887	* 9	3122.51	32,016
8	2504.59	39,915	*40	3223.59	31,012

[7] Shenstone and Blair, Phil. Mag. **8**, 765 (1929).

[8] Bacher and Goudsmit, Phys. Rev. **46**, 948 (1934).

The agreement is good considering the fact that the coupling is probably not extreme Russell-Saunders.

The lines given in Table IV are the only ones of considerable intensity in the data which are unassigned. Those marked with a star were listed by Arnolds[9] as tin lines. Some of the stronger unclassified lines may belong to the arc spectrum of tin, although they do not fit in the existing term scheme.[1]

Perturbations

A consideration of the effective quantum numbers in Table III indicates that the ^2P and ^2F series are regular, as is to be expected in view of the absence of perturbing terms of the same parity. Likewise, the ^2G terms are expected to be regular, since they have no J values in common with the other even terms.

Irregularities occur, however, among the other even terms; the 7^2S term is displaced somewhat from the predicted location while the 5^2D terms are markedly displaced and have a larger separation than expected. These irregularities are shown graphically in Fig. 1, where the Rydberg correction term a is plotted against the principal quantum number n. The fact that the quantum numbers of these terms are higher than expected is interpreted as being due to repulsion from the lower lying perturbing terms $p^2\,^2S$ and $p^2\,^2D$. The perturbing terms, themselves, are probably displaced downward because of the interaction. Thus the $p^2\,^2S$ term is found between the $p^2\,^2P$ terms, whereas its normal position would be above them. A rough calculation, assuming the Slater interval relations,[10] indicates that the $p^2\,^2D$ terms are lower by some 9000 cm^{-1} than their predicted position. These series terms and the corresponding perturbing terms share characteristics to such an extent that it is nearly impossible to distinguish between them.

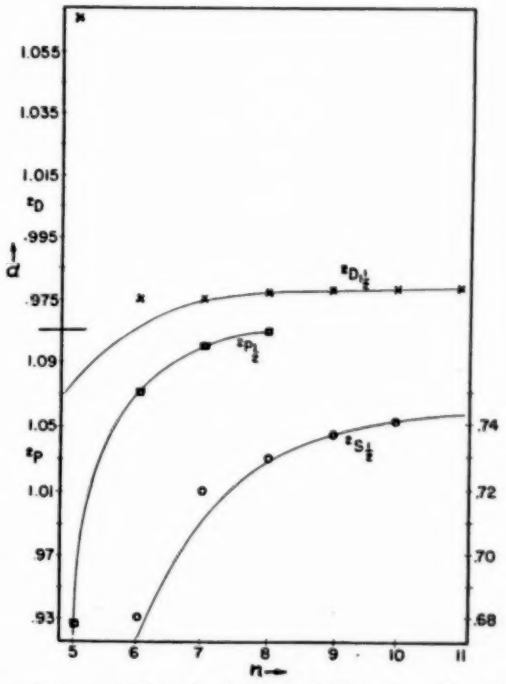

Fig. 1. Irregularities in the ^2S and ^2D terms of Sn II, as shown by plot of the Rydberg correction term, a, vs. principal quantum number, n.

Comparisons with the isoelectronic spectra In I and Sb III were made by investigation of the regular and the irregular doublet laws. Unfortunately, data on these spectra are not very complete so that the number of comparisons which could be made was not large.

From the expression:

$$\Delta\nu=\frac{R\alpha^2(Z-s)^4}{n^3l(l+1)}$$

the values of the screening constant s have been computed and are shown in Table V. The agreement is satisfactory for heavy atoms, particularly in view of the existing perturbations. The large changes in the values of s for the $5D$ terms of successive isoelectronic spectra is indicative of the perturbation of these terms by the $p^2\,^2D$ terms.

Table V. *The regular doublet law. Values of the screening constant, s, from the relation* $\Delta\nu=\frac{R\alpha^2(Z-s)^4}{n^3l(l+1)}$.

	5P	6P	7P	8P	
In I	31.44		38.30	39.04	
Sn II	29.32	33.99	35.62	36.55	
Sb III	27.94	32.24			
	5D	6D	7D	8D	9D
In I	41.58	38.73	39.21	39.13	
Sn II	33.04	37.49	38.24	38.78	38.93
Sb III	27.80	35.84			

[9] Arnolds, Zeits. f. Wiss. Phot. **13**, 313 (1913–14).

[10] Slater, Phys. Rev. **34**, 1293 (1929).

The Thermal Expansion of Crystalline Sodium Between 80°K and 290°K*

SIDNEY SIEGEL AND S. L. QUIMBY
Columbia University, New York, N. Y.

(Received May 5, 1938)

The observed linear thermal expansion of crystalline sodium is tabulated at ten degree intervals between 80°K and 290°K. The behavior of this material is in accord with the relation obtained by Gruneisen between thermal expansion and heat content, within the precision measure of the latter quantity. A description of the thermal expansion and cryostatic apparatus is given.

THE only data on the thermal expansion of sodium that the writers have been able to discover are the observations of Dewar,[1] who measured the density of sodium at the temperature of boiling liquid oxygen, and those of Richards and Brink,[2] who measured the density at 20°C. This circumstance blocked the completion of a research on the temperature variation of the principal elastic constants of crystalline sodium, in which the dynamical method of Balamuth[3] and Rose[4] was used. Accordingly the investigation here reported was undertaken.

Apparatus and Method

The specimen material is triply distilled Mallinckrodt sodium, the first and last quarters of the distillate having been rejected in the first distillation. The specimens are single crystals in the form of right circular cylinders 0.47 cm in diameter and 4 cm long.[5]

A cross-sectional elevation and two cross-sectional plans of the thermal dilatometer are shown in Fig. 1. The dilatometer proper, represented by the cross hatched portion of the figure, is constructed entirely of clear fused quartz. The envelope is Pyrex glass. The specimen is loosely encased in a thin-walled glass tube, which is held vertical against guides on a vertical support by a silk thread. This thread passes around the tube at its middle, over pulleys on opposite sides of the support, and down to a 15 gm weight, not shown, hanging below. The specimen rests on a hemispherical protuberance on a horizontal plate fused to the bottom of the support.

A bit of microscope cover glass is placed on top of the specimen, and on this rests a 2 mm quartz rod held vertical in guides. This rod can be raised or lowered into position by means of a silk thread attached near the top and wrapped around a spindle operated through a ground glass joint. The top of the rod is drawn out to a very fine, short, vertical fiber. Immediately adjacent to this fiber is another, attached to the support. The tips of both fibers are viewed simultaneously through a compound microscope equipped with a 32 mm objective and a filar micrometer eyepiece. The change in length of the specimen is measured by measuring the change in the distance between the fixed and moving fiber tips.

The temperature of the specimen is measured with a copper-constantan thermojunction located near its midpoint. The thermojunction leads are brought out of the envelope at the points labeled *T.C.* in the figure.

The dilatometer and microscope are mounted in common on a heavy metal fitting, which is firmly secured to an elevating table. The specimen is inserted in the cryostat described below, or in an appropriate constant temperature bath, by lowering this table. This procedure leaves the entire measuring equipment undisturbed.

Observations below 100°K are made with the lower part of the dilatometer immersed in a dewar of liquid nitrogen and liquid oxygen. Above 220°K the bath liquid is methanol containing a suitable amount of solid carbon dioxide. Thermal contact between the specimen

* Publication assisted by the Ernest Kempton Adams Fund for Physical Research of Columbia University.

[1] Dewar, Proc. Roy. Soc. **70**, 237 (1902).
[2] Richards and Brink, J. Am. Chem. Soc. **29**, 117 (1907).
[3] Balamuth, Phys. Rev. **45**, 715 (1934).
[4] Rose, Phys. Rev. **49**, 50 (1936).
[5] The experimental methods for growing and handling the crystals will be described in the paper dealing with the elastic constants, shortly to be submitted for publication in this journal.

and these constant temperature baths is secured by filling the dilatometer with helium at atmospheric pressure. Temperatures between 100°K and 220°K are obtained with the cryostat shown diagrammatically in Fig. 2.

C (Fig. 2) is a copper tube 10 inches long, $\frac{13}{16}$ inch internal diameter, and $\frac{3}{4}$ inch wall thickness, about which is wound a single layer of No. 22 copper wire. It hangs suspended by three Bakelite screws from a copper pan, *D*, and is surrounded by an unsilvered dewar, *B*, which can at will be evacuated or filled with helium. This dewar rests on a brass and Bakelite frame, not shown, in a large high vacuum silvered dewar, *A*, which is mounted in a wooden box. The top of this box supplies the support for the pan, *D*, and the suspended copper tube. The pan is filled with a slush of solid carbon dioxide and methanol, and the large dewar with liquid nitrogen.

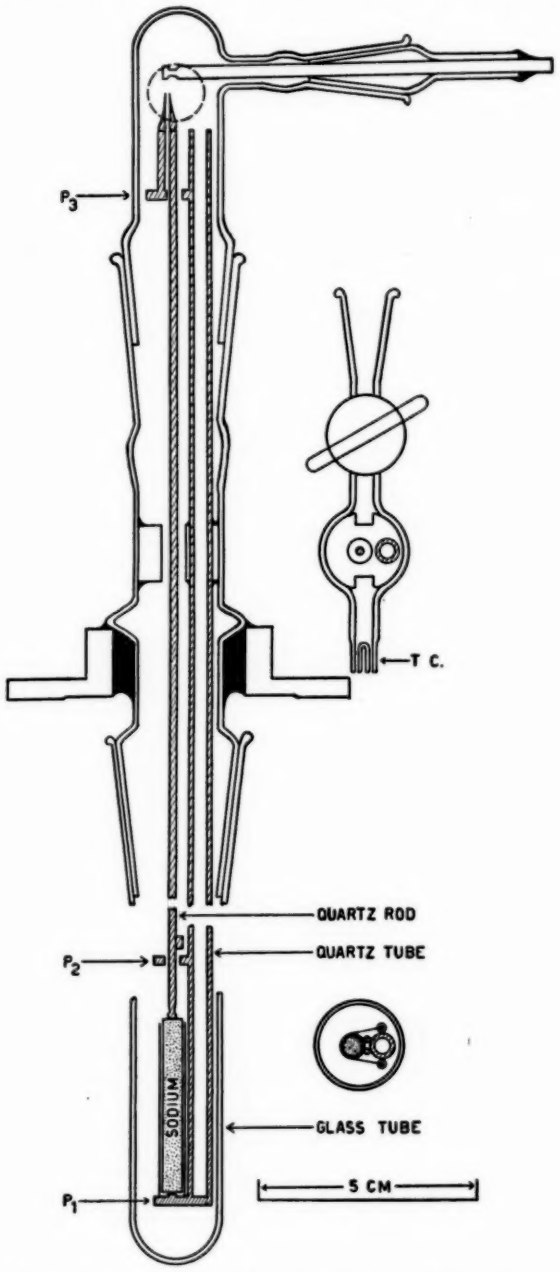

FIG. 1. Diagram of the thermal expansion apparatus.

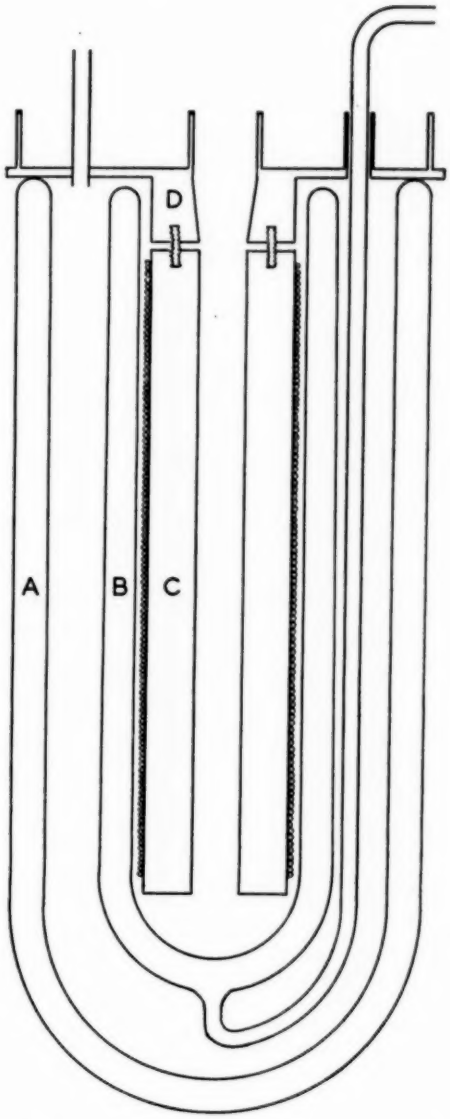

FIG. 2. The cryostat for obtaining temperatures between 100°K and 220°K.

The temperature of the cryostat is adjusted by manipulating the current in the coil and the

vacuum in the dewar, B. The maximum temperature difference between the top and the bottom of the tube is about 1°K. The temperature of the specimen in the cryostat is easily stabilized to 0.1°K for several minutes. A single run from 220°K to 100°K, with observations every 10°K, takes about 8 hours and consumes about 15 lb. of liquid nitrogen.

Results

The data given in Table I represent the mean of observations on three single crystals of sodium. The data on one of these crystals is plotted in Fig. 3. None of the observations on any of the crystals departs from the mean by more than 0.3 percent of the total change in length between 80°K and 290°K.

The last column in Table I contains the ratio of the change in length per unit length here observed to the corresponding change in the heat content, ΔH, as calculated from the data given in the *International Critical Tables*.[6] In accordance with a simplified relation obtained by Gruneisen from the lattice theory of crystals[7] this ratio should be independent of the temperature. The agreement is well within the precision measure of ΔH.

TABLE I. *The thermal expansion of crystalline sodium. The last column gives the ratio of the thermal expansion to the corresponding change in the heat content.*

Temp. (°K)	Total Expansion in Percent of the Length at 273°K	$(\Delta L/L)/\Delta H$
80	−1.155	2.36
90	1.114	
100	1.071	2.41
110	1.022	
120	0.970	2.40
130	0.917	
140	0.860	2.42
150	0.801	
160	0.742	2.44
170	0.682	
180	0.621	2.46
190	0.557	
200	0.493	2.46
210	0.428	
220	0.361	2.47
230	0.294	
240	0.226	2.51
250	0.158	
260	0.090	2.50
270	0.022	
280	+0.047	
290	+0.116	2.31

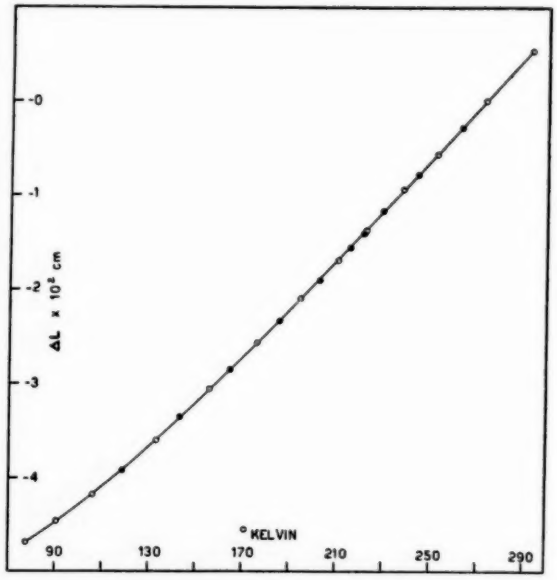

FIG. 3. The thermal expansion of a single crystal of sodium. The circles represent observations made with the temperature decreasing, and the dots observations made subsequently with the temperature increasing.

Accuracy

The filar micrometer screw was calibrated on a large Geneva Society comparator. The calibration constant of the microscope is 0.00145 mm per scale division of the screw head, and is uniform over the working range. Settings can be repeated within a single division. The correction for the thermal expansion of 4 cm of quartz amounts to only 1 percent. The thermocouple was temperature calibrated before and after the observations against a platinum resistance thermometer certificated by the National Bureau of Standards. The two calibrations agreed to 0.2°K. Accordingly it is estimated that the measurements of ΔL are accurate to 0.002 mm.

In conclusion, the writers acknowledge their indebtedness to the Ernest Kempton Adams Fellowship of Columbia University for the financial assistance which made this research possible.

[6] *International Critical Tables*, V, p. 88.

[7] Gruneisen, *Handbuch der Physik*, Vol. 10, p. 42. Durand (Physics **7**, 297 (1936)) has shown that single crystals of MgO obey Gruneisen's relation over the same temperature range.

A Generalization of the Theory of Ferromagnetism*

F. BITTER
Massachusetts Institute of Technology, Cambridge, Massachusetts

(Received May 18, 1938)

The Weiss-Heisenberg theory of ferromagnetism is discussed and generalized in a plausible way. Whether this generalization is theoretically sound must be determined by a quantum-mechanical investigation. The proposed equations of state, however, may be regarded as an attempt to describe antiferromagnetism (i.e., the case in which oppositely directed spins on adjacent atoms have the lowest energy), pure metals having less than one spin per atom, and the magnetic properties of alloys. No attempt is made to compare the results with the properties of actual alloys, but it is shown that the proposed equations do give systems in which the Curie temperature depends on composition and atomic order; in which nonmagnetic metals may combine to produce a ferromagnetic alloy; in which wasp waisted hysteresis loops occur; and in which heat treatment may radically affect magnetic properties. Large effects are predicted which should make it easy to verify experimentally whether or not the proposed approach to the problem is on the right track.

THE theory of ferromagnetism as developed by Weiss, Heisenberg, and others, has been used chiefly to interpret the magnetic properties of crystals of like atoms in which internal forces tend to make elementary magnetic moments point in the same direction. In this field even the simplest form of the theory has been quite successful in accounting for the dependence of spontaneous magnetization, magnetic susceptibility, and specific heat on temperature. The simple magnetic equation of state which gives these results is admittedly only approximate, but its success has been sufficient to give point to the question of how it might be generalized to include systems of unlike atoms and systems in which conflicting internal forces may be present. There is at present no hope of setting up such equations rigorously, and we shall consequently have to content ourselves with plausible guesses based on the theories of Weiss and Heisenberg, which we shall first briefly review. We shall assume systems containing dipoles that are either parallel or antiparallel to each other and to the externally applied field. In a system containing N such dipoles of which $N+$ are pointing to the right and $N-$ are pointing to the left, the relative intensity of magnetization is defined as $i=(N_+-N_-)/(N_++N_-)$, and the total intensity of magnetization is defined as $I=\mu Ni$. The Langevin theory of paramagnetism states that if these elementary dipoles do not interact with each other, the magnetization i, absolute temperature T, and magnetic field H are related by the equation $i=\tanh(\mu H/kT)$. The Weiss theory generalizes this by saying that if the dipoles do interact, this interaction may be represented as an additional field proportional and parallel to the intensity of magnetization and the equation of state becomes

$$i=\tanh\left[(Di+\mu H)/kT\right]. \tag{1}$$

From this equation of state one can calculate the physical properties of the system. The spontaneous magnetization (i as a function of T for $H=0$) and volumes susceptibility ($K_0=\mu N\,\partial i/\partial H$ for $H=0$) follow directly. If the equation has more than one solution, the most stable one is defined as that having the lowest free energy $f=u-\mu iH-T\varphi$, the internal energy u and entropy φ per atom being defined by[1]

$$du=s_I dT-\left(T\frac{\partial H}{\partial T}-H\right)\frac{dI}{N}, \tag{2}$$

$$d\varphi=\frac{s_I dT}{T}-\frac{\partial H}{\partial T}\frac{dI}{N}, \tag{3}$$

where s_I is the atomic specific heat at constant magnetization. Substituting from the equation of state and integrating one finds that

$$u=-\tfrac{1}{2}Di^2, \tag{4}$$

$$\varphi=-\tfrac{1}{2}k\left[(1+i)\ln(1+i)+(1-i)\ln(1-i)\right], \tag{5}$$

* The outlines of this paper were first presented at a meeting of the American Physical Society, December 28–30, 1936, and at the Symposium on the Structure of Metallic Phases, held by the department of physics of Cornell University, July 1, 1937.

[1] See F. Bitter, *Introduction to Ferromagnetism* (McGraw-Hill, 1937) Chapter IX.

terms independent of i being omitted. s_I can be shown to be independent of i.

The Heisenberg theory is the quantum-mechanical counterpart of an earlier theory due to Ising[2] which was first developed for the case of linear chains of atoms, but which we shall run through in a more general way. The magnetic moments are assumed to be distributed on the lattice points of a crystal, and each dipole has z nearest neighbors. It is assumed that only nearest neighbors interact, and that the total energy of the crystal may be taken as the sum of the mutual energies of all pairs of nearest neighbors

$$Nu=\epsilon_{++}\nu_{++}+\epsilon_{+-}\nu_{+-}+\epsilon_{--}\nu_{--}.$$

ϵ_{++} is the interaction energy of a pair of positive dipoles, ν_{++} is the number of these present in some particular configuration of the crystal, and it is assumed for simplicity that the total volume of the crystal is one cubic centimeter. It can be shown that this expression can be rewritten in terms of a new parameter σ, sometimes called the short range order, defined by

$$\nu_{+-}=\tfrac{1}{4}Nz(1-\sigma).$$

From this definition it follows that

$$\begin{aligned}\nu_{++}&=\tfrac{1}{4}Nz\{1+i-\tfrac{1}{2}(1-\sigma)\},\\ \nu_{--}&=\tfrac{1}{4}Nz\{1-i-\tfrac{1}{2}(1-\sigma)\},\\ u&=-\tfrac{1}{2}D\sigma\end{aligned}\qquad(6)$$

where D is a constant derived from the interaction energies. The variables i and σ define the state of the crystal. Unfortunately it is not possible to write the entropy as a function of i and σ except for the case of a linear chain of atoms, because we do not know how to estimate the number of configurations corresponding to given values of i and σ. We do know, however, that there are far more configurations for $\sigma=\bar{\sigma}$ than for any other configuration; in fact that the total number of configurations for all values of σ with a fixed i is very nearly equal to the number of configurations for $\sigma=\bar{\sigma}$ and the same value of i. It can easily be shown that the mean value[3] of σ is

$$\bar{\sigma}=i^2$$

and that if we neglect states with values of $\sigma\neq\bar{\sigma}$, the entropy must have the forms given in Eq. (5). With these assumptions one can readily obtain the equation of state (1) by minimizing the free energy.

Heisenberg's theory differs from the above form of Ising's theory in two respects. First, if electronic spins are responsible for the magnetization i, the mean value of σ must be found by calculating the mean value[4] of the product of two spin operators $\langle s_j\cdot s_k\rangle_{Av}$ instead of the mean value of the product two numbers $\langle x_jx_k\rangle_{Av}$. For the case of a pure ferromagnetic metal, however, this calculation gives $\bar{\sigma}=i^2$ as in Ising's theory, and to this approximation the two theories give the same result. Heisenberg, however, goes on to assume a Gaussian distribution of states about the mean value, and adjusts the spread of this assumed distribution, so that the quantity $\overline{\sigma^2}-\bar{\sigma}^2$ has its correct value. In this approximation the two theories give different results. Ising's approximation is[5]

$$i=\tanh\left\{\frac{\mu H}{kT}+\frac{Di}{kT}\left[1-\frac{D}{kT}\frac{(1-i^2)}{z}\right]\right\},\qquad(7)$$

which behaves "sensibly" at all temperatures, while Heisenberg's more correct treatment gives

$$i=\tanh\left\{\frac{\mu H}{kT}+\frac{Di}{kT}\left[1-\frac{D}{kT}\frac{(2-i^2)}{z}\right]\right\},\qquad(8)$$

which breaks down at low temperatures. The physical properties derived by means of these equations differ only slightly from those obtained from the simpler equation of state (1).

This is the foundation on which we shall proceed with our generalization. The inclusion of fluctuations[6] adds so much to the complexity of the work, and so little to the physical content of the equations, that we shall omit them here. Eq. (1) is consequently our starting point. In

---

[2] E. Ising, Zeits. f. Physik **31**, 253 (1925).

[3] Let x_k be a number which is $+1$ when the kth lattice point is occupied by a positive moment, and -1 when occupied by a negative moment. $\sum_{k=1}^{N}x_k=N_+-N_-=Ni$; $\sum_{k=1}^{N}x_k^2=N$; $\frac{1}{2}\sum_{\text{all pairs}}(1-x_jx_k)=\nu_{AB}$; $\sum_{\text{all pairs}}x_jx_k=Nz\sigma/2$; $\langle x_jx_k\rangle_{Av}=\bar{\sigma}$; $\sum x_j\sum x_k=i^2N^2=\sum x_k^2+N(N-1)x_jx_k=N(N-1)\bar{\sigma}$; and for large values of N therefore $\bar{\sigma}=i^2$.

[4] See Van Vleck, *Electric and Magnetic Susceptibilities* (Oxford, 1932) Chapter XII.

[5] A similar equation has been obtained by J. G. Kirkwood, J. Chem. Phys. **6**, 73 (1938) for the order-disorder problem.

[6] L. Néel has attempted to include the effects of fluctuations in a different way. Ann. de physique **17**, 1 (1932).

discussing it we may use the language of any of the three derivations given above, which we shall refer to briefly by the names of Weiss, Ising, and Heisenberg. Of these we shall choose the method of Weiss because it is best suited to discussing the physical ideas in words with a minimum of calculation. The same results follow from the theory of Ising if we limit ourselves to the mean values of the energy, but it seems hardly worth while to go through the calculations in print. Whether or not the Heisenberg theory gives the same result to this approximation has not been determined.

Equation (1) applied to pure ferromagnetic media for which $D>0$ gives a spontaneous magnetization which vanishes for $T>D/k=T_c$; a specific heat having a discontinuity for $T=T_c$; and an initial susceptibility given by the formula

$$K_0=\frac{N\mu^2/k}{T/(1-i^2)-T_c}. \tag{9}$$

This quantity is $\partial I/\partial H$ for $H=0$ as calculated from Eq. (1). Below the Curie point it represents the small increase in the spontaneous magnetization which can be produced by strong fields. This has not yet been measured. Above the Curie temperature there is no spontaneous magnetization, $i=0$, and the behavior of actual materials is fairly well described by Eq. (9). The internal field in Eq. (1) is assumed to be proportional to the intensity of magnetization. This statement should be made more precise by saying, instead, that the field acting on any one atom is proportional to the intensity of magnetization of that group of atoms with which it interacts. It can be shown that for the case under discussion the positive and negative spins are randomly arranged among each other, and that, therefore, the intensity of magnetization of all groups of atoms within a region of spontaneous magnetization will be the same. The question of the range of the interatomic forces is, therefore, irrelevant, and Eq. (1) will hold whether we assume short range forces as in the Ising and Heisenberg treatments, or arbitrarily long range forces.

The question of the range of the forces,[6] however, becomes important when we consider antiferromagnetism, or the case in which the internal forces are such as to make interacting spins antiparallel to each other. To illustrate this, we shall consider two limiting cases. If the range of the forces is sufficiently large, we may assume as before that the internal field is proportional to the spontaneous magnetization, since the average magnetization of a sufficiently large group of atoms is likely to be equal to the spontaneous magnetization. The equation of state is then Eq. (1), with $D/k=T_c<0$. The spontaneous magnetization is now zero for all temperatures, the specific heat is constant, and the initial susceptibility is given by

$$K_0=\frac{N\mu^2/k}{T-T_c}. \tag{10}$$

This formula predicts a finite susceptibility at the absolute zero, continuously decreasing with rising temperature, and with small values of N and large negative values of T_c its contribution to the total susceptibility is of the same order of magnitude as that observed for some metals.

If the range of the internal forces is exceedingly short, we may neglect the interaction of all but nearest neighbors. In this case we must consider the possibility of orderly arrangements of magnetic moments in such a way that the average intensity of magnetization of the nearest neighbors of an atom is not equal to the total average intensity of magnetization of nearby atoms. In the case of a body-centered cubic lattice, for instance, it is convenient to break the lattice up into two simple cubic lattices which have the property that any atom on one of these sublattices has its eight nearest neighbors on the other sublattice. In the absence of interactions between next nearest neighbors[7] we may assume the magnetization of these sublattices to be uniform. Denoting the relative intensity of magnetization of these sublattices by i_1 and i_2, we may write

$$i_1=\tanh\frac{Di_2+\mu H}{kT}, \tag{11}$$

$$i_2=\tanh\frac{Di_1+\mu H}{kT}, \tag{12}$$

[7] For a suggestion as to how these and more remote interactions may be taken into account, see a note by the author to appear shortly in J. Chem. Phys. and footnote 12 below.

since the internal field acting on the atoms of one sublattice is proportional to the intensity of magnetization of the atoms on the other sublattice. It is convenient to replace these variables by the total relative intensity of magnetization $i=(i_1+i_2)/2$ and an order parameter $p=(i_1-i_2)/2$ similar to the order parameter S in the theory of order-disorder in alloys. In terms of these variables Eqs. (11) and (12) may be written

$$\tfrac{1}{4}\ln\frac{(1+i+p)(1+i-p)}{(1-i-p)(1-i+p)}=\frac{Di+\mu H}{kT}, \tag{13}$$

$$\tfrac{1}{4}\ln\frac{(1+i+p)(1-i+p)}{(1-i-p)(1+i-p)}=-\frac{Dp}{kT} \tag{14}$$

and the expression for the internal energy becomes

$$u=-\tfrac{1}{2}D(i^2-p^2). \tag{15}$$

For ferromagnetic substances $D>0$, and the solution of the above equations is $p=0$, and i satisfies Eq. (1). For antiferromagnetic substances $D<0$, and in the absence of a magnetic field the solution of (13) and (14) is

$$i=0,$$

$$p=\tanh(-T_cp/T). \tag{16}$$

$$K_0=\frac{N\mu^2/k}{T/(1-p^2)-T_c}. \tag{17}$$

The specific heat has an anomaly for $T=-T_c$ identical with that of a ferromagnetic at the Curie temperature, and the susceptibility has the form shown in Fig. 1. No material exhibiting such properties is known.

Néel[8] has pointed out that manganese probably is an antiferromagnetic substance in the above sense, as it has an anomaly in the specific heat near 350°C. Its magnetic susceptibility, however, is constant below the critical temperature and falls off slightly above it. Our considerations were based on the assumption that the elementary magnetic moments were parallel or antiparallel to the applied field. Néel[9] shows that if this assumption is dropped, it seems

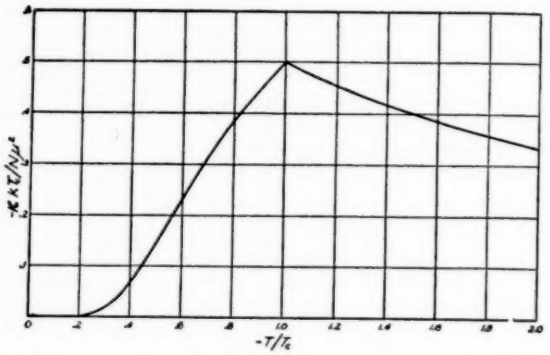

FIG. 1. Susceptibility of an antiferromagnetic substance as a function of temperature.

quite reasonable to expect susceptibilities for $T=0$ of the same order of magnitude as for $T=T_c$, because of the rotation of individual magnetic moments.

Hulthen[10] has also calculated the susceptibility of antiferromagnetic materials at low temperatures, using a method due to Heller and Kramers.[11] He finds that in small fields the magnetic moments tend to set themselves at right angles to the applied field and antiparallel to their nearest neighbors. At low temperatures the susceptibility has the form $A-BT^2$. In actual materials the behavior will be complicated by crystalline fields tending to orient magnetic moments with reference to the crystallographic axes. If anomalies of the type shown in Fig. 1 do actually occur, they will be superimposed on other effects due to causes which have not been considered in this article.

The results obtainable for alloys[6] are very complicated, and we shall attempt here only to indicate the general outlines of a theory. If it is assumed that we may neglect the interactions of all but nearest neighbors, it is at once apparent that the ordering tendency of different types of atoms in an alloy will play an important part in determining magnetic properties. Furthermore, the internal fields responsible for ferromagnetism will influence the degree of order at any particular temperature, and these effects may be large, as the critical temperatures for ferromagnetism are of the same order of magni-

[8] L. Néel, Comptes rendus **203**, 304 (1936).
[9] L. Néel, Ann. de physique **17**, 63 (1932).
[10] L. Hulthen, Proc. Roy. Acad. Amsterdam **39**, 190 (1936).
[11] G. Heller and H. A. Kramers, Proc. Roy Acad. Amsterdam **37**, 378 (1934).

tude as the critical temperatures for the order-disorder transitions. One ought really to build up a theory on the assumption that atoms of two kinds, A and B, each having a magnetic moment μ_A or μ_B, can interact in several ways, and that the total energy of any configuration of the alloy is the sum of the energies of pairs of nearest neighbors. This would give different values to parallel and antiparallel pairs of types $A-A$, $A-B$, and $B-B$. One ought then to calculate the equilibrium degree of order and magnetization for every temperature. The equations defining such equilibrium may be readily set up in a nice symmetrical form, but their solution is so laborious that we shall simply treat the order parameter and the concentration as independent variables, and omit the question of determining the conditions that homogeneous phases of given composition and order may exist.[12]

For simplicity we shall again consider a body-centered cubic lattice which may be broken up into two sublattices having the property that any atom of one interacts only with atoms on the other, if we consider nearest neighbor interaction only. If N_{A1+} are the number of atoms of type A on sublattice one whose magnetic moments point to the right, and other similar symbols are used for the number of atoms of other types we have

$$N_{A1+}+N_{A1-}=N_{A1},$$
$$N_{A1}+N_{B1}=N_1,$$
$$N_{A1}+N_{A2}=N_A$$

and similarly for atoms of type B and sublattice two. The concentration of atoms of types A and B on one sublattice is defined by

$$y_1=(N_{A1}-N_{B1})/N_1,$$
$$N_{A1}/N_1=\tfrac{1}{2}(1+y_1); \qquad N_{B1}/N_1=\tfrac{1}{2}(1-y_1).$$

The total mean concentration is

$$y=(N_A-N_B)/N=\tfrac{1}{2}(y_1+y_2)$$

and the long range order is defined by

$$S=\tfrac{1}{2}(y_1-y_2).$$

The relative intensity of magnetization is defined by

$$i_{A1}=(N_{A1+}-N_{A1-})/N_{A1}$$

with similar variables for both types of atoms on either lattice. If we assume that the internal field acting on any one atom is made up of two parts, one due to the atoms of the same type, and one due to atoms of the opposite type, and that either of these fields is proportional to the

[12] The formulation of this problem may be undertaken quite generally as follows: Suppose we have an arbitrary number of kinds of atoms, arranged on the lattice points of a crystal. Among the various kinds of atoms we may distinguish between atoms of the same chemical species, but in different states. Our calculations are based on the assumptions that the energy of interaction of any two atoms is independent of the arrangement of the remaining atoms of the lattice. With this assumption interactions over arbitrarily large distances may be included. To do this, break up the lattice into a set of interpenetrating sublattices such that the nearest neighbors on each sublattice are a distance apart greater than some arbitrarily chosen distance, Ro, which we define as the range of the atomic interactions. The atoms of any one sublattice may then be considered to have no interaction with each other. Consider now any two sublattices in their mutually correct positions. It will always be possible to break up the original lattice into a sufficient number of sublattices such that each atom of one of any pair of sublattices j and k has a certain number of neighbors on the other sublattice a distance $R_{jk}<Ro$ away, and that in this pair of sublattices there are no other neighbors at distances less than Ro. If n_j represents the total number of lattice points on the jth sublattice, and n_{jA} the number of these lattice points occupied by atoms of type A, we may define any configuration of the lattice in terms of the concentration variables $x_{jA}=n_{jA}/n_j$. The entropy may be written as a sum of terms of the form $-x_{jA}\ln x_{jA}$. Numerical factors will appear in some of these terms if the number of atomic sites is not the same for all the sublattices. The energy may be expressed as a sum of terms of the form $\epsilon_{jkAB}\nu_{jkAB}$ where the first factor represents the energy of interaction of two atoms A and B a distance R_{jk} apart, and the second factor represents the number of such pairs on the j and k sublattices in any particular configuration. If, as above, we replace the energy distribution by its mean value, we must calculate the mean values of the quantities ν_{jkAB}. These can readily be calculated by the following device. Let ν_{jk} be the total number of pairs of nearest neighbors on sublattices j and k. Let $\delta_{ij}^{(\alpha)}$ be a number equal to unity if the ith lattice point on the jth sublattice in some particular configuration designated by (α) is an atom of type A, otherwise $\delta=0$. Similarly let $\gamma_{ij}^{(\alpha)}$ be unity if the site is occupied by an atom of type B, otherwise $\gamma=0$.

$$\nu_{jkAB}^{(\alpha)}=\sum_{il}{}^{*}(\delta_{ij}^{(\alpha)}\gamma_{lk}^{(\alpha)}+\gamma_{ij}^{(\alpha)}\delta_{lk}^{(\alpha)}),$$

$$\langle\nu_{jkAB}\rangle_{Av}=\frac{\sum_{(\alpha)}\nu_{jkAB}^{(\alpha)}}{\dfrac{n_j!}{n_{jA}!n_{jB}!\cdots}\dfrac{n_k!}{n_{kA}!n_{kB}!\cdots}}.$$

$\sum_{il}{}^{*}$ means sum over all pairs of nearest neighbors, and $\sum_{(\alpha)}$ means sum over all configurations of the system. Substituting the first expression in the second, and summing first over (α) keeping i and l fixed, one finds that

$$\langle\nu_{jkAB}\rangle_{Av}=\nu_{jk}(x_{jA}x_{kB}+x_{jB}x_{kA}).$$

These expressions define the system thermodynamically. In many cases the number of independent variables can be reduced by arguments concerning the symmetry of the equations defining equilibrium.

concentration of the type of atom in question and to its intensity of magnetization, then the equations of state can be written directly in the following form

$$\begin{aligned} i_{A1} &= \tanh \frac{Di_{A2}(1+y_2)+Gi_{B2}(1-y_2)+\mu_A H}{kT}, \\ i_{B1} &= \tanh \frac{Gi_{A2}(1+y_2)+Fi_{B2}(1-y_2)+\mu_B H}{kT}, \\ i_{A2} &= \tanh \frac{Di_{A1}(1+y_1)+Gi_{B1}(1-y_1)+\mu_A H}{kT}, \\ i_{B2} &= \tanh \frac{Gi_{A1}(1+y_1)+Fi_{B2}(1-y_1)+\mu_B H}{kT}. \end{aligned} \tag{17A}$$

D, F, and G are constants. D and F determine the behavior of pure A and pure B, respectively. μ_A and μ_B are the dipole moments of an atom of A or B, and G determines the interactions of dipoles of A and B with each other. Even with all the above simplifications these equations are quite formidable, and we shall discuss only a few special cases.

It is well known that ferromagnetic metals do not in general have an absolute saturation corresponding to one magnetic moment per atom, but that only some fraction of the atoms contribute to the ferromagnetism. A way of introducing such a feature into the above theory is to let A represent those atoms having a magnetic moment, and to let B represent atoms with no moment. The equations then reduce to

$$\begin{aligned} i_{A1} &= \tanh \frac{Di_{A2}(1+y_2)+\mu_A H}{kT}, \\ i_{A2} &= \tanh \frac{Di_{A1}(1+y_1)+\mu_A H}{kT}. \end{aligned} \tag{18}$$

The solutions of these equations are determined to a large extent by assumptions which we must make concerning the arrangement of the nonmagnetic atoms in the lattice. If they are arranged at random, we may put $y_1=y_2=y$. Since the substance is ferromagnetic $D>0$, and hence, $i_{A1}=i_{A2}$. The equations reduce to the form of Eq. (1), and the nonmagnetic atoms have no influence on the properties of the system.

If, on the other hand, the nonmagnetic atoms tend to arrange themselves in an orderly fashion, then $y_1 \neq y_2$, and the equation of state is modified. If we measure the mean concentration of nonmagnetic atoms by the parameter $y=\frac{1}{2}(y_1+y_2)$, and the long range order by $s=\frac{1}{2}(y_1-y_2)$, the Curie temperature can be written in the form

$$T_c=(D/k)[(1+y)^2-s^2]^{\frac{1}{2}}.$$

It can be shown that $0 \leqslant s^2 \leqslant (1-|y|)^2$; that for $0 \geqslant y \geqslant -1$, or for concentrations involving fewer magnetic atoms A than nonmagnetic atoms B, the metal may become paramagnetic simply because the magnetic atoms may be completely surrounded by nonmagnetic atoms; and that for $0 \leqslant y \leqslant 1$ there is a real Curie temperature which rises as the degree of order diminishes. Under these circumstances, one should expect additional anomalies in the specific heat due to the changes of order.

The topics discussed so far have had to do with the possibilities of long range order in the electronic states of similar atoms in a pure metal, and the results obtained do not seem to indicate that such a behavior actually exists except possibly in Mn. In discussing alloys, we shall therefore concern ourselves with ferromagnetic metals, as in this case the antiparallel moments will be arranged at random, and we shall discuss metals with one magnetic moment per atom only, so as to avoid assumptions as to how nonmagnetic atoms are arranged in the lattice.

If the pure metals A and B used for the alloy described in Eq. (17A) are ferromagnetic, then D and F must be positive. To illustrate the effect of order-disorder on the magnetic properties, we shall consider the case of an alloy having A and B in equal proportions, but in one case fully disordered $y_1=y_2=y$, $s=0$; and again fully ordered $y_1=-y_2=1$, $y=0$, $s=1$. For the disordered case it can be shown that the two sublattices are identical, $i_{A1}=i_{A2}$, $i_{B1}=i_{B2}$, and the equations reduce to

$$\begin{aligned} i_A &= \tanh \frac{Di_A+Gi_B+\mu_A H}{kT}, \\ i_B &= \tanh \frac{Gi_A+Fi_B+\mu_B H}{kT}. \end{aligned} \tag{19}$$

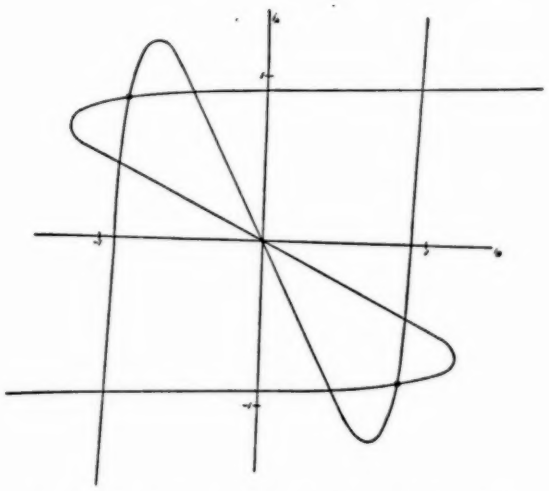

FIG. 2. Plot of Eqs. (21) as functions of i_A and i_B.

For the completely ordered case, on the other hand $i_{A2}=i_{B1}=0$ because there are no atoms of B on lattice 1 or atoms of A on lattice 2, and the equations reduce to

$$i_A=\tanh\frac{2Gi_B+\mu_A H}{kT},\qquad i_B=\tanh\frac{2Gi_A+\mu_B H}{kT}. \tag{20}$$

If, for instance, $D=F=0$ but $G>0$, it is easily seen that the Curie temperature is G/k for the disordered alloys, but $2G/k$ for the ordered alloy. The main point which it is desired to emphasize is that equations of this sort can give radical changes of properties with heat treatment and can make understandable, in principle at least, the appearance of ferromagnetism in alloys of nonmagnetic elements.[13] Whether a more detailed comparison with the behavior of actual systems is possible remains to be seen.

In order to demonstrate somewhat more fully the predictions of Eqs. (17A) we shall discuss them for the case of an alloy of two ferromagnetic elements in any proportions in which the atoms are arranged at random. In this case the two sublattices are identical, and we may put $y_1=y_2=y$, and $i_{A1}=i_{A2}$, $i_{B1}=i_{B2}$, and the equations become

$$i_A=\tanh\frac{Di_A(1+y)+Gi_B(1-y)+\mu_A H}{kT},\qquad i_B=\tanh\frac{Gi_A(1+y)+Fi_B(1-y)+\mu_B H}{kT}. \tag{21}$$

These equations may be plotted as functions of i_A and i_B as in Fig. 2. They have the form of an S, and may have as many as nine solutions. The solutions for the largest absolute values of i_A and i_B have the lowest free energy, and are, therefore, the most stable. For this solution i_A and i_B will have the same sign if $G>0$, or opposite signs if $G<0$. If there are nine solutions, then, in addition to the two mentioned, there will be two solutions corresponding to subsidiary minima of the free energy at the points indicated by circles in the figure. None of the other solutions correspond to minima of the free energy, and are, therefore, not stable solutions. For high temperatures the curves cross only at the origin, if there is no applied magnetic field. The condition for the appearance of spontaneous magnetization is that the slope of the two curves at the origin shall be equal. This may occur for two temperatures, but the higher one of the two is, of course, the Curie point. The subsidiary minima of the free energy appear at temperatures below the lower of the above-mentioned temperatures. The Curie temperature is given by[14]

$$T_c=(1/2k)[D(1+y)+F(1-y)+\{[D(1+y)-F(1-y)]^2+4G^2(1-y^2)\}^{\frac{1}{2}}]. \tag{22}$$

If G is small, the behavior of the alloy will be almost that of two coexisting pure ferromagnetic metals; the Curie point of each will be proportional to its concentration in the alloy. At the Curie point one of these will become ferromagnetic. As the temperature is lowered the magnetization of this component will increase until at some point the second component becomes magnetized. The magnetization of this component will be parallel or antiparallel to that of the first depending on whether G is greater than or less than zero, and the mag-

[13] Experimental work in this connection is summarized by F. C. Nix and W. Shockley, Rev. Mod. Phys. **10**, 59 (1938).

[14] Expressions similar to (22) and (23) were first obtained by L. Néel, reference 6.

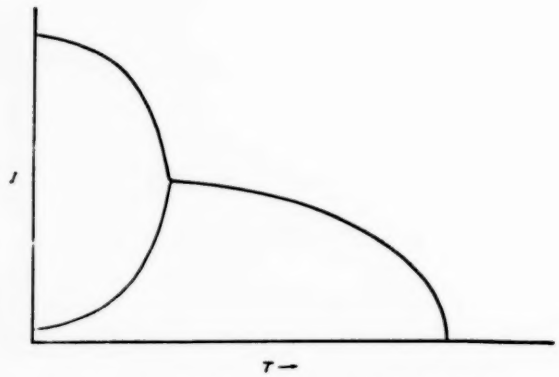

FIG. 3. Intensity of magnetization of an alloy.

netization of the alloy will either increase or decrease with the temperature, as shown in Fig. 3. In the latter case the magnetization can be shifted from the lower to the upper of the two curves in Fig. 3 by the application of a sufficiently strong magnetic field. Hysteresis effects are to be expected in the neighborhood of this field strength because of the presence of two minima in the free energy of almost equal depth. This behavior is similar to that found in the so-called "wasp waisted" hysteresis loops of certain iron-nickel-cobalt alloys.[15] Further experiments on the less complex alloys of this type over wide ranges of field and temperature are greatly to be desired.

[15] Such loops are briefly described by T. D. Yensen in F. Bitter, *Introduction to Ferromagnetism* (McGraw-Hill, 1937).

For other values of G one may expect a behavior of the spontaneous magnetization ranging from that shown in Fig. 3 to that of a pure substance. If $G^2=DF$, the Curie temperature is a linear function of the concentration, and if in addition $D=F$ all alloys behave like either pure substance.

The anomalies in the spontaneous magnetization will, of course, be reflected in the behavior of the specific heats. Also the initial susceptibility above the Curie point will no longer be given by the simple formula, Eq. (9) with $i=0$, but by the expression

$$K_0=\frac{N\mu^2}{k}\frac{T+(1/2k)(2G-D-F)(1-y^2)}{(T-T_1)(T-T_2)}, \quad (23)$$

T_1 being the Curie temperature as defined in Eq. (22), and T_2 a lower temperature defined by this same expression with a negative sign in front of the square root. It is assumed that $\mu_A=\mu_B=\mu$.

The behavior of an alloy in the neighborhood of its Curie point is not completely determined by Eqs. (17A). For a range of temperatures near the critical temperature the alloy may break up into a paramagnetic and a ferromagnetic phase having different compositions. This behavior is influenced by interaction energies which do not appear in the magnetic equation of state, and will, therefore, not be discussed further at this point.

LETTERS TO THE EDITOR

Prompt publication of brief reports of important discoveries in physics may be secured by addressing them to this department. Closing dates for this department are, for the first issue of the month, the eighteenth of the preceding month, for the second issue, the third of the month. Because of the late closing dates for the section no proof can be shown to authors. The Board of Editors does not hold itself responsible for the opinions expressed by the correspondents.

Communications should not in general exceed 600 words in length.

The Heat Capacity of Rochelle Salt

Kobeko and Nelidow[1] and Rusterholz[2] have reported the existence of a rather large anomaly (~5 percent) in the heat capacity of Rochelle salt near its upper Curie point.

The undersigned, working in the department of physics by the method of adiabatic electric heating and independently in the department of chemistry with a Nernst-type vacuum calorimeter, have made a careful investigation of the heat capacity of Rochelle salt in a range including both Curie points. The absolute magnitudes of the heat capacity determined by the two methods agree within 0.3 percent.

At the upper Curie point we have found very little indication of an anomaly and believe that if our samples possess one its amplitude is less than 0.5 percent of the total heat capacity. Fig. 1 shows a set of measurements made with the adiabatic calorimeter near the upper Curie point. Rusterholz' curve, decreased by about 11 percent to make the absolute magnitudes agree, is superposed for comparison.

At the lower Curie point both methods suggest a small anomaly with a maximum amplitude of somewhat less than 1 percent. Fig. 2 shows the measurements made with the adiabatic calorimeter.

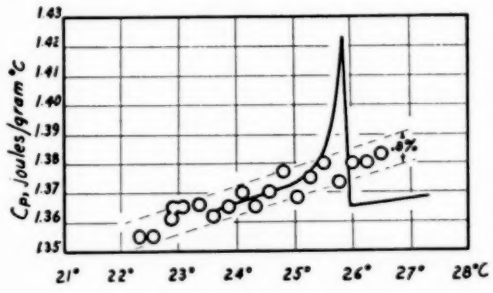

FIG. 1.

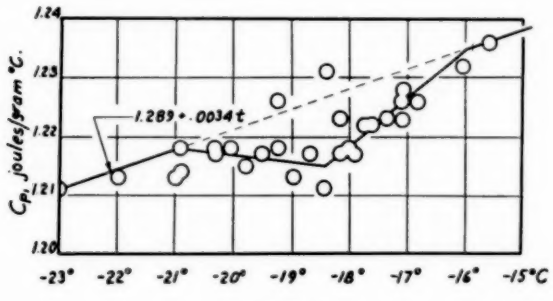

FIG. 2.

Full reports of the separate investigations will be published shortly.

A. J. C. WILSON
J. F. G. HICKS
J. G. HOOLEY

Department of Physics (A. J. C. W.),
Research Laboratory of Physical Chemistry,
Massachusetts Institute of Technology,
Cambridge, Massachusetts,
June 12, 1938.

[1] P. P. Kobeko and J. G. Nelidow, Phys. Zeits. d. Sowjetunion **1**, 382 (1932).
[2] A. A. Rusterholz, Helv. Phys. Acta **8**, 39 (1935).

Asymmetric Distribution of Protons from Deuteron-Deuteron Reaction

We find that the distribution in the center of mass system of the protons from the deuteron-deuteron reaction is not symmetric with respect to a plane perpendicular to the direction of motion of the incident deuterons. More protons are ejected backward than forward. The asymmetry increases rapidly with energy, being just definitely perceptible at 200 kv,[1] whereas at 350 kv it amounts to 13 percent. The observed distribution reduced to the center of mass system may be represented by

$$100+66.7\cos^2\theta+28.2\cos^4\theta-1.1\cos\theta-3.5\cos^3\theta$$

at 200 kv and by

$$100+63\cos^2\theta+62.3\cos^4\theta-2.85\cos\theta-12.7\cos^3\theta$$

at 350 kv. Scattering of the *d*-type is clearly evident at the higher energy and preliminary observations at 400 kv show it still increasing.

The asymmetry appears to indicate the existence of a velocity dependent part of the nuclear forces, perhaps of the nature of a spin-orbit interaction.[2]

These observations have been made with a *thin* target, deuterium gas at a pressure of about 1 mm Hg. The energy loss in such a target is of the order of 500 volts, so that the transformation to the center of mass system introduces no error.

A. ELLETT
R. D. HUNTOON

State University of Iowa,
Iowa City, Iowa,
June 16, 1938.

[1] With thicker targets the asymmetry may be expected to be even less, and this may explain the failure of Kempton, Brown, and Maasdorp (Proc. Roy. Soc. **A157**, 386 (1936)), of Neuert (Physik. Zeits. **38**, 122, 618 (1937)) and of Haxby, Allen and Williams (Phys. Rev. **53**, 921 (1938)) to observe it.
[2] Various types of velocity dependence have been discussed by Breit (Phys. Rev. **51**, 248 (1937); **51**, 778 (1937); **53**, 153 (1938)) and by Wheeler (Phys. Rev. **50**, 643 (1936)).

Long-Lived Radioactive Silver

Several reports of a long-lived activity induced in silver by slow neutrons have appeared recently. Mitchell refers[1] to a weak activity of about 3 months half-life: Alexeeva gives the figure 1.2 to 2.0 years[2] (amended in a private communication to 300±90 days); Reddemann and Strassmann quote[3] a half-life equal to 190±40 days, with observations extending for 3 months, and have shown the activity to be chemically identifiable with silver, so that it must be ascribed to either Ag^{108} or Ag^{110}.

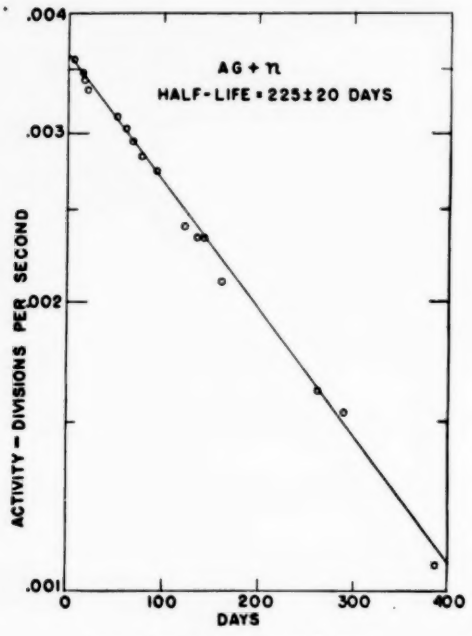

FIG. 1. Decay of radioactive silver.

We wish to add further confirmation to this neutron-induced activity and to give the half-life with somewhat greater precision, after having followed the decay for over a year. Our value is 225±20 days, as may be seen from Fig. 1.

This research has been supported by the Research Corporation, the Chemical Foundation and the Josiah Macy Jr. Foundation.

J. J. LIVINGOOD
G. T. SEABORG

Radiation Laboratory, Dept. of Physics (J. J. L.),
Dept. of Chemistry (G. T. S.),
University of California,
Berkeley, California,
June 9, 1938.

[1] A. C. G. Mitchell, Phys. Rev. **53**, 269 (1938).
[2] K. Alexeeva, Comptes Rendus U.R.S.S. **18**, 553 (1938).
[3] H. Reddemann and F. Strassmann, Naturwiss. **26**, 187 (1938).

Cosmic-Ray Particles of Intermediate Mass

A Geiger-counter placed inside a cloud chamber and coupled by means of a coincidence circuit to a second counter placed above the chamber has been employed to increase the probability of observing cosmic-ray particles near the ends of their ranges, and thus to provide information concerning the mass and stability properties of the particles of intermediate mass. One photograph obtained by this method showing a positively charged particle of $H\rho = 1.7 \times 10^5$ gauss cm, which after traversing the counter emerges with an energy low enough for it to be brought to rest in the gas of the chamber, is of special interest and is reproduced in Fig. 1.

The gas in the chamber consisted of $\frac{2}{3}$ helium and $\frac{1}{3}$ argon at a combined pressure of 1 atmosphere, which together with the alcohol vapor corresponds in stopping power to about 0.5 atmosphere of air. Partly for this reason and partly because of a lower light intensity used in these experiments the tracks are somewhat fainter than those normally obtained. The specific ionization of the particle of Fig. 1 before it traverses the counter, although not accurately measurable, is greater than that of a fast electron.

Although four independent mass estimates can be made from the data provided by the photograph, the most accurate value is to be obtained merely from the initial $H\rho$ of the particle and the thickness of matter traversed before it comes to rest. Both of these quantities can be accurately measured; in particular the track is sharp and an accurate curvature measurement is possible.

The details of the computation and a discussion of the errors of measurement will be deferred until the thickness of matter traversed has been accurately measured after breaking the counter. The uncertainty in the final estimate will probably lie more in the theoretical relation between energy loss and velocity than in the experimental measurements themselves. The final determination should be considerably more accurate than any so far made. From the best guess we can make at present as to the thickness of matter traversed in the counter, the mass appears to be about 240 electron-masses. The other three determinations of the mass, (1) by the relation between the specific ionization and the value of $H\rho$ for the upper portion of the track, (2) by the ionization and $H\rho$ below the counter, and (3) by the $H\rho$ and residual range below the counter, all give values consistent with the one above. The initial energy of the particle before it traverses the counter is 10 Mev and the energy with which it emerges is about 210,000 ev. It is perfectly clear that this particle cannot possibly have either electronic or protonic mass (see caption to Fig. 1).

An interesting feature of the photograph is the fact that the particle is actually observed to come to rest in the gas of the chamber. No completely certain evidence of a subsequent disintegration can be found on the photograph. There are, however, three droplets which appear on the left-hand image, which is the direct view, and also on the right-hand mirror image. Stereoscopic observation shows that these droplets line up so as to indicate a short segment of an electron track emanating from the point in the gas at which the particle came to rest and directed toward the counter. Because of the relatively weak light used in these experiments electron tracks are very faint. These droplets may therefore indicate that the particle after coming to rest disintegrated by the emission of a positive electron.

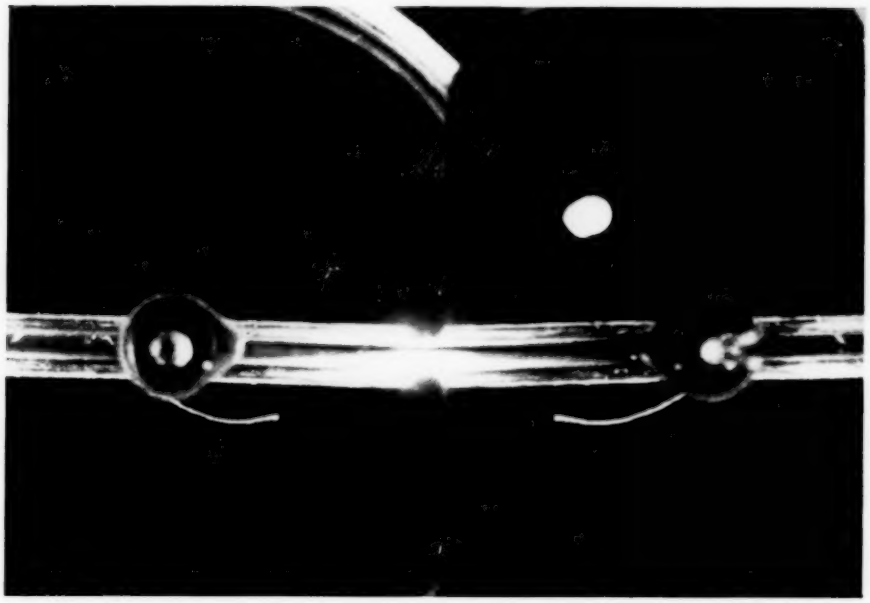

FIG. 1. A positively charged particle of about 240 electron-masses and 10 Mev energy passes through the glass walls and copper cylinder of a tube-counter and emerges with an energy of about 0.21 Mev. The magnetic field is 7900 gauss. The residual range of the particle after it emerges from the counter is 2.9 cm in the chamber (equivalent to a range of 1.5 cm in standard air). It comes to rest in the gas and may disintegrate by the emission of a positive electron not clearly shown in the photograph. It is clear from the following considerations that the track cannot possibly be due to a particle of either electronic or protonic mass. Above the counter the specific ionization of the particle is too great to permit ascribing it to an electron of the curvature shown. The curvature of the particle above the counter would correspond to that of a proton of 1.4 Mev and specific ionization about 7000 ion-pairs/cm, which is at least 30 times greater than the specific ionization exhibited in the photograph. The curvature ($\rho \cong 3$ cm) of the portion of the track below the counter would correspond to an energy of 7 Mev if the track were due to an electron. An electron of this energy would have a specific ionization imperceptibly different from that of a usual high energy particle which produces a thin track, and in addition it would have a range of at least 3000 cm in standard air instead of the 1.5 cm actually observed. Moreover if the particle had electronic mass and emerged from the counter with a velocity such that its specific ionization were great enough to correspond to that exhibited on the photograph, its residual range (in standard air) would be less than 0.05 cm instead of the 1.5 cm observed. A proton of the curvature of the track below the counter would have an energy of only 25,000 ev and a range in standard air of less than 0.02 cm.

Since the particle itself is positively charged it could not have been removed by absorption into a nucleus.

The "intermediate mass" hypothesis offered by the writers[1] to provide an interpretation both of energy loss data and of ionization-range data of the above kind has been given strong support by many experimenters.[2] Various mass estimates have been made from data of the latter type, yielding values ranging from 120 to about 400 electron masses. Our energy loss data have moreover recently been confirmed in all essential details by Blackett.[3] His main conclusion that the penetrating particles always become indistinguishable from electrons when their energies fall below 200 Mev cannot, however, be maintained. In any event this energy value needs to be corrected for the mass, and becomes in fact only 110 Mev for a mass of 240 electrons. A particle of this mass with a curvature corresponding to 100 Mev for an electron would have an actual energy of only 37 Mev and should have a range somewhat less than 1 cm of Pb. Thus, the scarcity of "penetrating" particles with small curvatures (which is clearly evident in our own data) could possibly be understood in terms of the short residual range.

A more detailed discussion, including evidence based on several other photographs of intermediate mass particles, will be given elsewhere.

It is a pleasure to express our indebtedness to Professor R. A. Millikan, and to the Carnegie Institution of Washington, whose grant of funds to Professor Millikan has provided the chief support for these researches. We wish to thank also Dr. J. K. Boggild and Mr. I. C. Kuo for their assistance in operating the apparatus.

SETH H. NEDDERMEYER
CARL D. ANDERSON

California Institute of Technology,
Pasadena, California,
June 16, 1938.

[1] Anderson and Neddermeyer, Phys. Rev. **50**, 263 (1936); Neddermeyer and Anderson, Phys. Rev. **51**, 884 (1937). A discussion of certain fundamental difficulties with identifying the penetrating component with either electrons or protons was given in the former paper and also by Anderson and Neddermeyer, *Report of London Conference*, Vol. I (1934), p. 179.

[2] Street and Stevenson, Phys. Rev. **52**, 1003 (1937); Nishina, Takeuchi and Ichimiya, Phys. Rev. **52**, 1198 (1937); Brode and Starr, Phys. Rev. **53**, 3 (1938); Auger, Comptes Rendus **206**, 346 (1938); Ruhlig and Crane, Phys. Rev. **53**, 266 (1938); Corson and Brode, Phys. Rev. **53**, 773 (1938); Ehrenfest, Comptes Rendus **206**, 428 (1938); Williams and Pickup, Nature **141**, 684 (1938).

[3] Blackett, Proc. Roy. Soc. **A165**, 11 (1938).

Search for an Excited State of the H^3 Nucleus

Evidence for the existence of an excited state of the He^3 nucleus formed in the reaction

$$H^2+H^2 \rightarrow He^3+n^1$$

has been presented by Bonner[1] and by Baldinger, Huber and Staub.[2] Difficulties encountered in accounting for such an excited state have been discussed by Share[3] and by Schiff.[4] Since the short range forces between elementary particles are thought to be identical except for the Coulomb forces, one expects a similar excited state of the H^3 nucleus formed in the companion reaction

$$H^2+H^2 \rightarrow H^3+H^1.$$

We have looked for such an excited state of H^3 by searching for a lower energy group of protons in this reaction. We find no evidence for it.

Both heavy ice and contamination targets were bombarded with a magnetically resolved deuteron beam of 120 to 160 kv. Protons were observed at 90° to the direction of the incident beam by means of a differential ionization chamber, linear amplifier, and thyratron "scale-of-four" counter. The disintegration protons emerged from the target chamber through a thin collodion window (approx. 0.15 cm stopping power) mounted on a grid of 19 holes each 0.05 cm in diameter confining the beam to a width of 0.35 cm at a distance of 11 cm from the target. Three collimating diaphragms, each 0.4 cm in diameter, were placed in the chamber to reduce scattering. Range measurements were obtained by using air up to about 5 cm stopping power, and rolled aluminum foils each of 1.14 cm air equivalent beyond this. Measurements were taken from a minimum absorption determined by the presence of counts from H^3 of 1.6 cm range.

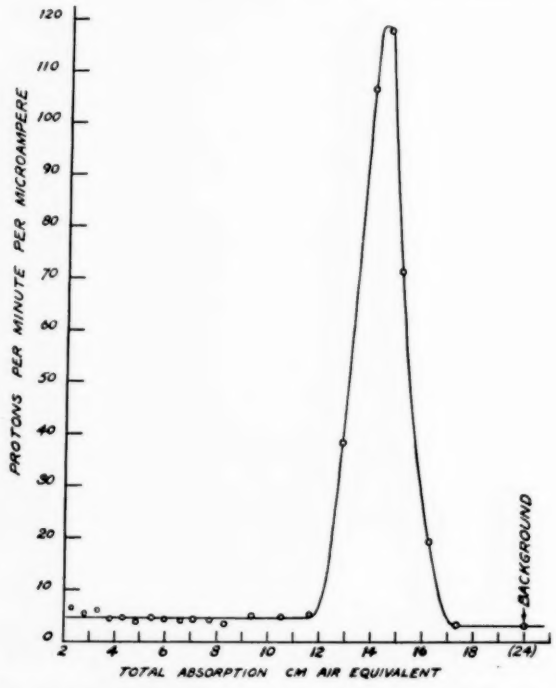

FIG. 1. Differential range curve of the protons from the reaction $H^2+H^2 \rightarrow H^3+H^1$.

The two halves of the differential ionization chamber were each 1 cm deep and were separated by an aluminum foil of 1.14 cm air equivalent. The construction of the chamber and the angular definition were such that all particles of sufficient energy to go through both halves of the chamber would cancel unless scattered in the front half of the chamber. To reduce this scattering, the usual grid over the opening to the chamber was replaced by seven parallel equally spaced 3 mil tungsten wires. The output of the linear amplifier was monitored continuously with a cathode ray oscillograph, and the thyratron counter was biased to count all pulses greater than a minimum of about three times the noise background. Protons which did not penetrate the collecting foil between the two halves of the chamber gave pulses approximately three times the size of the minimum counted.

Data were taken first at 160 kv then at 120 kv with a contamination target. To improve the sensitivity additional data were obtained at 120 kv with a heavy-ice target. Finally, in order to test the possibility of a resonance effect data were taken at 110 kv and with the unresolved ion beam falling on as thick a heavy-ice target as could be maintained. Particles were counted for intervals of one to five minutes depending on the counting rate. A fresh surface of heavy ice was deposited before counting at each point, and the constancy of the apparatus was checked by returning to the peak of the main group at frequent intervals. Resolved ion currents of 5 to 11μa were used, while the unresolved ion current was about 50μa. In no case was a second group of protons observed, and under the worst conditions a group of five percent the intensity of the main group should have been easily detected. The data taken at 120 kv with the resolved beam and a heavy-ice target are shown in Fig. 1, where the abscissa is the total absorption from the target to the collection foil in the ion chamber. In this case, a group of two percent of the main group should have been readily observed. No great accuracy is claimed for the range measurement of the main group since no corrections were applied for possible thin spots in the foils, and since the chamber was too deep for precise range measurements.

We wish to express our appreciation to Dr. Henry Primakoff for many helpful discussions.

FRANK E. MYERS
LAWRENCE M. LANGER

Department of Physics,
New York University,
University Heights,
New York, N. Y.,
June 16, 1938.

[1] Bonner, Phys. Rev. **53**, 711 (1938).
[2] Baldinger, Huber and Staub, Helv. Phys. Acta **XI**, 245 (1938).
[3] Share, Phys. Rev. **53**, 875 (1938).
[4] Schiff, Bulletin of the American Physical Society, San Diego meeting (1938).

The Theory of the Transverse Doppler Effect

The ingenious and exceedingly precise observations made recently by Ives* on the spectrum of hydrogen canal rays verify a long standing prediction of the special theory of relativity—the prediction that the frequencies

of spectral lines will be found to vary with the velocity v of the particles producing them as $(1-v^2/c^2)^{\frac{1}{2}}$.

That this effect was to be expected could be shown by transforming the expression for the phase of a train of spherical light waves from the space-time coordinates of the reference frame in which the radiating particle was at rest to a second frame—that of the observer—with respect to which the first was moving with uniform velocity v. By this procedure it is found that the observer should perceive the ordinary Doppler effect with respect not to the "rest frequency" of the radiation ν_0, but with respect to a lower frequency $\nu_0'=\nu_0(1-v^2/c^2)^{\frac{1}{2}}$. For an observer looking at right angles to the particle's velocity the ordinary Doppler effect vanishes, and this relativistic red shift should alone remain—hence the designation "transverse Doppler effect."

It is interesting, though not surprising perhaps, to find that the prediction might have been based equally well on the relativistic mechanics of photon emission. Consider an excited atom of total rest energy E_1. Its rest mass is $m_1=E_1/c^2$. In motion with velocity v_1 its total energy is $m_1c^2/(1-v_1^2/c^2)^{\frac{1}{2}}=E_1/(1-\beta_1^2)^{\frac{1}{2}}$. Suppose now that it ejects a photon of energy $h\nu$ in transition to a lower state of total energy $E_2/(1-\beta_2^2)^{\frac{1}{2}}$. Conservation of energy requires that

$$h\nu+E_2/(1-\beta_2^2)^{\frac{1}{2}}=E_1/(1-\beta_1^2)^{\frac{1}{2}}. \tag{1}$$

Consider next the momenta. The initial momentum of the atom is $m_1v_1/(1-\beta_1^2)^{\frac{1}{2}}=(E_1\beta_1/c)/(1-\beta_1^2)^{\frac{1}{2}}$. After ejecting the photon its momentum is $(E_2\beta_2/c)/(1-\beta_2^2)^{\frac{1}{2}}$ with components parallel and normal to v_1 proportional, respectively, to $\cos\gamma$ and $\sin\gamma$ where γ represents the angle between v_1 and v_2. The corresponding components of the photon's momentum are $(h\nu/c)\cos\alpha$ and $(h\nu/c)\sin\alpha$, where α represents the angle between v_1 and the direction in which the photon has been ejected. The three vectors are in a plane, and conservation of momentum requires that

$$\frac{E_2\beta_2/c}{(1-\beta_2^2)^{\frac{1}{2}}}\cos\gamma+\frac{h\nu}{c}\cos\alpha=\frac{E_1\beta_1/c}{(1-\beta_1^2)^{\frac{1}{2}}} \tag{2}$$

and

$$\frac{E_2\beta_2/c}{(1-\beta_2^2)^{\frac{1}{2}}}\sin\gamma-\frac{h\nu}{c}\sin\alpha=0. \tag{3}$$

If one uses these relations to eliminate β_2 and γ, and writes β for β_1 one finds that

$$\nu=\nu_0(1-\beta^2)^{\frac{1}{2}}/(1-\beta\cos\alpha),$$

where $\nu_0=[(E_1+E_2)/2E_1](E_1-E_2)/h$. It may be noted in passing that this differs from the usual expression for the "rest frequency" by the factor $(E_1+E_2)/2E_1$ (equal sensibly to one) which represents the fraction of the energy (E_1-E_2) carried off by the photon; the remainder appears as kinetic energy of the recoiling atom.

The expression for ν is identical with that obtained by the transformation of space-time coordinates. Rewritten in terms of wave-lengths it becomes

$$\lambda=\lambda_0/(1-\beta^2)^{\frac{1}{2}}(1-\beta\cos\alpha).$$

If the particle approaches the observer along his line of sight, $\alpha=0$ and $\lambda=\lambda_1=\lambda_0[(1-\beta)/(1+\beta)]^{\frac{1}{2}}$; if it recedes from him along his line of sight $\alpha=\pi$ and $\lambda=\lambda_2=\lambda_0[(1+\beta)/(1-\beta)]^{\frac{1}{2}}$. The mean of these wave-lengths,

$$(\lambda_1+\lambda_2)/2=\lambda_0/(1-\beta^2)^{\frac{1}{2}}.$$

It is the prediction in this particular form which Ives has verified.

C. J. DAVISSON

Bell Telephone Laboratories,
New York, New York,
June 2, 1938.

* Ives, Nature **141**, 551 (1938). J. O. S. A., July 1938.

Structure of Oxidized Silicon Film

Electron diffraction photographs were obtained by the transmission of electrons (0.058 to 0.063A) through thin films of silicon.

These films were obtained by condensing silicon vapor on a polished rocksalt surface. The vapor is obtained from silicon metal which is heated electrically in a thoria crucible placed in a vacuum container. Free films are obtained by dissolving the crystal base in water.

The diffraction pattern obtained by this film consists of three diffused rings corresponding to $(\sin\theta/2)/\lambda=0.12$ (strong), $=0.29$ (weak), $=0.40$ (medium), which are quite different from those of silicon crystal. This resu't, somewhat similar to that of Maxwell and Mosley's[1] on a fused silica film, can be discussed as scattering from amorphous SiO_2 as previously treated by Warren.[2] It may be concluded that a thin silicon film changes to an amorphous silica film by spontaneous oxidation in air.

By heating the film at various temperatures ranging from 410 to 800°C the diffraction pattern changes as follows:

(1) Intensity maxima of films after the heat treatment.

Temp. °C	Time (min.)	$(\sin\theta/2)/\lambda$						
410	3	0.13(*st*)	0.20	—	0.26(*w*)	—	—	0.41(*m*)
440	3	0.13(*st*)	0.20	0.24	0.26(*w, s*)	0.29(*w, s*)	0.34	0.41(*m*)
515	3	0.13(*st*)	0.20		0.25(*d*)	—	—	0.39(*m*)
615	3	0.13(*st, s*)	0.20	—	—	—	—	0.40(*m*)
800	3	0.13(*st, s*)	0.19	—	—	—	—	0.41(*m*)

Note: (*st*): strong. (*st, s*): strong and sharp. (*w*): weak. (*w, s*): weak and sharp. (*m*): medium. (*d*): diffuse and (doublet?).

(2) Diffused ring at $(\sin\theta/2)/\lambda=0.13$ becomes gradually sharper with the rise of the temperature of heat treatment.

(3) Weak halos at $(\sin\theta/2)/\lambda=0.24$, 0.26, and 0.34, appear only when it is heated at about 450°C and these halos can not be expected from Warren's model, but coincide with Shishacow's[3] result if we allow an experimental error of ±0.01.

A more detailed account will be published elsewhere.

HIROSI KAMOGAWA

Research Laboratory,
Tokyo Electric Company,
Kawasaki, Japan,
May 26, 1938.

[1] Maxwell and Mosley, Phys. Rev. **47**, 331 (1935).
[2] B. E. Warren, Phys. Rev. **45**, 657 (1934).
[3] Shishacow, Nature **136**, 514 (1935); Comptes Rendus Acad. Sci. U.R.S.S. **1**, 19 (1936).

Excited State of He^3

Recent experiments of Bonner[1] indicate the existence of a bound excited state of He^3 1.9 Mev above the ground state. Since this is probably a P state, it involves interactions that are not determined by the normal state energies of the lightest nuclei or by existing data on scattering. It is therefore of considerable interest to see what information concerning the P interactions between like and unlike particles is implied by the existence of a P state of He^3 about 1.9 Mev above the ground state. It would seem *a priori* that there should be no excited state for a much larger distance above the ground state, since the saturation property of nuclear forces requires the interaction between two particles in an antisymmetric state to contribute much less to the binding than the interaction in a symmetric state.

We shall try here to make this argument somewhat sharper by using the variational method to compute the energies of the normal state and the lowest group of excited states. We assume for the moment that many-body and spin-orbit forces are negligible. The interactions are then:

$$V_{p\pi}(r) \doteq [(M+H\boldsymbol{\sigma}\cdot\boldsymbol{\sigma}')P^M+W+H\boldsymbol{\sigma}\cdot\boldsymbol{\sigma}']J(r),$$
$$V_{\pi\pi}(r)=(W'+B'\boldsymbol{\sigma}\cdot\boldsymbol{\sigma}')J(r)+e^2/r, \qquad J(r)=\exp(-\gamma r^2),$$

where the $\boldsymbol{\sigma}$'s have unit amplitude; with $\gamma^{-\frac{1}{2}}=2.25\times10^{-13}$ cm, the conditions $M+W=-32.0$, $H+B=-3.5$, $W'-3B'=-21.4$, all in Mev, insure agreement with data on the deuteron and on scattering.[2] As variational wave-functions we use:

$$\psi_0=(4\alpha\beta/\pi^2)^{3/4}\exp(-\alpha R^2-\beta r^2)\cdot{}^2\Sigma_-,$$
$$\psi_1=2\beta^{\frac{1}{2}}x(4\alpha\beta/\pi^2)^{3/4}\exp(-\alpha R^2-\beta r^2)\cdot{}^4\Sigma_+,$$
$$\psi_2=2\beta^{\frac{1}{2}}x(4\alpha\beta/\pi^2)^{3/4}\exp(-\alpha R^2-\beta r^2)\cdot{}^2\Sigma_+,$$
$$\psi_3=2\alpha^{\frac{1}{2}}X(4\alpha\beta/\pi^2)^{3/4}\exp(-\alpha R^2-\beta r^2)\cdot{}^2\Sigma_-,$$

where x is a cartesian component of $\mathbf{r}$, which joins the two protons, X is a cartesian component of $\mathbf{R}$, which joins the center of mass of the two protons with the neutron, and the Σ's are appropriate spin functions. ψ_0 is the even ^2S ground state, ψ_1 an odd ^4P excited state, and ψ_2 and ψ_3 odd ^2P excited states. We treat the Coulomb energy as a perturbation throughout. The minimization of ψ_0 gives -5.7 for the ground state energy, as compared with the experimental value -7.6; this result is insensitive to the values of M, H, and W', provided that $M+W=-32.0$, etc. The calculation of the energy of ψ_1 and the lower root of the second order secular equation, obtained from ψ_2 and ψ_3, and by the use of the usual saturating forces ($W=W'=0$, B and H both of the order of -3.5), shows that these quantities have poorly defined minima and are never negative; for reasonable values of α and β they are both greater than $+5$. Now since the excited state indicated by experiment is well bound (3.5 Mev below the continuum of deuteron plus proton) and since the variational method gives good results for the ground state, we may hope that the same method with similar wave functions will work reasonably well for the excited state. Therefore it seems likely that the usual choice of force constants, which leads to a lowest excited state far up in the continuum, is incompatible with the existence of Bonner's state.[3]

In order to show to what extremes it is necessary to go if one wishes to obtain an excited state at anywhere near the indicated place, the variational calculation was carried through for several sets of force constants, subject to the restrictions $M+W=-32.0$, etc. The constants: $M=+18.0$, $W=-50.0$, $H=-3.5$, $B=0.0$, $W'=-53.5$, $B'=-10.7$, satisfy these restrictions and give two bound excited states: the ^4P at -3.7 (2.0 Mev above the computed ground state), and the lower ^2P at -2.0 (3.7 Mev above the computed ground state); the other ^2P state is far up in the continuum. Any significant decrease of $-W$ or $-W'$ would raise both excited levels considerably. These force constants just avoid binding the ^1P deuteron, and are not far from binding the ^3P deuteron and ^3P He^2. Since they are in flagrant contradiction with the saturation requirement and would imply inacceptably large binding energies for nuclei such as He^5 and Li^6, we cannot regard them as being correct.

We have also investigated the possibility of accounting for the excited state in terms of a spin-orbit force of the form $(\boldsymbol{\sigma}\cdot\mathbf{r})(\boldsymbol{\sigma}'\cdot\mathbf{r})J(r)/r^2$. (An interaction of this general form and of magnitude comparable to that of the $(\boldsymbol{\sigma}\cdot\boldsymbol{\sigma}')$ interaction is suggested by dynaton theories of nuclear forces.[4]) However, it turns out that if saturating forces are used, the spin-orbit part of the interaction must be very much larger than the spin-spin part if the excited state is to be properly placed. This is contrary to the usual assumption that nuclear spin-orbit forces are small. We can thus conclude that an explanation of the position of Bonner's state would require the existence of strong attractive interactions which do not manifest themselves in the normal states of the lightest nuclei or in scattering experiments, and which entail far-reaching modifications of the usual ideas concerning nuclear forces.

It is a pleasure to thank Professor J. R. Oppenheimer and Dr. R. Serber for helpful discussion of this problem.

L. I. SCHIFF*

California Institute of Technology,
Pasadena, California,
June 1, 1938.

* National Research Fellow.

[1] Bonner, Phys. Rev. **53**, 711 (1938).

[2] Margenau and Warren, Phys. Rev. **52**, 790 (1937).

[3] These results do not seem to be sensitive to the breadth of the interaction.

[4] Yukawa, Sakata and Taketani, Proc. Phys.-Math. Soc. Japan **20**, 319 (1938); Frohlich, Heitler and Kemmer, Proc. Roy. Soc. **166**, 154 (1938).